DOT/FAA/AR-02/80

Office of Aviation Research
Washington, D.C. 20591

Impact Damage Characterization and Damage Tolerance of Composite Sandwich Airframe Structures – Phase II

October 2002

Final Report

U.S. Department of Transportation
Federal Aviation Administration

NOTICE

This document is disseminated under the sponsorship of the U.S. Department of Transportation in the interest of information exchange. The United States Government assumes no liability for the contents or use thereof. The United States Government does not endorse products or manufacturers. Trade or manufacturer's names appear herein solely because they are considered essential to the objective of this report. This document does not constitute FAA certification policy. Consult your local FAA aircraft certification office as to its use.

This report is available at the Federal Aviation Administration William J. Hughes Technical Center's Full-Text Technical Reports page: actlibrary.tc.faa.gov in Adobe Acrobat portable document format (PDF).

Technical Report Documentation Page

1. Report No.	2. Government Accession No.	3. Recipient's Catalog No.
DOT/FAA/AR-02/80		

4. Title and Subtitle	5. Report Date
IMPACT DAMAGE CHARACTERIZATION AND DAMAGE TOLERANCE OF COMPOSITE SANDWICH AIRFRAME STRUCTURES – PHASE II	October 2002
	6. Performing Organization Code

7. Author(s)	8. Performing Organization Report No.
Tomblin, John S., Raju, K.S., Acosta, J.F., Smith, B.L., and Romine, N.A.	

9. Performing Organization Name and Address	10. Work Unit No. (TRAIS)
Wichita State University 1845 Fairmount Wichita, KS 67260-0093	
	11. Contract or Grant No. 01-C-AW-WiSU-002

12. Sponsoring Agency Name and Address	13. Type of Report and Period Covered
U.S. Department of Transportation Federal Aviation Administration Office of Aviation Research Washington, DC 20591	Final Report
	14. Sponsoring Agency Code ACE-110

15. Supplementary Notes

The Federal Aviation Administration William J. Hughes Technical Center Technical Manager was Peter Shyprykevich.

16. Abstract

The impact responses and the damage states in flat composite sandwich panels with thin facesheets were investigated in Phase I and were found to be dependent on the diameter of the spherical steel impactor. The residual strength of impact-damaged sandwich panels under static in-plane compressive loads was reported to be dependent on the nature of the damage state. The impact damage due to blunt impactors is difficult to detect in service and depending on the size of the damage, can degrade the residual strength more than a punctured skin. The detectability of impact damage states using different field inspection techniques was experimentally investigated for different facesheet and core combinations. The impact damage in honeycomb core sandwich panels was better detected using instruments that exploit the local vibrational characteristics of the sandwich structure, while the damage in foam core panels was more amenable to acoustic-based techniques. The effect of facesheet stiffness on the sensitivity of the field inspection techniques was investigated and the results are reported. The behavior of the sandwich panels with impact damage and subjected to the in-plane static compressive loads was investigated in detail. The impact damage behaved in a characteristic sequence of events leading to contrasting final failure modes. The sequence of events was found to be dependent on the facesheet stiffness and the transverse compressive properties of the core material.

The effects of panel curvature on the impact damage resistance of sandwich panels were experimentally investigated for limited sandwich configurations. The effects of the radius of cylindrical panels, boundary conditions, facesheet type, and core type were also examined. The decreasing radius of curvature increased the global bending stiffness but decreased the local contact stiffness due to the radial compressive properties of the honeycomb core. The curved panel behavior was characterized in terms of the impact response and the damage metrics.

The fatigue behavior of honeycomb core and foam core sandwich panels with impact damage due to a 3″ diameter impactor was investigated. The effect of load ratio and load level on the fatigue life was observed and the results reported. The specimens surviving the predefined infinite life of 150,000 cycles were further tested for degradation in residual strength. Except for foam core sandwich panels with fiberglass/epoxy facesheets (inspected at 30 lbf-ft energy level where the residual strength degradation was 30%), the fatigue cycling did not degrade the static residual strength.

17. Key Words	18. Distribution Statement
Composites, Sandwich, Honeycomb, Foam, Damage tolerance, Impact, Field inspection techniques, Residual strength, Curvature, Fatigue	This document is available to the public through the National Technical Information Service (NTIS), Springfield, Virginia 22161.

19. Security Classif. (of this report)	20. Security Classif. (of this page)	21. No. of Pages	22. Price
Unclassified	Unclassified	87	

TABLE OF CONTENTS

LIST OF FIGURES

LIST OF TABLES

EXECUTIVE SUMMARY

The impact responses and the damage states in flat composite sandwich panels with thin facesheets were investigated in Phase I and were found to be dependent on the diameter of the spherical steel impactor. The residual strength of impact-damaged sandwich panels under static in-plane compressive loads was also found to be dependent on the nature of the damage state. The impact damage states due to blunt impactors, depending on the size of the damage, are difficult to detect in service and can degrade the residual strength more than a punctured skin. In Phase II, the detectability of impact damage states using different field inspection techniques was experimentally investigated for different facesheet and core combinations. The impact damage in honeycomb core sandwich panels was better detected using instruments that exploited the local vibrational characteristics of the sandwich structure, while the damage in foam core panels were more amenable to acoustic-based techniques. The effect of facesheet stiffness on the sensitivity of the field inspection techniques was investigated. The behavior of the sandwich panel with impact damage and subjected to in-plane compressive loads was investigated in detail. The impact damage behaved in a characteristic sequence of events leading to contrasting final failure modes. The sequence of events was dependent on the facesheet stiffness and the transverse compressive properties of the core material.

The effects of panel curvature on the impact damage resistance of sandwich panels were experimentally investigated for limited sandwich configurations. The effects of the radius of cylindrical panels, boundary conditions, facesheet type, and core type were also examined. The decreasing radius of curvature increased the global bending stiffness, but decreased the local contact stiffness due to the radial compressive properties of the honeycomb core. The decrease in radius increased susceptibility to damage for sharp impactors but decreased damage for blunt impactors.

The fatigue behavior of honeycomb core and foam core sandwich panels with impact damage due to a 3″ diameter impactor was investigated, including the effect of load ratio and load level on the fatigue life. No significant trend could be observed with load ratio. The load/life was very flat and exhibited a well known composites sudden death behavior. At higher fatigue loads, the early failures were attributed to impingement on the static strength distribution. The specimens surviving the predefined infinite life of 150,000 cycles were further tested for degradation in residual strength. Except for foam core sandwich panels with fiberglass/epoxy facesheets (impacted at 30 lbf-ft energy level where the residual strength demonstration was 30%), the fatigue cycling did not degrade the static strength. It should be noted that the fatigue cycling was at strain levels much higher than would be expected in service.

1. INTRODUCTION.

To successfully implement damage tolerance programs for composite sandwich airframe structures, a good understanding of the potential damage states in sandwich panels, the capability to detect and characterize these damage states, and the behavior of the damaged structure under service loads is required. The formation of damage in sandwich airframes has been attributed to transient transverse normal loads arising due to low-velocity impacts by foreign objects. The behavior of sandwich structures under such transient loads and the resulting damage states are governed by several variables, which have been classified as intrinsic variables and extrinsic variables [1]. The impact responses and the damage states in flat sandwich panels with thin facesheets were reported to be dependent on the diameter of the spherical steel impactor [2]. The smaller (1″) diameter impactor produced localized facesheet damage with noticeable residual indentations on the order of the facesheet thickness, while the larger (3″) diameter impactor produced widespread core damage with residual indentations on the order of ply thickness (0.01″) or less.

The damage tolerance of the impact damaged sandwich panels were evaluated by conducting compression-after-impact (CAI) tests. The residual strength and failure modes of the sandwich panels under in-plane compressive loads were governed by the relative distribution of facesheet and core damage states. The impact damage due to smaller impactors produced a stress concentration governed compressive failure of the facesheet across the width of the sandwich panel, with the crack originating from the damage zone and propagating towards the lateral edges. The impact damage due to the larger impactor promoted a local buckling initiated failure of the impacted facesheet. The residual strengths that corresponded to the compressive failure of the sandwich panels were consistently higher than the buckling initiated failure.

The normalized residual strengths of sandwich panels impacted with 1″ and 3″ diameter impactors are plotted as a function of planar damage area in figure 1(a). The data is scattered around a hypothetical degradation curve irrespective of the impactor diameter. However, the data points that correspond to the smaller diameter impactor are spread over the initial portion of the curve while those for the larger impactor fall over the asymptotic region of the curve.

The impact damage states in practice will only undergo a posteriori analysis based on the "damage metrics," without any knowledge of the associated impact energies. The maximum residual indentation has been typically used as a measure of the severity of impact damage. The threshold of detectability based on the residual indentation is known as barely visible impact damage (BVID). There is no consensus on a standard value for the BVID, even though it has been assumed that the strength degradation is proportional to the residual indentation depth based on data for impactors 1 in or smaller. It has been shown in the previous study [2] that the maximum residual indentation depth does not necessarily correlate well with the CAI strength particularly when considering larger impactor diameters and a range of sandwich design parameters. Figure 1(b) shows that large planar damage areas can exist while the maximum residual indentation is on the order of a few ply thicknesses (0.008″ in this case). It was concluded that BVID is not a reliable indicator of impact damage; rather planar damage size better reflects the residual strength degradation in sandwich panels. Thus, other damage detection techniques need to be identified and evaluated to quantify planar damage size.

Alternatively, knowledge of the shape of the residual strength curve can be used to set design strain levels sufficiently low such that large planar damage does not pose a safety threat. Such a solution imposes a weight penalty.

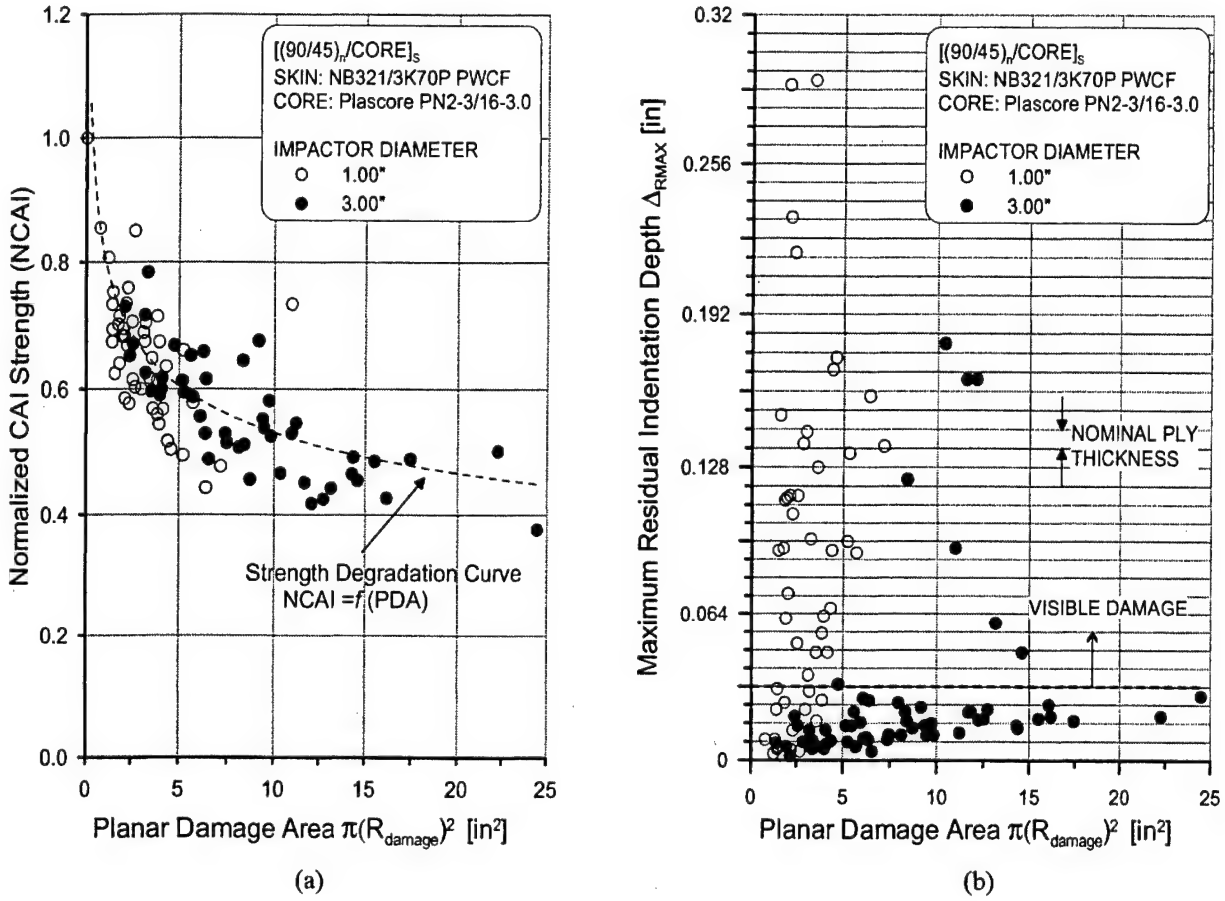

FIGURE 1. (a) NORMALIZED RESIDUAL STRENGTH FOR $[(90/45)N/CORE]_s$ (N=1,2,3)[1] SANDWICH PANELS WITH HONEYCOMB CORE (3/8″ AND 3/4″ THICK) AND (b) VARIATION OF MAXIMUM RESIDUAL INDENTATION DEPTH WITH PLANAR DAMAGE AREA FOR THE SANDWICH PANELS

In this report, the nature of the impact damage states based on destructive sectioning of sandwich panels [2 and 3] is discussed. The damage metrics associated with these damage states are presented, and the possibility of their detection using nondestructive methods is also discussed.

The detection and quantification of impact damage using candidate field inspection techniques were also investigated. The damage delineation using field inspection techniques was conducted at the Sandia National Laboratories. The techniques that were used by Sandia are either in common use by airlines, such as tap testing, or limit use such as Mitsui Woodpecker or V-95 Bond Tester. The effectiveness of each technique was evaluated by comparing the damage metrics delineated by candidate methods with those of ultrasonic C-scan method. The effects of

[1] The sandwich layup configurations listed throughout this document shall imply that the layup is symmetric about the core, i.e., $[(90/45)_n/CORE]_s$ means $[(90/45)_n/CORE/(45/90)_n]$

facesheet stiffness and core density (honeycomb and foam cores) on the detectability of the field inspection techniques were estimated by using limited experiments.

In Phase I of this investigation, the CAI test data were used to determine the degradation of the sandwich compression strength and the final failure mode. Since the far-field strain data and the end shortening were almost linear until the initiation of final failure, supplementary tests were conducted with additional instrumentation to monitor the growth of indentation under in-plane compressive loads. The tests also revealed characteristic behavior of the dimple, which was dependent on the initial indentation levels, planar damage area, facesheet stiffness, and the transverse compressive behavior of cores. Both honeycomb and foam cores were used in this study and the results are presented in this report.

The impact resistance of sandwich structures has been typically investigated using flat coupons. However, airframe structures are seldom flat and the effect of curvature should be known. In an effort to estimate the effects of the panel curvature on the impact responses and resulting damage states, a limited number of impact experiments were conducted on selected sandwich configurations with internal radii of 6″, 24″, and 48″. The specimens were cylindrical and supported along the edges formed by cylindrical generators. The effects of specimen cylindrical curvature on the impact responses, C-scan damage size, and residual indentations were observed. A limited study on the influence of the boundary supports on the impact resistance was also conducted.

Finally, the behavior of impact damage states under fatigue loads was investigated. Two types of sandwich panels were used in the study: (1) carbon fabric facesheets and honeycomb cores and (2) fiberglass fabric facesheets and foam cores. Sandwich configurations of $[(90/45)/CORE]_s$ and $[(90/45)_2/CORE]_s$ with 0.75″ thick cores were used. The impact damage states due to 3″ impactor at two impact energy levels corresponding to the knee region and the asymptotic region of the hypothetical residual strength degradation curve were considered. The results of the fatigue life at four different stress levels and three stress ratios are summarized and reported. The reduction in residual strength of sandwich specimens, which survived the N_∞ cycles, is also reported.

In summary, the following issues were addressed in this phase of the investigation:

- Among the different damage metrics that can be associated with impact damage in sandwich panels, which can be detected and which reflect the residual strength degradation better.
- Performance characteristics of different field inspection techniques to detect impact damage.
- Behavior of impact damage states under static loading.
- Effects of curvature (cylindrical) on the damage resistance of sandwich panels.
- Behavior of impact damaged sandwich panels under fatigue loads.

2. IMPACT DAMAGE IN SANDWICH PANELS.

The damage states in sandwich panels can be broadly classified as material damage states and geometric damage states. The material damage states include facesheet damage, core damage, and facesheet-core interface disbonds. The facesheet damage states encompass delaminations, matrix cracks, and facesheet and ply fractures. The core damage states may be comprised of core crushing (foam cores), cell wall buckling (honeycomb cores), and core fractures. The geometric damage state in sandwich panels manifests as a residual indentation distribution around the point of impact. The various damage states may occur simultaneously with the relative proportions being dictated by intrinsic and extrinsic variables. In this section, the damage states observed during the experimental program are enumerated.

2.1 FACESHEET DAMAGE.

The facesheet damage states may be comprised of facesheet delaminations, matrix cracking, and ply and facesheet fractures [3 and 4]. The initiation of facesheet damage was observed to be dependent on the impactor size (diameter). A limited number of sandwich panels ($[(90/45)_2/CORE]_s$) with fiberglass facesheets (Newport NB321/7781) and honeycomb cores (Plascore PN2-3/16-3.0; 0.75″ thick) were impacted to study the facesheet damage states in sandwich panels. The translucency of the fiberglass facesheets was exploited to observe the facesheet damage states, since the underlying core damage masked the facesheet damage during the through-transmission ultrasonic C-scan (TTU C-scan) measurements [2-4].

The facesheet damage was observed to initiate in the form of delaminations between the plies adjacent to the facesheet-core interface and these delaminations occurred above the honeycomb cell walls [4]. A network of delaminations was observed at higher impact energy levels. The area over which delamination networks occurred was found to increase with impact energy up to the point when facesheet fracture was initiated. The typical delamination networks in sandwich panels impacted with a 3″ diameter impactor are illustrated in figure 2. It was observed that the damage area measured by the TTU C-scan method was consistently higher than the area corresponding to the facesheet delaminations. This implies that in practice, facesheet damage may go undetected in the absence of a conspicuous facesheet fracture.

2.2 CORE DAMAGE.

The core damage in honeycomb core sandwich panels was observed to be predominantly cell wall buckling, core crushing, and cell wall fracture. The incipient failure mode in all cases was observed to be cell wall buckling, which propagated across the planar dimensions of the panel. The damage metrics associated with the core damage in sandwich panels (honeycomb core) are illustrated in figure 3. The TTU C-scan method measures the planar damage size $2R_{damage}$ of the core reasonably well. The damaged core increases the impedance of the honeycomb core to the ultrasonic waves and thus can be detected. The through thickness distribution of the core damage may be characterized by the maximum crush depth of the core Δ_{crush}. This damage metric is of particular importance in analytical models for predicting residual strength of impact damaged sandwich panels. The damaged core within the crushed region will offer no support to the facesheet under subsequent in-plane loads, until the indentation depth increases by Δ_{crush}. The ratio of planar damage size ($2R_{damage}$) to the maximum crush depth (Δ_{crush}) will, in general,

depend on the impactor size, facesheet stiffness, and the transverse compressive behavior of the core. Additional destructive sectioning of impact damaged sandwich panels will be necessary to characterize the effects of facesheet stiffness and core properties on the core crush depths associated with planar damage size.

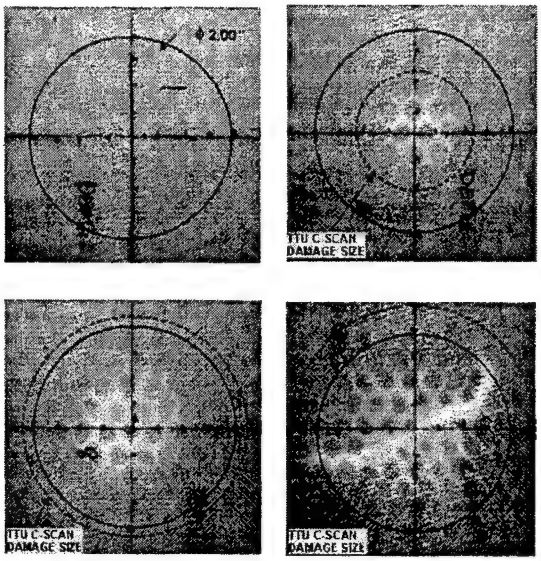

FIGURE 2. TYPICAL NETWORK OF DELAMINATIONS OBSERVED IN $[(90/45)_2/\text{CORE}]_s$ SANDWICH PANELS WITH FIBERGLASS FACESHEETS AND HONEYCOMB CORES, IMPACTED WITH 3″ DIAMETER IMPACTOR

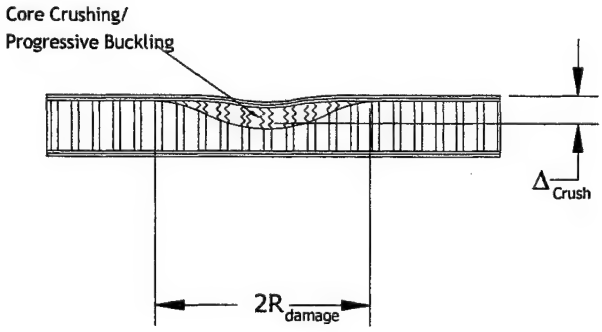

FIGURE 3. ILLUSTRATION OF CORE DAMAGE AND ASSOCIATED DAMAGE METRICS FOR HONEYCOMB CORE SANDWICH PANELS

2.3 RESIDUAL INDENTATION.

The material damage states in sandwich panels are confined to the facesheet and the core. However, due to the structural interaction between the damaged components of the sandwich panels, a geometric imperfection exists in impact-damaged sandwich panels. The geometric imperfection manifests as a residual indentation distribution as illustrated in figure 4. The residual indentation distribution is characterized by the maximum residual indentation Δ_{RMAX} occurring at the center of the indentation region (point of impact) and the planar size $2R_{ind}$ of the residual indentation. The residual indentation distribution is a result of the permanent

deformation of the core, due to the impact, as illustrated in figure 4. The Δ_{RMAX}, for a given planar damage size of the core $2R_{damage}$, will depend on the facesheet stiffness and the degraded tensile properties of the damaged core. The preceding argument is consistent with the experimental observations reported in reference 1, where the thicker skinned sandwich panels suffered smaller residual indentations in spite of large planar damage areas. Also, a core which fractures under the impact loads will provide no tensile resistance to the facesheet springback, further reducing the residual indentation and making it difficult to detect damage visually. The damage metrics associated with the sandwich components, quantification methods, and associated degraded properties are summarized in table 1.

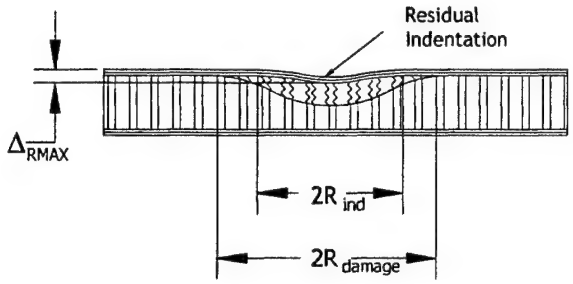

FIGURE 4. RESIDUAL INDENTATION IN IMPACTED SANDWICH PANELS

TABLE 1. SUMMARY OF DAMAGE METRICS AND ASSOCIATED DEGRADED PROPERTIES

Sandwich Component	Damage Metric(s)	Measurement Method	Degraded Properties	Comments
Facesheet	Planar facesheet damage size $2R_{skin}$	Visual, Destructive sectioning	Facesheet stiffness (flexural)	Region not necessarily circular
Core	Planar core damage size $2R_{damage}$	NDI	Transverse properties of core	Region not necessarily circular
	Maximum Core Crush depth Δ_{crush}	Destructive sectioning		
Facesheet	Maximum residual indentation Δ_{RMAX}	Coordinate measurement machine	N/A	Region not necessarily circular
	Planar size of residual indentation region $2R_{ind}$			
Interface	Residual traction field on facesheet due to damaged core	Analytical model	N/A	N/A

3. NONDESTRUCTIVE INSPECTION (NDI) AND QUANTIFICATION OF IMPACT DAMAGE USING FIELD INSPECTION TECHNIQUES.

Because the implementation of an effective damage tolerance program dictates continual monitoring of airframe structures in service, it would be desirable to use in situ NDI methods that can detect damage states critical to the performance of sandwich airframe structures. Some

of the in situ inspection techniques are the manual tap test (coin tap test), automated (instrumented) tap hammer, mechanical impedance analysis (MIA), etc. In this investigation, the effectiveness of different field inspection techniques (FITs) was assessed by comparing the damage size predicted by these techniques with that of the TTU C-scan. The damage size measured by TTU C-scan was found to correlate well with the underlying core damage [2]. The details of the TTU C-scan equipment, calibration standards, and damage quantification procedures can be found in reference 2. The damage delineation using FITs were conducted at the Sandia National Laboratories. The FITs used in the current study are manual impact tap hammer, the instrumented tap tester, and the mechanical impedance analysis. The details of these techniques are summarized in the following sections.

3.1 TAP TESTING.

Tap testing can be classified into mechanical tap testing and acoustical tap testing. Mechanical tap testing involves the analysis of the mechanical response of the structure subjected to a localized excitation. The acoustical tap test relies on the analysis of the characteristic resonant sound emanating from the location of the tap. The localized excitation in both cases is typically provided by a light impact using a spherical nosed impactor, with energy levels low enough to preclude any damage during the inspection itself. The tapping is done manually or by using a hand-held instrument where the impactor is driven by a solenoid mechanism.

In mechanical tap testing, the impact (tap) force is measured using an accelerometer that is mounted behind the impactor. The magnitude of the force and impact duration will depend on the constitutive properties of the sandwich components, impact energy, and impactor properties. The duration of impact (period) has been reported to be rather insensitive to the magnitude of the peak impact force for sandwich panels [5], which ensures repeatability. However, the impact duration will be significantly altered when the local stiffness of the sandwich structure is reduced due to the presence of damage. This change in impact duration is used to identify damage in sandwich structures. In the present investigation, the Mitsui Woodpecker Automated Tap Tester [6] (shown in figure 5) was used to identify the impact damage in sandwich panels.

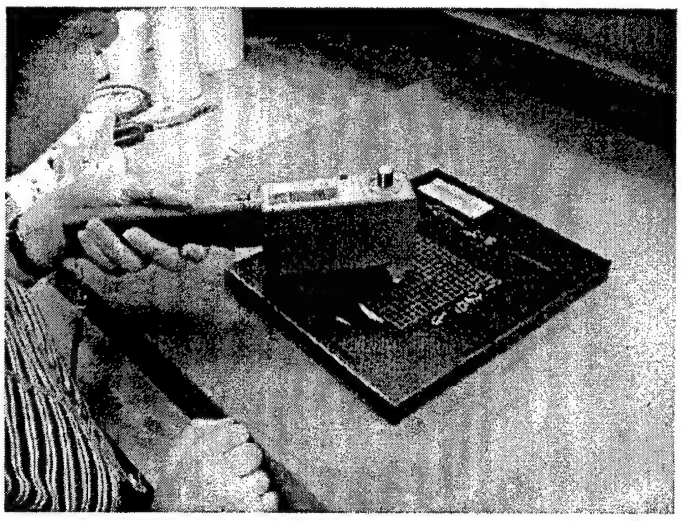

FIGURE 5. MITSUI WOODPECKER AUTOMATED TAP TESTER

In acoustical tap testing, the characteristic resonant sound emanating from the tap test is analyzed by the human ear. The audible resonant sound will depend on the sandwich local impedance and tap mass and hammer characteristics. The damaged region is characterized by a dull (dead) sound, which can be attributed to the decreased participation of the higher frequency modes. The manual tap test hammer (Airbus design) used in this investigation is shown in figure 6.

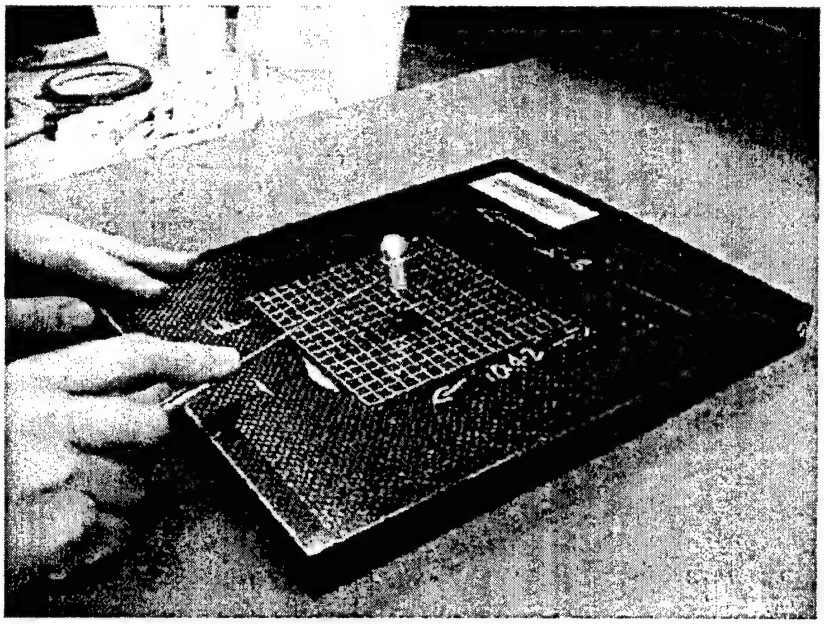

FIGURE 6. MANUAL IMPACT HAMMER (AIRBUS DESIGN)

3.2 MECHANICAL IMPEDANCE ANALYSIS.

In the MIA method [7], the stiffness of the structure in contact with a probe tip is measured. The mechanical impedance (stiffness) of the structure is a function of the constitutive properties of the sandwich components. The MIA method has been frequently used for identifying flaws in adhesive bonds. The presence of facesheet or core damage will reduce the mechanical impedance of the sandwich structure, and can result in a phase or amplitude change to the displayed signal, depending on the frequency of the probe. The probe consists of two piezoelectric crystals with the driver positioned behind the receiver within the same holder. The driver converts electrical energy into sonic vibrations and the receiver, in direct contact with the test surface, converts the modified vibrations into electrical signals for processing by the instrument. The V-95 Low-frequency bond tester used in the present study is illustrated in figure 7.

FIGURE 7. V-95 BOND TESTER USED FOR MECHANICAL IMPEDANCE ANALYSIS

3.3 EVALUATION OF FITs FOR IMPACT DAMAGE DETECTION.

The effectiveness of using FITs for detection and quantification of impact damage in honeycomb and foam core sandwich panels was investigated for different sandwich configurations. The honeycomb and foam core sandwich panels used in this program belong to the design of experiments (DOE) test matrix that was used to develop response surfaces for the impact resistance and damage tolerance of sandwich structures [8]. The material systems used for honeycomb and foam core sandwich panels are summarized in table 2.

TABLE 2. SANDWICH CONFIGURATIONS AND MATERIAL SYSTEMS

	Honeycomb Core Panels	Foam Core Panels
Facesheet Material Systems	Newport NB321/3K70P Plain Weave carbon prepreg	Newport NB321/7781 Satin Weave E-glass prepreg
Layup Schedules	$[(90/45)/CORE]_s$, $[(90/45)_2/CORE]_s$, $[(90/45)_3/CORE]_s$	
Core Types	Plascore Nomex Honeycomb PN2-3/16-3.0 PN2-3/16-4.5 PN2-3/16-6.0	Divinycell Foam cores HT-50 HT-70 HT-90
Nominal Core Densities (lb/ft^3)	3.0, 4.5 and 6.0	2.6, 4.2 and 5.5
Adhesive	Hysol 9628.060 PSF NW film adhesive	

The various sandwich configurations were impacted with impactor diameters of 1.00″, 2.00″, and 3″ with different impact energy levels. The honeycomb sandwich panels were then subjected to nondestructive inspection using TTU C-scan to obtain the planar damage diameter $(2R_{damage})_{C\text{-}scan}$. The maximum residual indentation depth was also measured for all the sandwich configurations. The impact damage in foam core sandwich panels, however, could not be quantified using TTU C-scan because of the practical limitations posed by the high-attenuation property of the foam cores. The V-95 mechanical impedance analysis was used to generate baseline damage size for foam core sandwich panels.

The FIT locations for impact-damaged sandwich panels are illustrated in figure 8. In each case, the center of the impact was identified by a cross-mark, around which the inspections were conducted. The inspection locations were along horizontal and vertical lines passing through the center of the impact and along lines at 45° to the horizontal and vertical lines. A network of grids spanning 4″ × 4″, (see figures 5 to 7) centered about the point of impact, was drawn on each specimen. The points along the boundary of the damaged region, as identified by the FIT equipment, were marked on a sheet of paper where a similar grid was drawn. The eight points along the boundary of damaged region were then joined by a smooth curve to identify the damaged region. The average diameter of the damaged region was then computed relative to the grid to obtain the damage size.

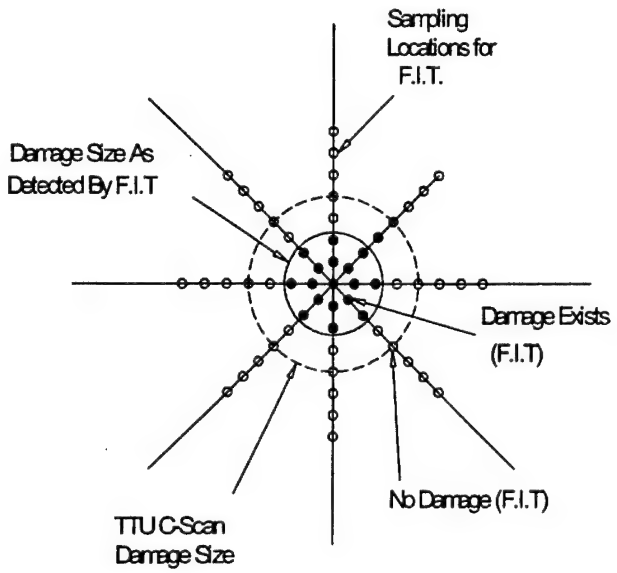

FIGURE 8. TYPICAL SAMPLING LOCATIONS FOR DAMAGE DELINEATION USING FITs

The impact energy levels, impactor diameter, and damage size obtained by different NDI methods are summarized in the following tables. The following nomenclature will be used to identify the facesheet material, layup schedule, and core type of different sandwich specimens.

The typical sandwich specimen is identified by the alphanumeric

XXF-S0X-CXTX-PX-0Y

where

XXF – Facesheet material system
CRF : Newport NB321/3K70P plain weave carbon prepreg
GLF : Newport NB321/7781 satin weave E-glass prepreg

S0X – Layup schedule
S04 : $[(90/45)\ /CORE]_s$
S05 : $[(90/45)_2/CORE]_s$
S06 : $[(90/45)_3/CORE]_s$

CX – Core type/density
C1 : Plascore PN2-3/16-3.0 (3.0 lb/ft^3) honeycomb core
C2 : Plascore PN2-3/16-4.5 (4.5 lb/ft^3) honeycomb core
C3 : Plascore PN2-3/16-6.0 (6.0 lb/ft^3) honeycomb core
C4 : Divinycell HT-50 (2.6 lb/ft^3) foam core
C5 : Divinycell HT-70 (4.2 lb/ft^3) foam core
C6 : Divinycell HT-90 (5.5 lb/ft^3) foam core

TX – Core thickness
T1 : 0.375″
T2 : 0.750″
T3 : 1.125″

PX – Panel number
0Y – Specimen number

The planar damage diameters obtained using the FITs were compared to the TTU C-scan data. The damage diameter obtained by TTU C-scan $[(2R_{damage})_{C\text{-}scan}]$ was used as the baseline for comparison for honeycomb core sandwich panels, while the damage diameter obtained by V-95 Bondcheck (MIA), $[(2R_{damage})_{V\text{-}95}]$, was used for foam core sandwich panels. In addition, the MAUS C-scan apparatus was used in the MIA mode for foam core sandwich panels. This system adds the scanning capability to the MIA mode and eliminates the need to inspect the panels at discrete locations. Further, the damage diameters obtained by the FITs were normalized by their respective baseline damage diameters. The data presented in tables 3 and 4 are summarized for honeycomb and foam core sandwich panels and the key observations are discussed in the following sections.

TABLE 3. SUMMARY OF IMPACT TESTS AND IMPACT DAMAGE SIZE OBTAINED BY DIFFERENT NONDESTRUCTIVE INSPECTION METHODS (Honeycomb core panels)

Specimen ID	Impactor Diameter (inches)	Impact Energy (lbf-in)	Planar Damage Diameter $2R_{damage}$ (inches)			
			TTU C-scan	V-95 (MIA)	Mitsui Woodpecker	Airbus Tap Hammer
CRF-S04-C1T2-P1-02	3	84.9	1.87	1.50	1.32	0.98
CRF-S04-C1T2-PX-X2	3	125.8	2.28	1.86	1.95	2.00
CRF-S04-C1T2-P1-03	3	149.1	2.59	1.88	2.00	1.00
CRF-S04-C1T2-P2-02	3	121.2	2.00	1.67	1.48	1.20
CRF-S04-C1T2-P2-03	2	148.5	1.36	1.73	1.58	1.97
CRF-S04-C2T1-P1-01	3	117.6	2.37	2.00	1.59	1.00
CRF-S04-C2T3-P1-01	3	117.6	1.63	1.79	1.50	1.00
CRF-S04-C3T2-P1-01	3	117.6	2.29	1.85	1.40	1.29
CRF-S05-C1T2-P1-02	3	121.2	2.13	1.45	1.34	0.93
CRF-S05-C1T2-P1-03	3	121.1	2.05	1.50	1.50	1.05
CRF-S05-C1T2-P1-04	3	121.6	2.06	1.64	1.50	0.69
CRF-S05-C1T2-PX-13	3	143.6	3.25	2.44	2.82	2.00
CRF-S05-C1T2-PX-10	3	146.4	3.26	2.53	2.20	1.48
CRF-S05-C1T2-PX-X6	3	87.1	2.41	1.98	1.93	1.50
CRF-S05-C1T2-PX-X9	3	87.4	2.31	1.73	1.35	1.48
CRF-S05-C1T2-P2-03	1	89.1	1.44	0.95	1.15	0.98
CRF-S05-C1T2-P2-04	3	84.6	1.81	1.40	1.32	0.59
CRF-S05-C1T2-P3-03	1	148.5	1.57	1.37	1.28	2.50
CRF-S05-C1T2-PX-15	3	152.6	3.26	2.92	1.96	2.00
CRF-S05-C1T2-PX-14	2	117.5	2.39	2.00	1.98	1.98
CRF-S05-C1T1-PX-X1	3	114.2	2.00	2.00	0.67	2.00
CRF-S05-C1T3-P1-01	3	117.6	2.08	1.65	1.68	1.10
CRF-S05-C2T2-P1-01	3	113.0	2.51	1.41	1.52	0.70
CRF-S05-C2T2-P1-02	3	117.6	2.64	1.58	1.41	0.78
CRF-S05-C2T2-P1-03	3	117.6	2.47	1.70	1.40	0.51
CRF-S05-C3T1-P1-01	3	117.6	2.76	1.61	1.62	0.78
CRF-S05-C3T3-P1-01	3	117.6	2.06	1.69	1.40	1.21
CRF-S06-C1T2-P1-02	3	88.3	1.72	1.10	0.92	0.77
CRF-S06-C1T2-P1-03	3	143.3	2.25	1.48	0.72	0.90
CRF-S06-C1T2-PX-X4	3	117.7	3.31	1.48	0.69	0.98
CRF-S06-C1T2-P1-05	2	90.2	1.75	1.22	0.60	0.75
CRF-S06-C1T2-PX-X1	2	148.6	3.13	2.02	1.50	1.48
CRF-S06-C1T2-PX-X2	1	118.8	2.25	1.60	0.42	1.00
CRF-S06-C1T2-PY-06	3	122.1	2.87	1.60	0.80	1.50
CRF-S06-C1T2-P1-04	3	118.8	2.09	2.00	1.26	1.00
CRF-S06-C2T1-P1-01	3	117.6	2.84	1.50	1.00	0.50
CRF-S06-C2T3-P1-01	3	113.0	1.74	1.45	1.45	0.92
CRF-S06-C3T2-P1-01	3	117.6	1.96	1.18	1.10	0.60

TABLE 4. SUMMARY OF IMPACT TESTS AND IMPACT DAMAGE SIZE OBTAINED BY DIFFERENT NONDESTRUCTIVE INSPECTION METHODS (Foam core panels)

Specimen ID	Impactor Diameter (inches)	Impact Energy (lbf-in)	Planar Damage Diameter $2R_{damage}$ [inches]			
			V-95 (MIA)	MAUS-C-Scan (MIA mode)	Mitsui Woodpecker	Airbus Tap Hammer
GLF-S04-C4T2-P1-03	3	87.3	1.53	1.62	1.20	1.10
GLF-S04-C4T2-P1-04	3	121.7	1.90	1.80	1.15	0.95
GLF-S04-C4T2-P2-01	3	126.7	1.73	2.00	1.26	1.20
GLF-S04-C4T2-P2-02	3	150.1	1.82	2.20	1.48	1.52
GLF-S04-C4T2-P2-03	2	88.4	1.52	1.60	0.97	1.02
GLF-S04-C4T2-P2-04	1	122.8	1.60	1.80	1.19	1.97
GLF-S04-C4T2-P3-01	3	117.1	2.00	2.00	1.54	1.95
GLF-S04-C4T2-P3-02	2	155.6	2.10	2.10	1.88	2.00
GLF-S04-C4T2-P3-03	3	117.1	2.07	2.10	1.60	1.97
GLF-S04-C5T1-P1-01	3	117.9	1.00	1.21	0.87	0.97
GLF-S04-C5T3-P1-01	3	119.7	1.21	1.40	1.07	1.04
GLF-S04-C6T2-P1-01	3	119.7	1.21	1.50	1.01	0.98
GLF-S05-C4T1-P1-01	3	117.1	1.22	1.25	0.48	1.00
GLF-S05-C4T2-P1-01	3	91.1	1.22	1.50	0.75	0.84
GLF-S05-C4T2-P1-02	3	90.5	1.00	1.70	0.48	1.00
GLF-S05-C4T2-P1-03	3	117.1	1.45	1.85	0.47	1.11
GLF-S05-C4T2-P1-04	3	117.1	1.27	1.85	0.50	0.97
GLF-S05-C4T2-P1-05	3	117.1	1.30	2.10	0.50	0.93
GLF-S05-C4T2-P2-01	3	155.7	1.90	2.40	0.98	1.23
GLF-S05-C4T2-P2-02	3	155.6	1.69	1.32	0.94	1.10
GLF-S05-C4T2-P2-03	1	86.4	1.54	1.51	0.50	1.95
GLF-S05-C4T2-P2-04	3	87.3	1.50	1.53	0.65	0.97
GLF-S05-C4T2-P2-05	2	119.8	1.75	1.62	0.77	1.00
GLF-S05-C4T2-P3-01	2	119.8	1.05	1.50	0.50	1.00
GLF-S05-C4T2-P3-02	2	119.8	1.02	1.50	0.59	1.00
GLF-S05-C4T2-P3-03	1	149.9	1.30	1.90	0.98	1.88
GLF-S05-C4T2-P3-04	3	155.7	1.30	1.70	0.57	1.00
GLF-S05-C4T3-P1-01	3	124.8	1.00	1.28	NONE	1.00
GLF-S05-C5T2-P1-01	3	117.1	1.00	1.80	0.48	1.00
GLF-S05-C5T2-P1-02	3	117.1	1.07	1.50	NONE	1.08
GLF-S05-C5T2-P1-03	3	117.1	0.98	1.90	0.48	1.00
GLF-S05-C6T1-P1-01	3	117.1	0.53	1.50	NONE	1.02
GLF-S05-C6T3-P1-01	3	117.1	0.82	1.38	NONE	1.00
GLF-S06 C4T2-P2-04	3	117.1	0.97	1.48	NONE	0.94
GLF-S06 C5T1-P1-01	3	117.1	0.10	1.50	NONE	NONE
GLF-S06-C4T2-P1-01	3	87.3	0.84	1.25	NONE	0.90
GLF-S06-C4T2-P1-02	3	124.7	0.58	1.42	NONE	0.55
GLF-S06-C4T2-P1-03	3	126.7	0.88	NONE	NONE	1.04
GLF-S06-C4T2-P1-04	3	155.7	1.00	2.00	0.51	1.00
GLF-S06-C4T2-P1-05	2	87.1	0.86	NONE	NONE	1.00
GLF-S06-C4T2-P2-01	1	122.8	0.93	1.72	0.49	1.02
GLF-S06-C4T2-P2-02	3	117.1	0.98	2.05	0.48	0.93
GLF-S06-C4T2-P2-03	2	144.7	1.12	1.85	0.98	1.02
GLF-S06-C5T3-P1-01	3	125.9	0.50	NONE	NONE	1.00
GLF-S06-C6T2-P1-01	3	117.1	0.50	1.20	NONE	NONE

Note: NONE indicates that the instrument could not sense any damage.

3.3.1 Honeycomb Core Sandwich Panels.

Since the honeycomb core sandwich panels used in this study belonged to the Design of Experiments test matrix [8], no control on the damage metric could be exercised. Thus, only a limited range of damage sizes was available for the appraisal of FITs. The planar damage diameters ranged between 1.36″ to 3.3″ for honeycomb core panels based on TTU C-scan measurements. Thus, the minimum damage size that could be detected by the different FITs used in the study could not be estimated.

The effect of baseline damage size on the detectability of FITs is illustrated in figures 9 through 11. The V-95 Bondcheck (MIA) proved to be the best method for all facesheet configurations and the range of planar damage sizes investigated. However, none of the FITs could match the damage size measured by the TTU C-scan, except in cases where appreciable facesheet damage (in the form of facesheet fracture) was present. In the presence of surface skin fractures, the FITs overestimated the damage size. The performances of FITs were dependent on the amount of degradation in the local transverse stiffness. The skin fractures influence the transverse stiffness of the neighboring locations producing a halo effect, which results in larger detected damage areas. The manual impact (tap) hammer was the least sensitive method, except in the case of $[(90/45)_3/CORE]_s$ sandwich panels, where it performed better than the Mitsui Woodpecker.

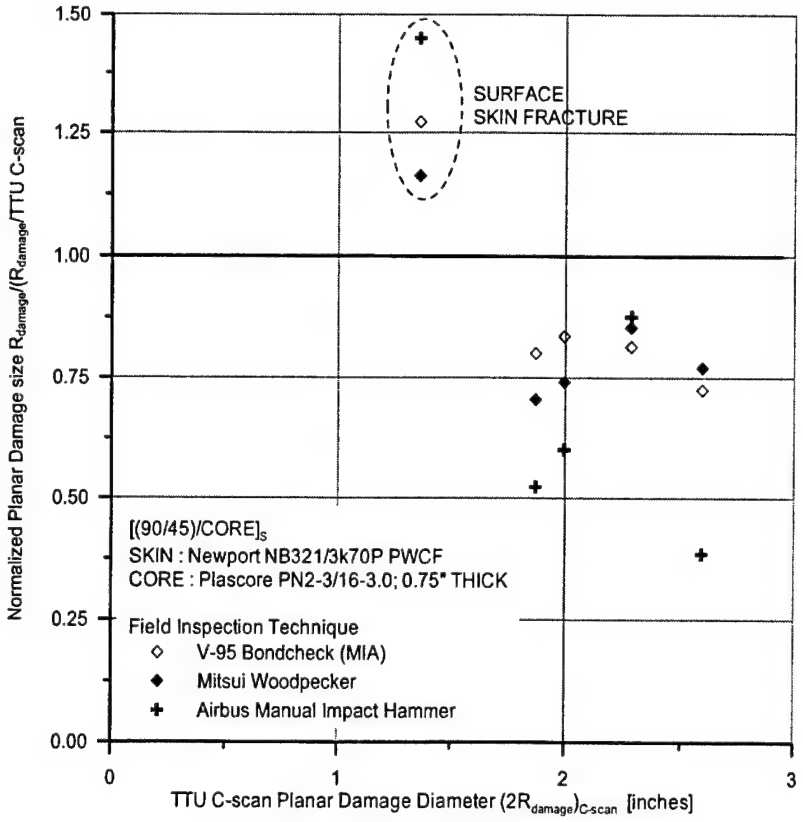

FIGURE 9. NORMALIZED DAMAGE SIZES FOR $[(90/45)/CORE]_s$ HONEYCOMB CORE SANDWICH PANELS USING DIFFERENT FITs

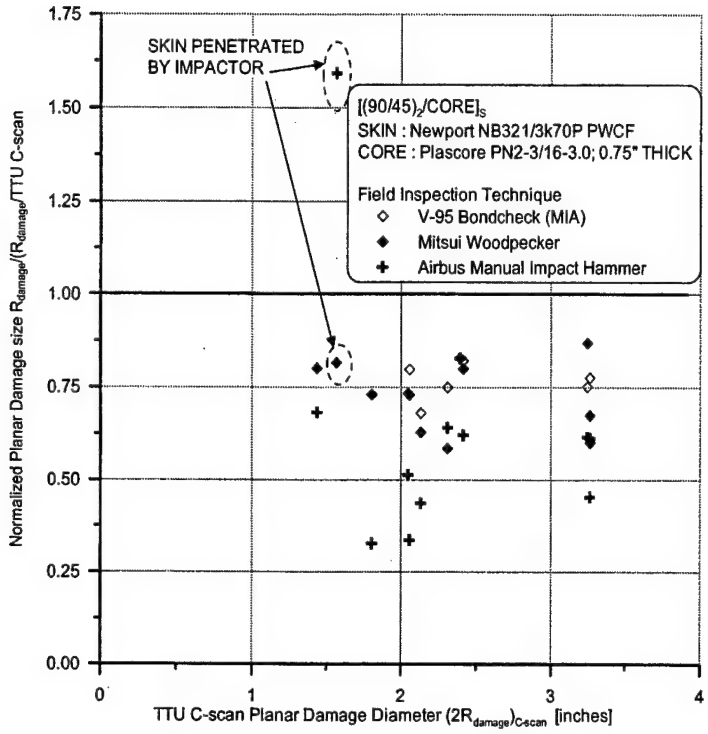

FIGURE 10. NORMALIZED DAMAGE SIZES FOR $[(90/45)_2/CORE]_S$ HONEYCOMB CORE SANDWICH PANELS USING DIFFERENT FITs

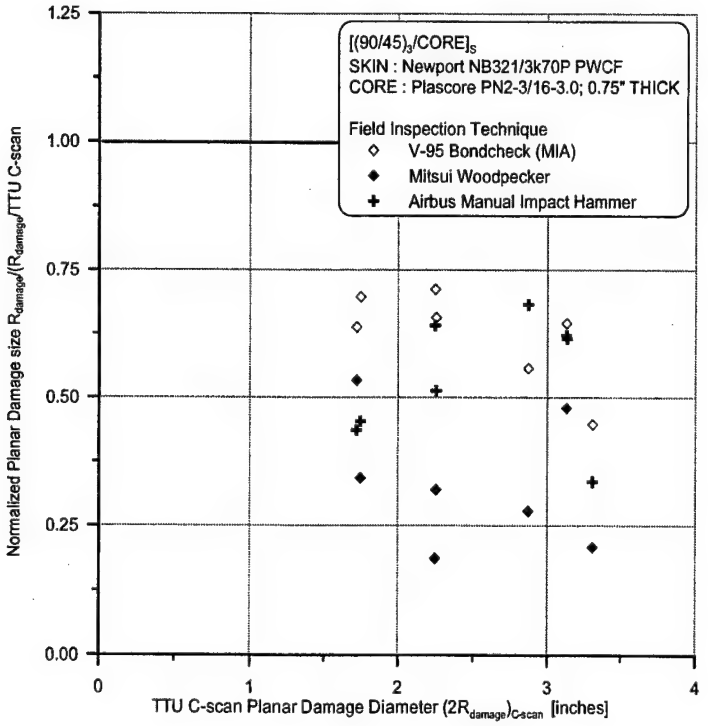

FIGURE 11. NORMALIZED DAMAGE SIZES FOR $[(90/45)_3/CORE]_S$ HONEYCOMB CORE SANDWICH PANELS USING DIFFERENT FITs

The effects of facesheet thickness on the detection capability of FITs were analyzed by comparing the average of all the normalized planar damage sizes for each facesheet type. The results are summarized and plotted as a function of the number of (90/45) ply groups in the facesheets in figure 12. The error bars shown in this figure correspond to one standard deviation about the respective mean value. From the figure, it can be observed that the FITs performed better with thinner facesheets. However, relatively higher scatter was observed for thinner facesheets. As the facesheets get thicker, the contribution of the core to the local stiffness (flexural) decreases, especially at the edge of the damage region. Thus, the facesheet tends to mask the core damage underneath, reducing the effectiveness of FITs, which rely on either the mechanical or the acoustical impedance of the sandwich panel. These trends are consistent with the observations of Georgeson, et al. [9] who used an electronic tap hammer for damage assessment.

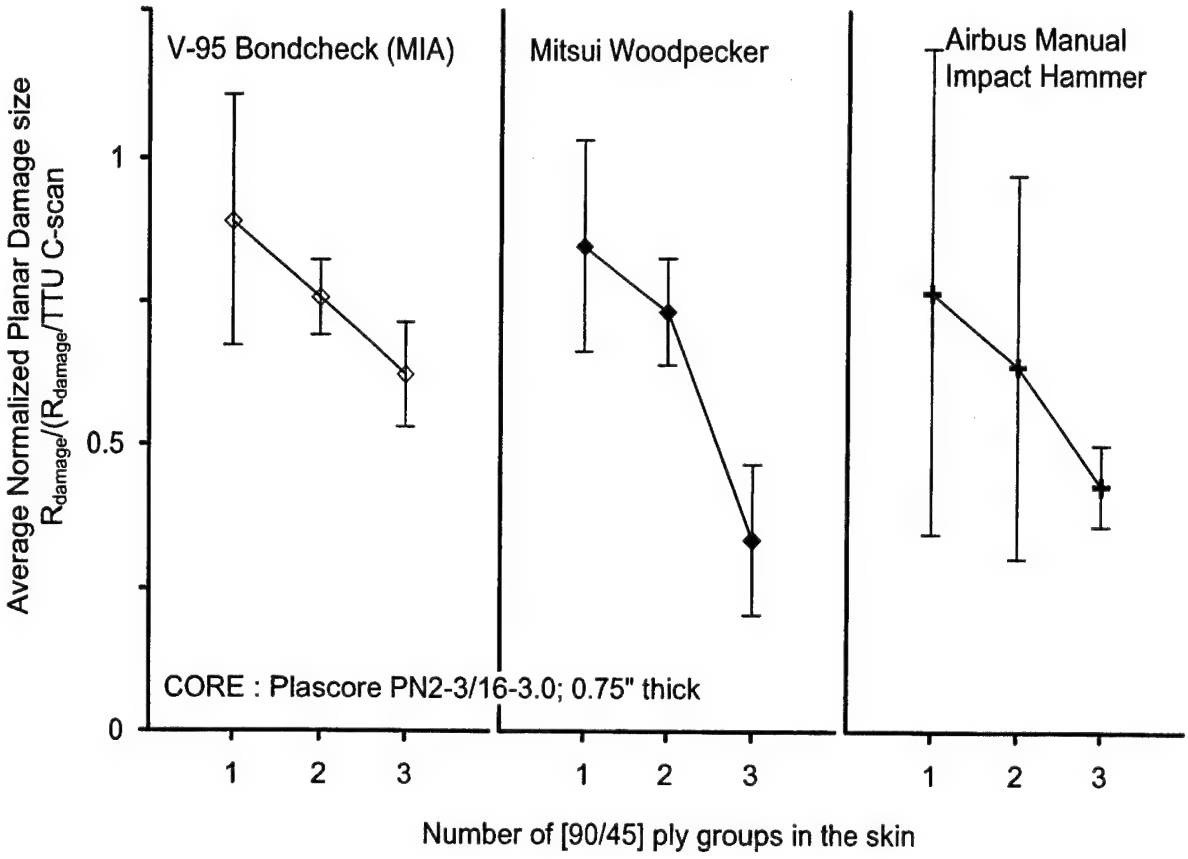

FIGURE 12. AVERAGE NORMALIZED DAMAGE SIZE FOR SANDWICH PANELS WITH DIFFERENT FACESHEET CONFIGURATIONS, WITH 0.75″ THICK, 3.0 lb/ft^3 CORES ONLY

3.3.2 Foam Core Sandwich Panels.

Similar to the honeycomb core sandwich panels, the foam core sandwich panels used in this study belonged to the Design of Experiments test matrix that were used to generate response surfaces. The sandwich panels were impacted with different combinations of impact energies and impactor diameters that are listed in table 4. Unlike honeycomb core sandwich panels, a

baseline damage size could not be obtained using TTU C-scan, because of the high acoustical impedance of the foam cores. Therefore, one of the FITs was used as the baseline damage detection method. In this study, the V-95 bondcheck (MIA) method was used as the baseline method since it was the only method able to detect damage in all the specimens used. In addition to the FITs described for honeycomb core sandwich panels, MAUS C-scan was also used to detect damage in foam core sandwich panels. This method was, however, used in the MIA mode rather than the through transmission (TT) mode and was used as verification for the V-95 bondcheck data.

The effects of baseline damage size on the detection capability of different FITs are compared in figures 13, 14, and 15 for different facesheets configurations. The damage size predicted by MAUS C-scan (MIA mode) almost always matched or exceeded the V-95 damage size. Unlike in the case of honeycomb core panels, the manual tap test performed better than the Mitsui Woodpecker instrumented tap hammer. This was more pronounced especially in the case of $[(90/45)_3/CORE]_s$ sandwich panels, where the Mitsui Woodpecker was unable to detect damage when the baseline damage size ($(2R_{damage})_{V\text{-}95}$) was less than 1.00″.

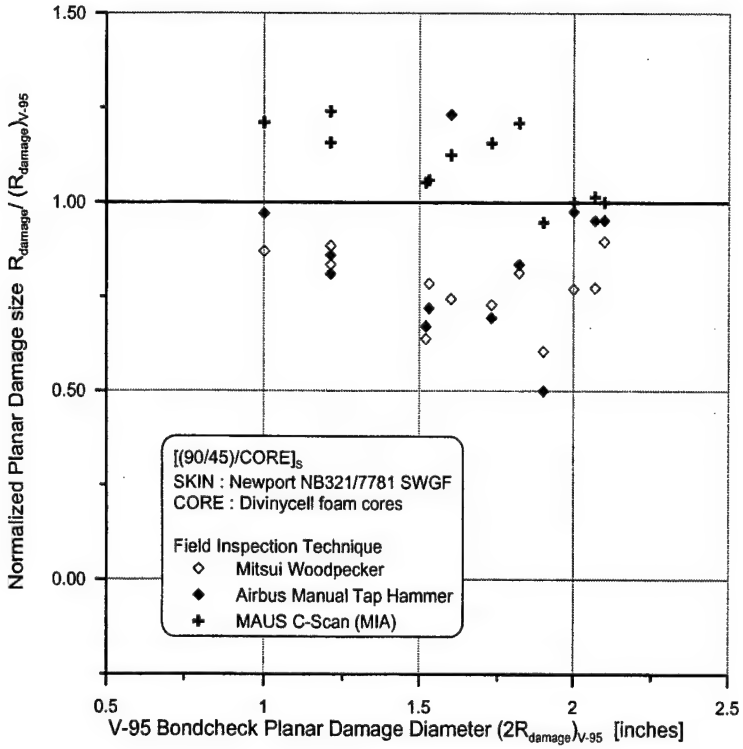

FIGURE 13. NORMALIZED DAMAGE SIZES FOR $[(90/45)/CORE]_s$ FOAM CORE SANDWICH PANELS USING DIFFERENT FITs

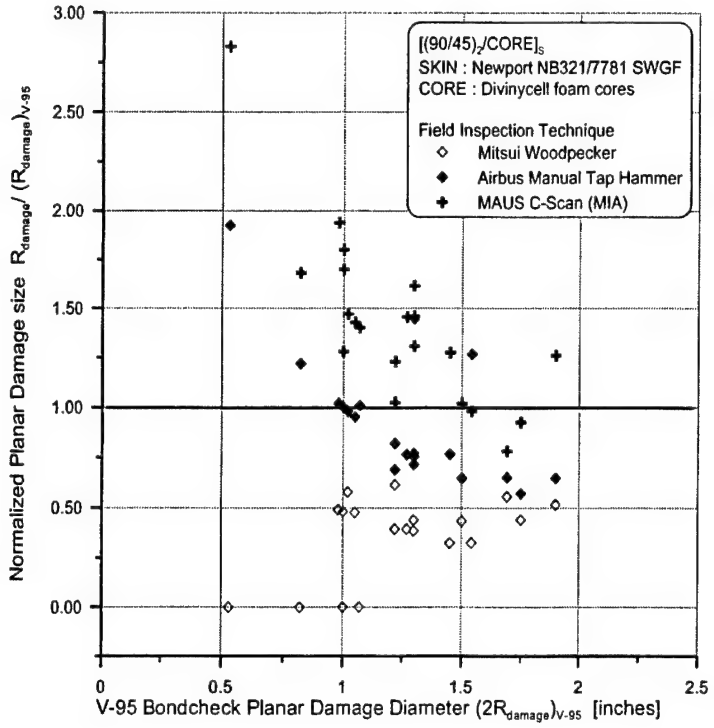

FIGURE 14. NORMALIZED DAMAGE SIZES FOR $[(90/45)_2/CORE]_s$ FOAM CORE SANDWICH PANELS USING DIFFERENT FITs

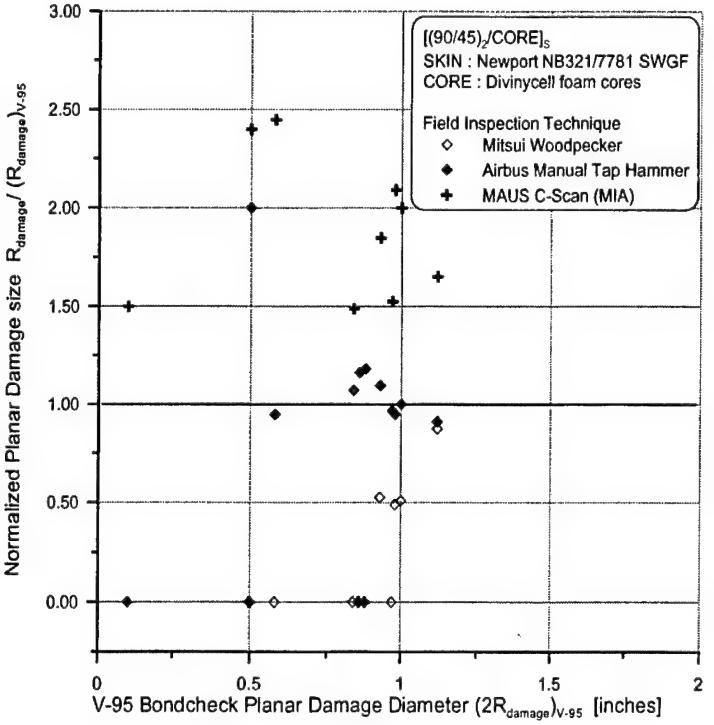

FIGURE 15. NORMALIZED DAMAGE SIZES FOR $[(90/45)_3/CORE]_s$ FOAM CORE SANDWICH PANELS USING DIFFERENT FITs

The effects of facesheet thickness on the detection capability of FITs were analyzed by comparing the average of all the normalized planar damage sizes for each facesheet type. The results are summarized and plotted as a function of the number of (90/45) ply groups in the facesheets in figure 16. The error bars shown in this figure correspond to one standard deviation about the respective mean value. Unlike in the case of honeycomb core sandwich panels, the Mitsui Woodpecker performs comparatively poorly with respect to the manual (acoustic) tap tests, especially as the facesheet gets thicker. This implies that the acoustic impedance of foam core sandwich panels is relatively more sensitive to impact damage.

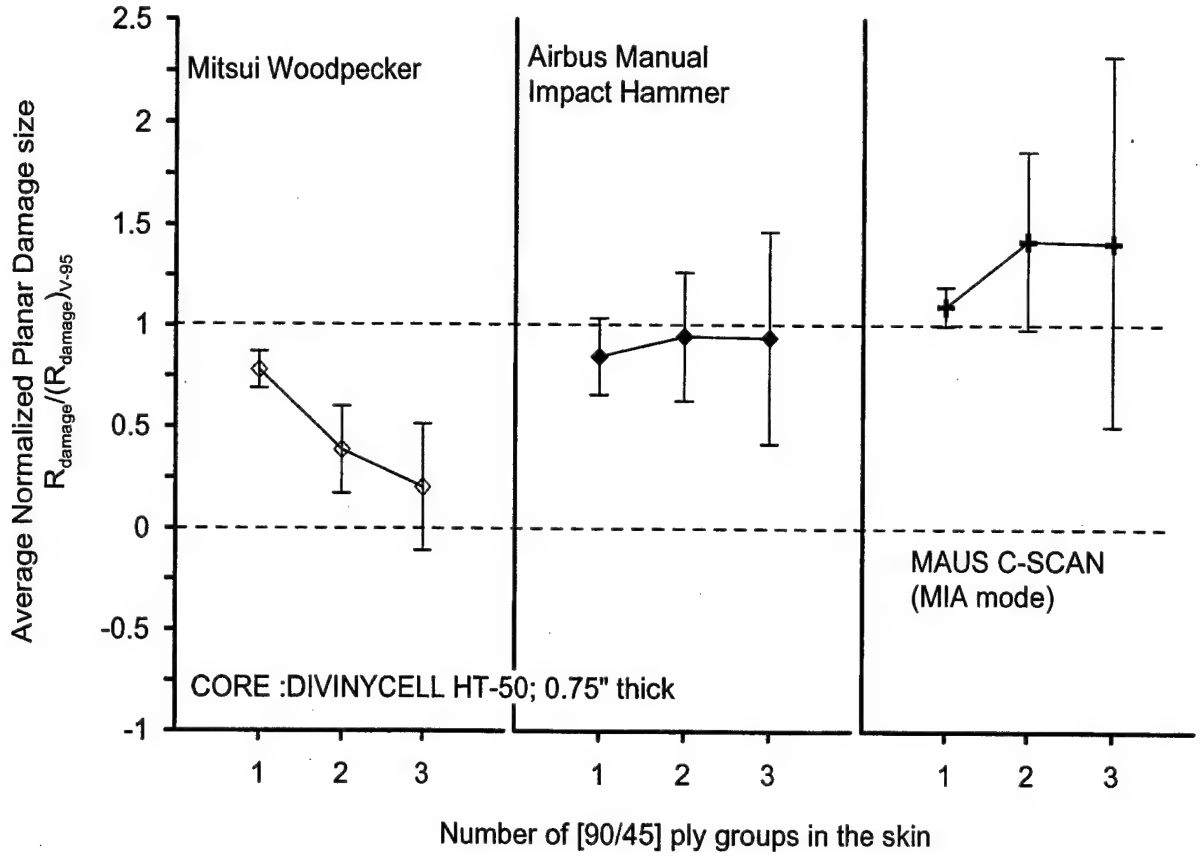

FIGURE 16. AVERAGE NORMALIZED DAMAGE SIZE FOR SANDWICH PANELS WITH DIFFERENT FACESHEET CONFIGURATIONS, WITH 0.75″ THICK, 2.6 lb/ft^3 CORES ONLY

In summary, based on the limited experimental results, it can be concluded that the detection of impact damage in honeycomb and foam core sandwich panels cannot be done with the same level of accuracy using a single FIT. The experimental data suggests that the impact damage in honeycomb core sandwich panels can be better detected by a technique that measures the local stiffness of the sandwich, while the damage in foam core panels can be better assessed with a technique relying on the measurement of acoustic impedance. The trends observed for foam core panels may be biased by the normalization procedure due to the inability to corroborate the damage size using destructive sectioning.

4. BEHAVIOR OF IMPACT DAMAGE UNDER IN-PLANE COMPRESSIVE LOADS.

The compression-after-impact tests were conducted to measure the severity of a given impact damage state in terms of the residual strength. However, the behavior of the various impact damage states, under in-plane compressive loads, leading to contrasting failure modes has received limited attention. In this section, the results of a limited experimental investigation on the behavior of impact damage in both honeycomb core and foam core sandwich panels are presented. The trends observed in impact damage behavior are in terms of the displacement and strain data corresponding to the center of the planar damage area.

4.1 EXPERIMENTAL SETUP.

The test fixturing and boundary conditions used in the current experiments are similar to that reported in reference 2. The specimen geometry along with the locations of the strain gages and the location for the measurement of out-of-plane displacement are illustrated in figure 17. An additional strain gage was mounted at the center of the damage region to monitor the surface strains in the skin. A spring-loaded linear variable differential transformer (LVDT) was used to measure the out-of-plane displacement at aforementioned location. In addition, a deflectometer was used to measure the end shortening of the specimen. The LVDT, the deflectometer, and the specimen in the test fixture are illustrated in figure 18.

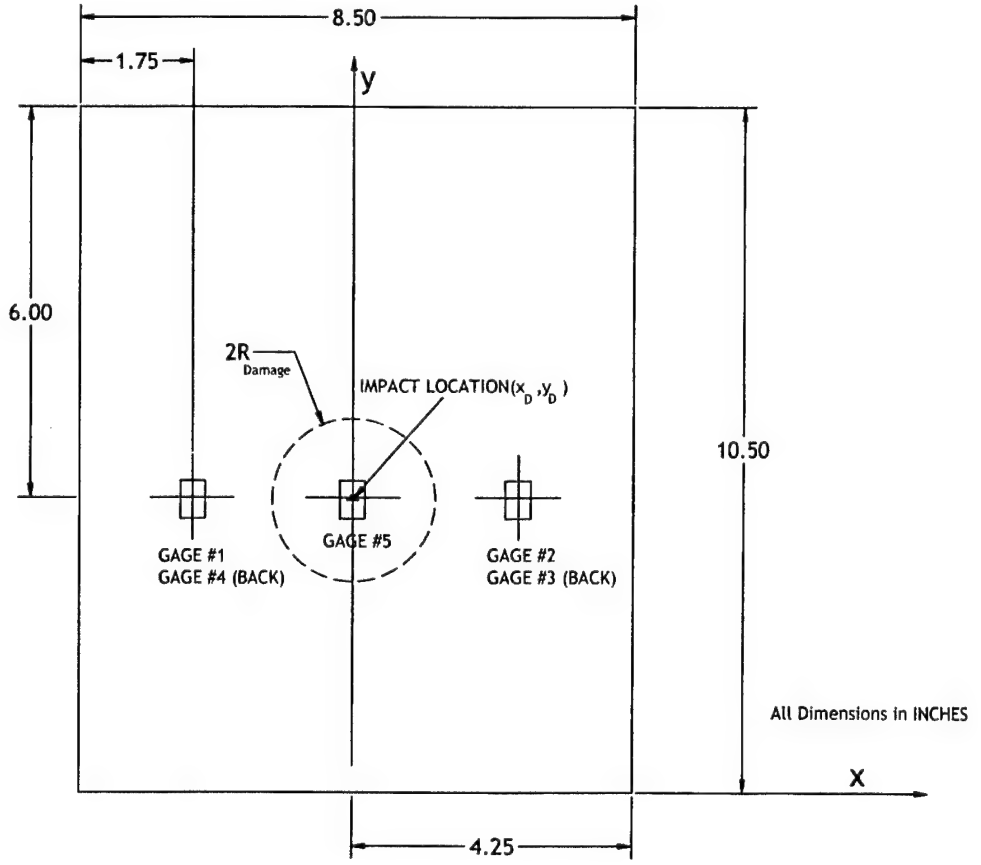

FIGURE 17. SPECIMEN GEOMETRY AND STRAIN GAGE LOCATIONS

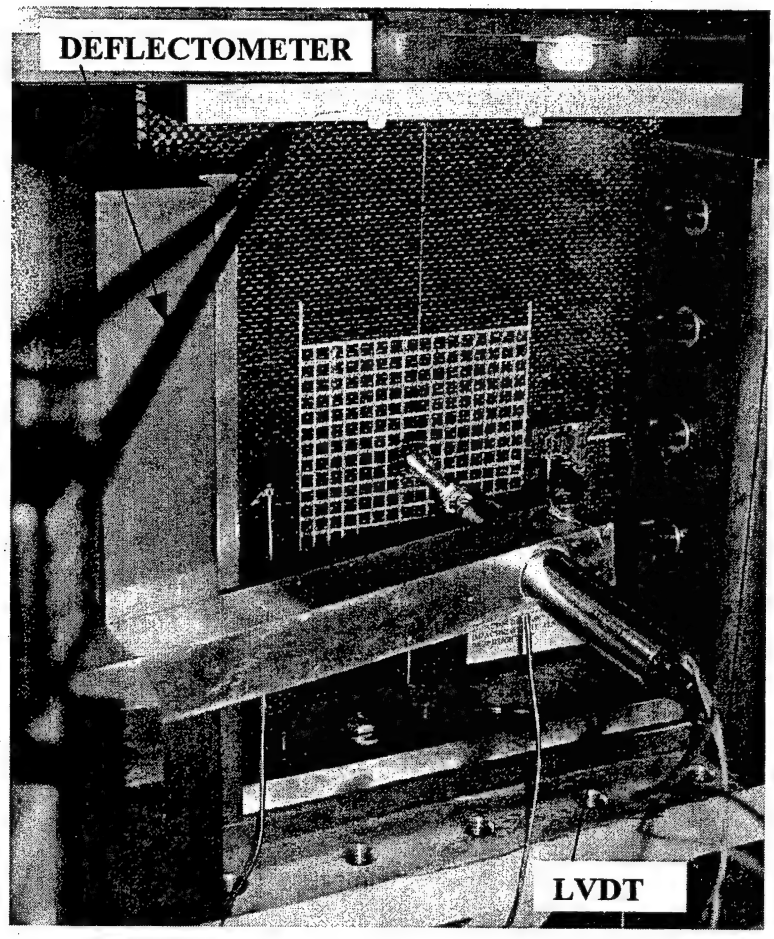

FIGURE 18. THE SANDWICH SPECIMEN IN THE TEST FIXTURE, THE LVDT, AND THE DEFLECTOMETER

The $[(90/45)/CORE]_s$ and $[(90/45)_2/CORE]_s$ sandwich panels with honeycomb and foam cores were impacted and tested under compressive loads using the previously discussed instrumentation. The test data obtained for each specimen along with the associated damage metrics, proposed damage growth mechanisms, and final failure modes are summarized and presented in the following sections.

4.2 CAI TESTING OF $[(90/45)/CORE]_s$ SPECIMEN WITH HONEYCOMB CORE.

The $[(90/45)/CORE]_s$ sandwich panel with NB321/3K70P PWCF facesheets was impacted with a 3″ diameter impactor at an energy level of 125 lbf-in. The planar damage area associated with the impact damage was D_A=4.02 in^2 ($2R_{damage}$=2.28 in). The maximum residual indentation depth associated with the damage was measured to be Δ_{RMAX}=0.017 in. The sandwich specimen was then statically tested to failure under in-plane compressive loads. The test data for this specimen is plotted in figure 19.

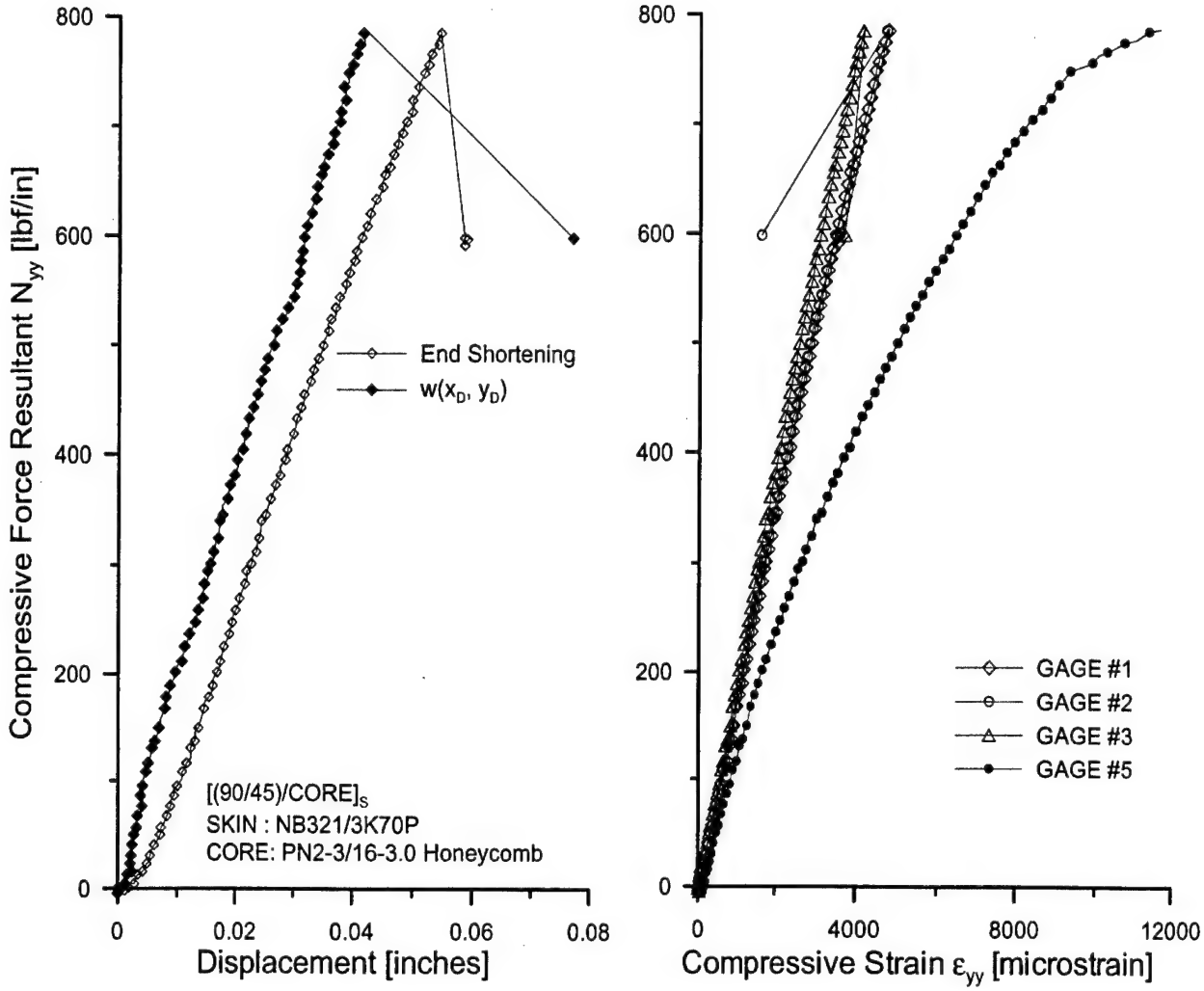

FIGURE 19. CAI TEST DATA FOR $[(90/45)/CORE]_s$ SANDWICH PANEL WITH NB321/3K70P PWCF FACESHEETS

The end-shortening displacement and the out-of-plane displacement at center of damage varied linearly with the applied load. The strain gage at the center of the damage, however, was nonlinear and more compliant compared to the far-field strain gages. This can be attributed to the additional bending component of strain associated with the skin in the damage/dimple region. The linearity of the out-of-plane displacement at the center of damage implies that there was no increase (growth) in damage area. However, the skin within the damage region was subjected to high bending strains leading to a strain-related failure. The damage growth mechanism resulting in final failure process is illustrated in figure 20. The in-plane compressive loads bend the skin within the damage zone due to the lack of support from the damaged core. This bending increases until the strains in the skin exceeds a critical strain value initiating skin fractures at the edge of the damage region. These compressive cracks propagate out laterally, towards the edges of the specimen leading to complete fracture.

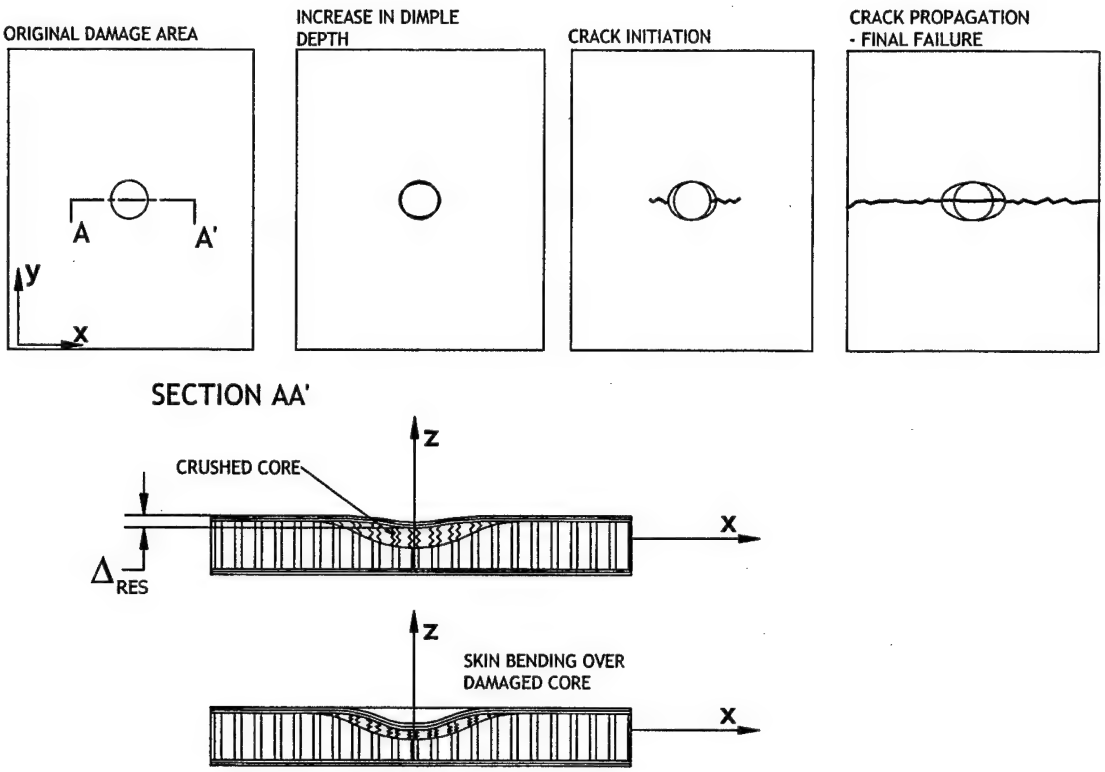

FIGURE 20. DAMAGE GROWTH MECHANISM AND FINAL FAILURE MODE OBSERVED IN $[(90/45)/CORE]_s$ SANDWICH PANEL WITH HONEYCOMB CORE

4.3 CAI TESTING OF $[(90/45)_2/CORE]_s$ SPECIMEN WITH HONEYCOMB CORE.

The $[(90/45)_2/CORE]_s$ sandwich panel with NB321/3K70P PWCF facesheets was impacted with a 3″ diameter impactor at an energy level of 87.4 lbf-in. The planar damage area associated with the impact damage was D_A=4.19 in^2 ($2R_{damage}$=2.31 in). The maximum residual indentation depth associated with the damage was measured to be Δ_{RMAX}=0.007 in. The sandwich specimen was then statically tested to failure under in-plane compressive loads. The test data for this specimen is plotted in figure 21.

The out-of-plane displacement and the strain measured at the center of damage region in the $[(90/45)_2/CORE]_s$ sandwich panels exhibited a characteristic response as shown in figure 21. A characteristic knee was observed for both the curves indicating a sudden change in compliance. The out-of-plane displacement response exhibited a nonlinear behavior past the knee point (A′ in the figure) with a slight stiffening tendency. The strain at the center of the damage region exhibits three distinct regions OA, AB, and BC. An abrupt increase in compliance occurs at point A beyond which the strain increases rapidly until point B is reached, where an appreciable increase in stiffness can be observed. The strain increases until point C, which corresponds to final failure, is reached. The observed behavior is explained using the illustrations in figure 22. The initial increase in strain and out-of-plane displacement (region OA and OA′ respectively) can be attributed to the bending of the skin over the impact pre-existing damaged core. The facesheet bends over the damaged core until the core consolidates and is able to transmit load

across the thickness. When point A (or A′) is reached, there is sufficient strain energy, and the moments generated in the skin are high enough to further crush the core in the thickness direction and initiate damage in the adjoining core, thereby increasing the damage area. This induces a reduction in stiffness associated with the local bending of the facesheet and is represented by the region AB in figure 21. The growth of the dimple in the lateral directions is arrested at point B due to the lack of sufficient energy to initiate additional core damage. The bending of the skin continues until point C is reached when there is enough energy in the skin to propagate the dimple in an unstable manner across the width of the panel, leading to final failure.

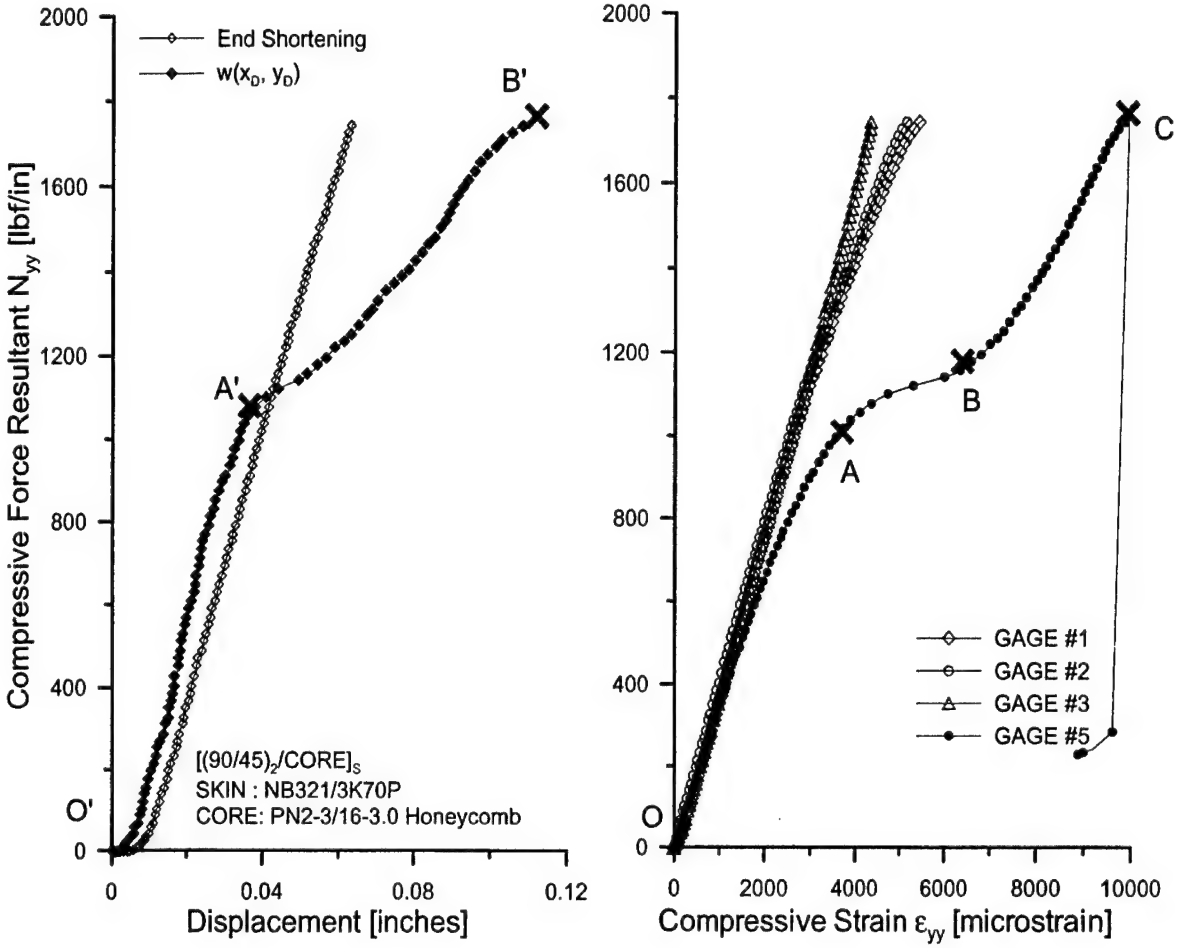

FIGURE 21. CAI TEST DATA FOR $[(90/45)_2/CORE]_s$ SANDWICH PANEL WITH NB321/3K70P PWCF FACESHEETS

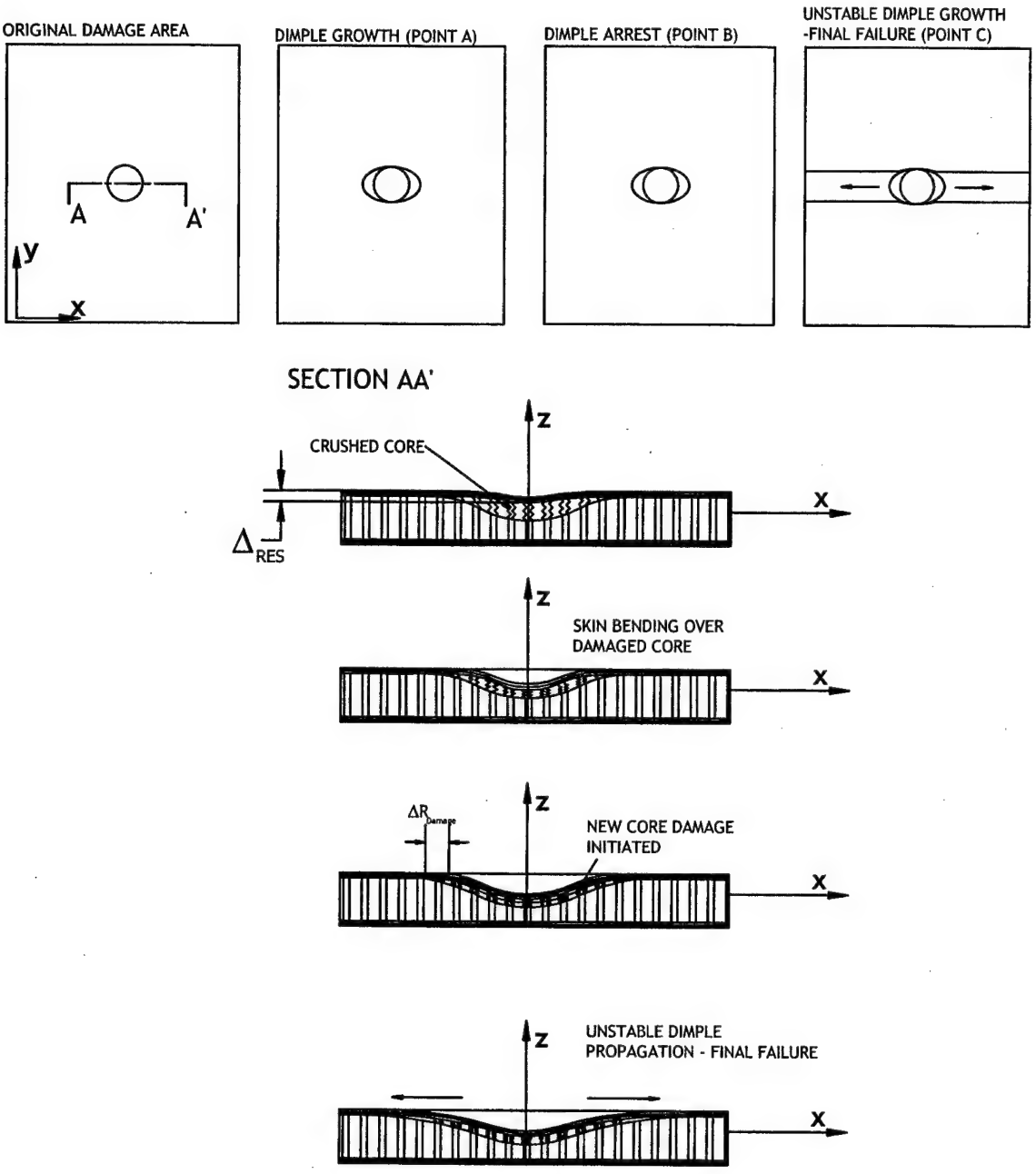

FIGURE 22. DAMAGE GROWTH MECHANISM AND FINAL FAILURE MODE OBSERVED IN $[(90/45)_2/CORE]_s$ SANDWICH PANEL WITH HONEYCOMB CORE

4.4 CAI TESTING OF $[(90/45)_2/CORE]_s$ SPECIMEN WITH FOAM CORE.

The $[(90/45)_2/CORE]_s$ sandwich panel with NB321/7781 SWGF facesheets was impacted with a 3″ diameter impactor at an energy level of 360 lbf-in. The maximum residual indentation depth associated with the damage was measured to be Δ_{RMAX}=0.04 in. The sandwich specimen was then statically tested to failure under in-plane compressive loads. The test data is plotted in figure 23.

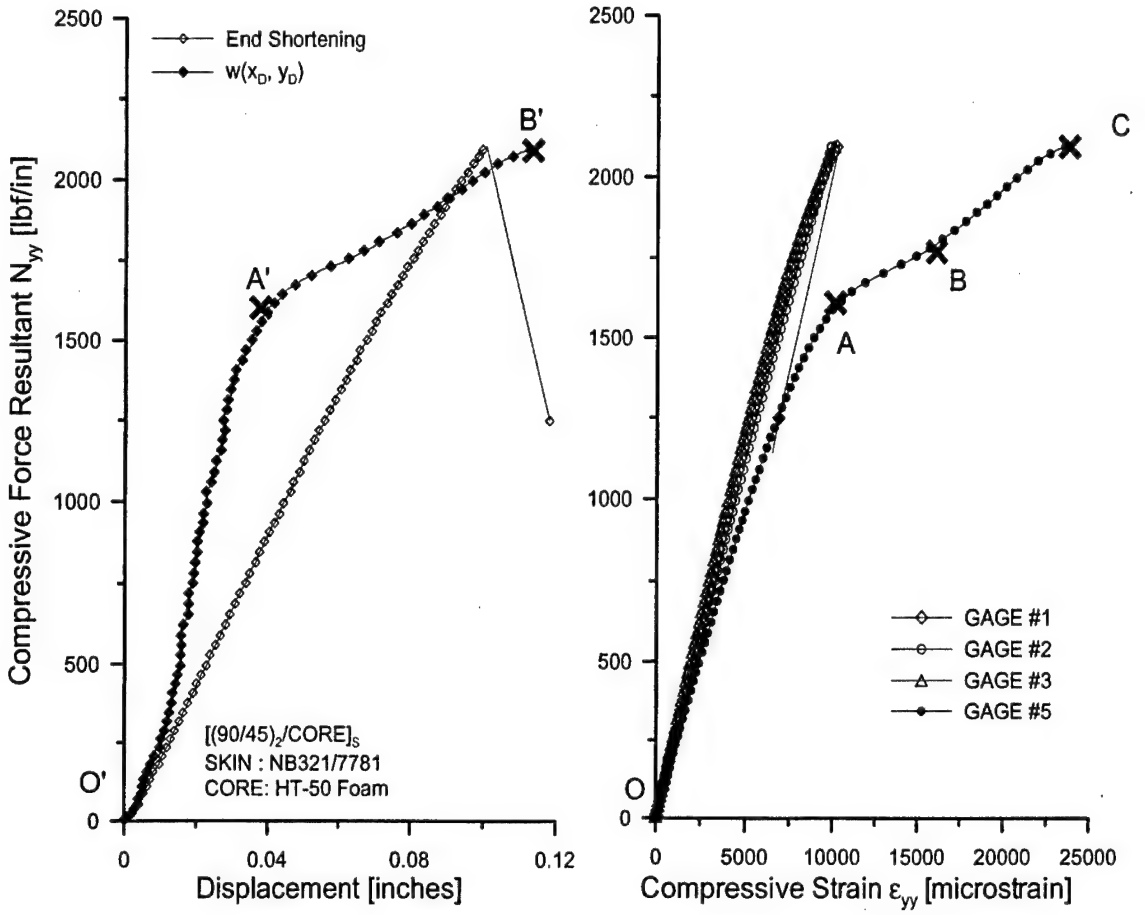

FIGURE 23. CAI TEST DATA FOR $[(90/45)_2/CORE]_s$ SANDWICH PANEL WITH NB321/7781 SWGF FACESHEETS

The impact damage in foam core sandwich panel exhibited behavior similar to the honeycomb core panel described in the previous section. However, upon the initiation of further core crushing, there was no evidence of dimple arrest mechanism, as seen from the strain data. This is due to the different transverse compressive behavior of the foam core when compared with the honeycomb cores [4 and 10]. Under transverse compression, the foam core behaves in an elastic-plastic manner, while the honeycomb cores can sustain transverse compressive loads several times that of their yield or crush load [4 and 5] before yielding or crushing is initiated.

The impact damage in sandwich panels, due to blunt impactors, behaves in a characteristic manner leading to contrasting final failure modes under in-plane compressive loads. The impact damage, which manifests in the form of a dimple, will be active well before the final failure occurs. The amount of this activity will be dependent on the flexural properties of the facesheet, transverse compressive properties of the core, and the damage metrics. A thin facesheet with negligible flexural stiffness will promote a strain-based failure mechanism, due to the inability of the skin to drive the dimple against the core. However, given enough flexural stiffness, the facesheet could drive the dimple through a characteristic sequence of events leading to a stability-based failure mechanism.

5. EFFECTS OF CURVATURE ON THE DAMAGE RESISTANCE OF CYLINDRICAL SANDWICH PANELS.

The damage resistance and tolerance investigations for sandwich panels have been mostly limited to flat panels. However, real airframe structures are not necessarily flat and certain curvatures are associated with their geometry as dictated by the aerodynamic design. It would, thus, be important to understand the effects of panel curvature on the impact response and associated impact damage metrics in sandwich panels. In this study, a limited experimental investigation was conducted to observe the effects of curvature on the damage resistance of cylindrical sandwich panels. The specimen geometry, specimen fabrication, test fixturing, and summary of test results are reported in the following sections.

5.1 SPECIMEN GEOMETRY AND BOUNDARY CONDITIONS.

The typical cylindrical sandwich geometry used in this study is illustrated in figure 24. The sandwich panel geometry is characterized by the internal radius of curvature R_{INT}, the chord length L_{CHORD}, sandwich thickness T_{sw}, and the cylindrical generator length (panel height) H. The chord length was limited to 8.5″ and the height of the panel was limited to 10.50″ for all the sandwich configurations used.

Three internal radii of curvature of R_{INT1}=6.00″, R_{INT2}=24.00″, and R_{INT3}=48.00″ were used for the specimens in the present study. The above radii are representative of different locations on a general aviation airframe. The internal radius was controlled as it formed the tool-side of the sandwich specimen during the fabrication process. Thus, the external radius (R_{INT} + T_{sw}) was not constant across different sandwich configuration.

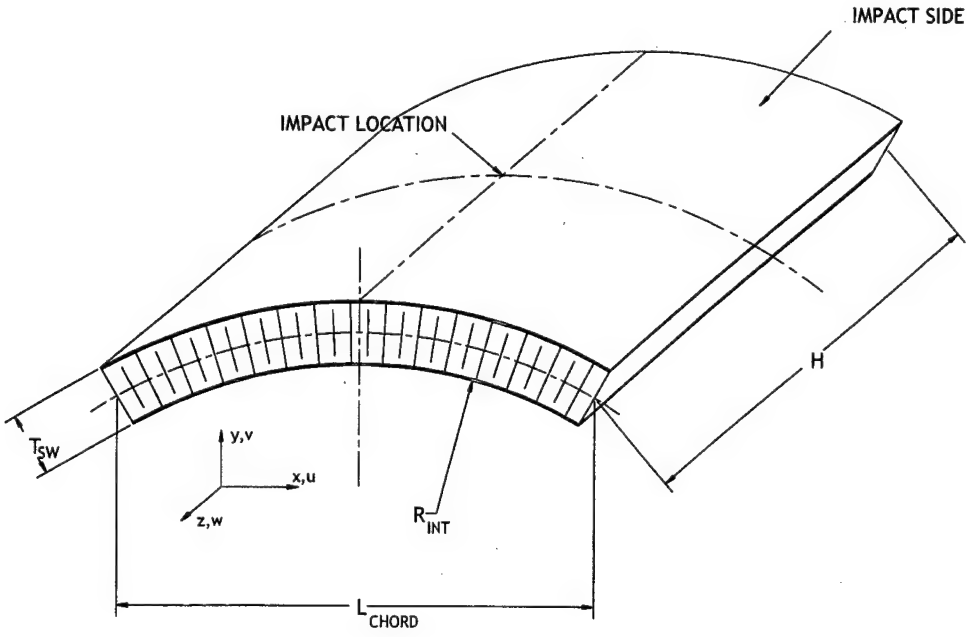

FIGURE 24. GEOMETRY OF CYLINDRICAL SANDWICH PANELS AND ASSOCIATED NOMENCLATURE

The cylindrical sandwich specimens were impacted on the convex side at their respective geometric centers. The specimens were supported along their longitudinal edges using three different boundary supports with varying degrees of end fixity. The boundary conditions investigated in this study are illustrated in figure 25.

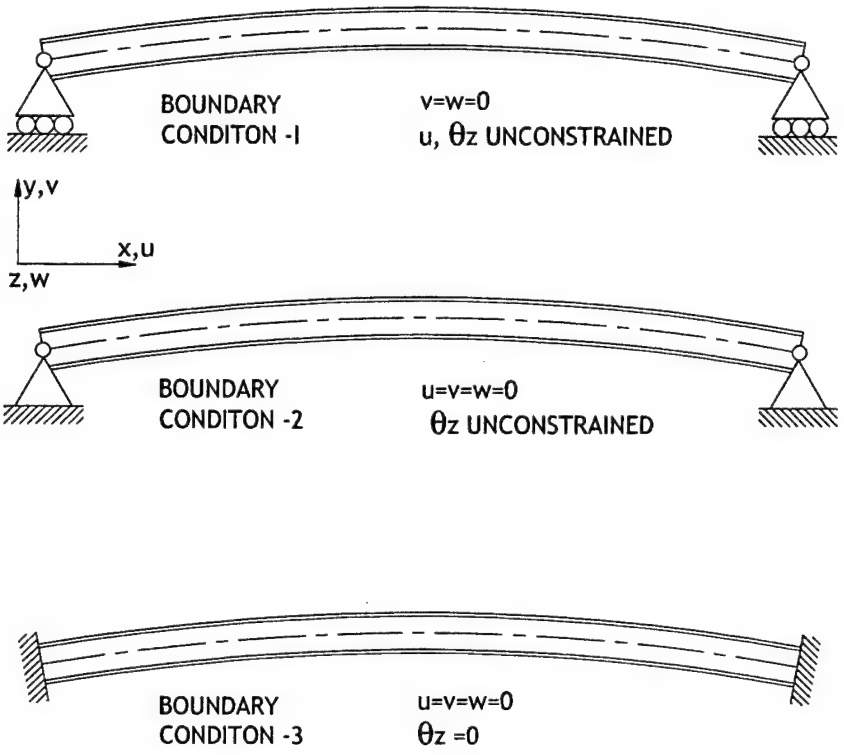

FIGURE 25. BOUNDARY SUPPORT CONDITIONS USED DURING IMPACT TESTING OF CYLINDRICAL SANDWICH PANELS

The three boundary conditions were used to simulate the adjoining structure in an actual airframe. The sandwich specimens are free to translate and rotate at the boundaries under boundary condition-1. Boundary condition-2 allows free rotation at the ends but constrains the translations while boundary condition-3 simulates a rigid adjoining structure. The three boundary conditions will generate different levels of flexural stiffnesses in the curved panels. The edges along the width are, however, unconstrained in all the three cases. Boundary condition-1 will be used for all sandwich configurations, while boundary conditions-2 and -3 will be used in a limited number of tests to observe the boundary constraint effects.

5.2 MATERIAL SYSTEMS AND SPECIMEN FABRICATION.

The facesheets of the curved sandwich panels were made of NB321/3K70P plain weave carbon prepreg. The core material used was Plascore PN2-3/16-x.x with a thickness of 0.375″. The core density used for majority of the sandwich panels was 3.0 lb/ft^3, while a limited number of specimens were made with core densities of 4.5 and 6.0 lb/ft^3. The facesheets were bonded to the core using Hysol 9628.060 PSF NW film adhesive, in a cocure, cobond process. The sandwich layup configurations investigated were $[(90/45)/CORE]_s$ and $[(90/45)_2/CORE]_s$.

The curved sandwich panels were fabricated on curved molds. The molds were assembled by bending aluminum sheet metal (0.032″ thick) over mold profile templates placed at intervals of 12″. The profile templates were secured by fastening them to two runner beams, as shown in the figure 26. The sheet metal was then fastened to the profile templates at the ends, as shown in the figure. The sheet metal extended by 2″ on either side of the profile template to accommodate sealant tape used for bagging purposes.

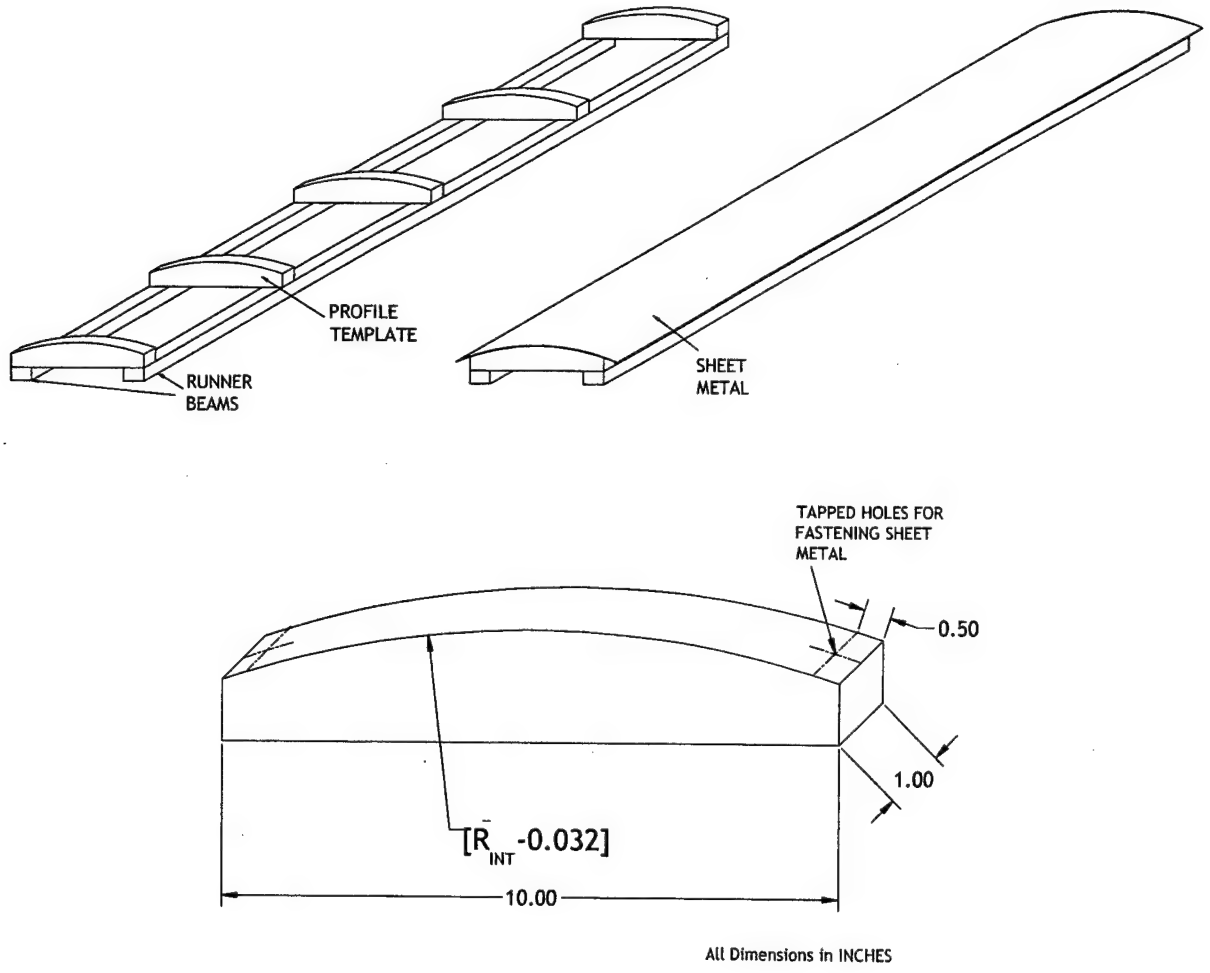

FIGURE 26. TOOLING FOR FABRICATING CYLINDRICAL SANDWICH PANELS AND DIMENSIONS OF A TYPICAL PROFILE TEMPLATE

5.3 TEST MATRIX.

The primary objective of the study was to investigate the effects of panel curvature on the impact response and the damage resistance of sandwich panels. The effects of boundary constraint were investigated for sandwich configurations of $[(90/45)/CORE]_s$ and $[(90/45)_2/CORE]_s$ with 3.0 lb/ft^3 core. The three boundary conditions described in the previous sections were used. The transverse compressive properties of the core have been shown to dominate the impact response of sandwich structures [1, 2, and 4]. To estimate the effects of the core stiffness, $[(90/45)_2/CORE]_s$ sandwich panels with core densities of 4.5 and 6.0 lb/ft^3 were also used. The

various combinations of sandwich configurations, impactor diameter, and boundary conditions investigated are summarized in table 5. The sandwich specimens corresponding to each of the marked combinations were impacted at five different energy levels. However, when the skin penetration was observed at any intermediate energy level, further testing was discontinued.

TABLE 5. TEST MATRIX FOR STUDYING CURVATURE EFFECTS

Sandwich Configuration	Boundary Condition	1			2			3		
	Impactor Diameter $2R_{IMP}$ (inches)	Nominal Radius R_{INT} (inches)			Nominal Radius R_{INT}			Nominal Radius R_{INT}		
		6	24	48	6	24	48	6	24	48
$[(90/45)/CORE]_s$ Plascore PN2-3/16-3.0	1.00	×	×	×		×			×	
	3	×	×	×		×			×	
$[(90/45)_2/CORE]_s$ Plascore PN2-3/16-3.0	1.00	×	×	×						
	3	×	×	×		×			×	
$[(90/45)_2/CORE]_s$ Plascore PN2-3/16-4.5	1.00		×							
	3		×							
$[(90/45)_2/CORE]_s$ Plascore PN2-3/16-6.0	1.00		×							
	3		×							

5.4 TEST FIXTURE.

A test fixture to hold the specimen and simulate the three different boundary conditions described in the previous sections was designed and fabricated. The schematic of the test fixture is shown in figure 27. The fixture mounts on a multipurpose base plate described in reference 2, as shown in figure 28, with multiple through-holes. The holes are used to fasten the slide mechanism, which is used to simulate the translating supports. The slide mechanism consists of precision shafts mounted on support rails. The support rails are then fastened to the base plate, as shown in figure 27. The specimen is clamped between two clamping edges. The lower clamping edge is mounted on a hinge, which is fastened to a translating beam. The beams are mounted on bearing blocks, which ride the shafts.

Boundary condition-1 is simulated by clamping the specimen between the clamping edges. Since the hinges are free to rotate and the translating bar is free to slide, the specimen is free to rotate and translate at its boundaries. Boundary condition-2 is simulated by securing the two translating blocks by passing an all-thread shaft through the holes provided in the blocks. The two blocks were then locked together using lock nuts on either side, constraining relative translation motion. Finally, for boundary condition-3, in addition to locking the translation of the blocks, the rotation of the hinges is constrained by locking the bottom clamp edge against the translating block. The translating block and the bottom clamp edge contain tapped holes that are aligned with each other. Bolts fastened into these holes can be used to prevent the rotation of the

hinges under load. It should be noted that the above constraints are not strictly rigid in nature but have some stiffness associated with them.

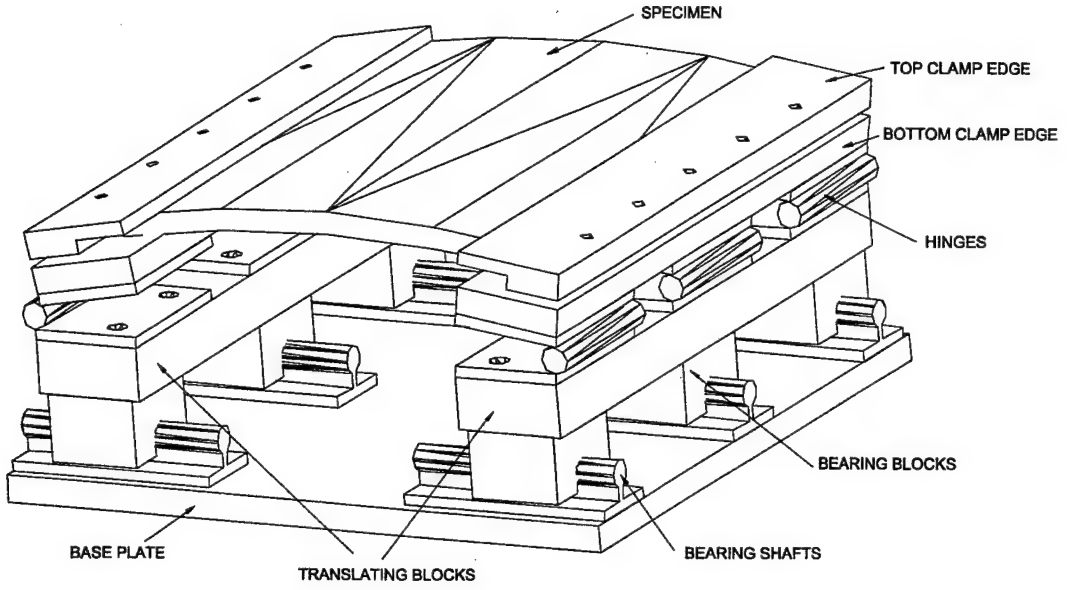

FIGURE 27. ILLUSTRATION OF THE TEST FIXTURE FOR CURVED PANELS
(Boundary condition-1 shown)

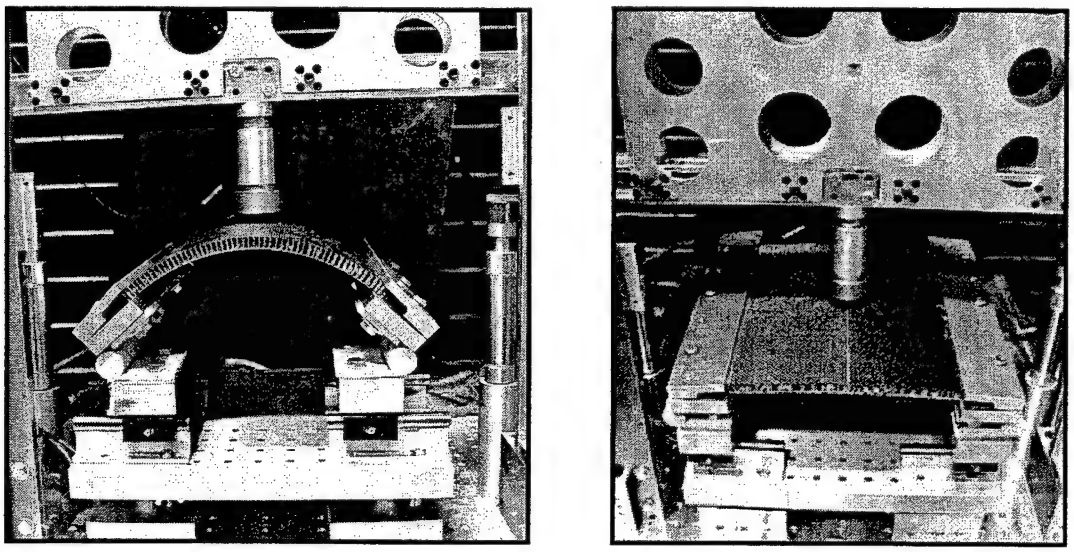

FIGURE 28. FIXTURE INSTALLED ON THE IMPACT TESTING MACHINE

The sandwich specimen was clamped between the clamping edges and the required boundary conditions were simulated as discussed above. The specimen was centered under the impactor by sliding the entire assembly over the bearing shafts. The impactor assembly was then raised to a desired height and the sandwich specimen was impacted by dropping the impactor assembly. The test data was recorded at a rate of 25 kHz and the data reduced using the method described in reference 2.

5.5 RESULTS AND DISCUSSIONS.

The curved sandwich specimens listed in the test matrix were impacted at suitable energy levels to inflict subsurface damage states. The impacted panels were then inspected for damage using TTU C-scan and the maximum residual indentation depth was measured. The effects of curvature were characterized in terms of the impact response and the damage metrics. The results of the test program are reported in the following sections.

5.5.1 Impact Event Characterization.

The impact responses of curved sandwich panels were influenced by their curvature, boundary condition type, impactor size, and core density. The typical impact responses of $[(90/45)_2/CORE]_s$ sandwich panels with nominal internal radii of 6″, 24″, and 48″ at comparable energy levels are shown in figures 29 and 30. The specimens were tested under boundary condition-1 with an impactor diameter of 3″. At an energy level of 40 lbf-in, the peak impact force increases with decreasing R_{INT}, which can be attributed to the higher flexural stiffness associated with the specimen with smaller R_{INT}. However, at an energy level of 140 lbf-in, the trend was found to be opposite. A logical explanation for this phenomenon can be provided by considering the local contact stiffness of the impactor-sandwich system. The contact stiffness depends on the relative radii of the impactor and the sandwich surface. The contact stiffness is dependent on the area of contact between the impactor and the sandwich specimen [4], which increases with specimen radius. In addition, the stiffness is also dependent on the transverse compressive properties of the core [4]. The core reaction is, however, dependent on the radius of the specimen due to the alignment of the cell walls along the radial direction, as illustrated in figure 31. The reaction force offered by the core adjacent to the point of impact will be lower, due to the eccentricity of the cell walls. This reduction in core support reaction will reduce the contact stiffness and, thus, result in a compliant impact response.

The effects of specimen curvature on the impact responses cannot be characterized based on the force-time history alone. The curvature affects the global bending stiffness and the local contact-indentation stiffness. The force-time responses may scale proportionally to the global bending stiffness when the impact energy levels are low enough to promote a near elastic impact. However, at higher energy levels, the contact stiffness will dominate the responses, which will in turn be affected by the global bending of the panel. The effects of specimen internal radius R_{INT} on the peak impact force measured for $[(90/45)/CORE]_s$ and $[(90/45)_2/CORE]_s$ specimens are summarized in figures 32 and 33, respectively. The plots indicate no conclusive trends at all energy levels tested.

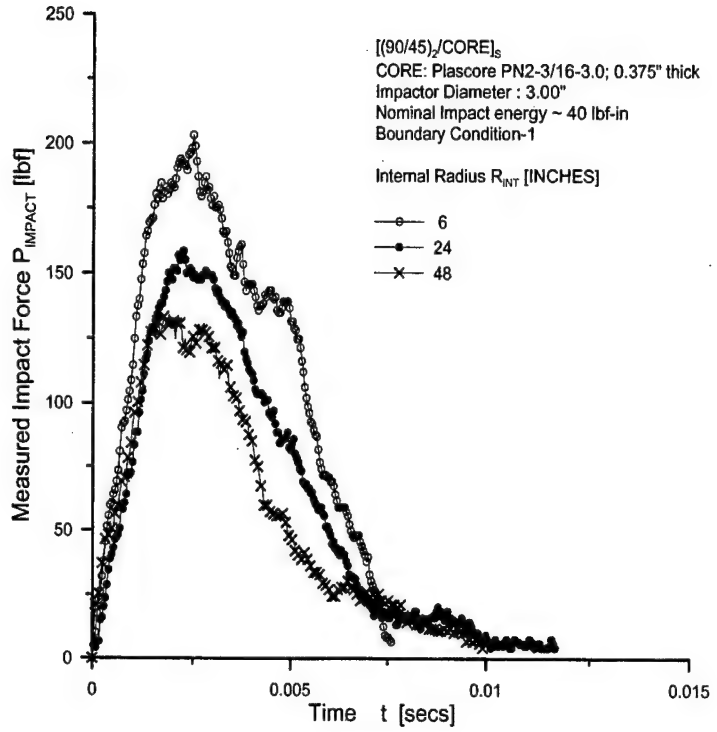

FIGURE 29. IMPACT RESPONSES OF $[(90/45)_2/CORE]_s$ SANDWICH PANELS WITH DIFFERENT INTERNAL RADIUS R_{INT} AT NOMINAL IMPACT ENERGY OF 40 lbf-in

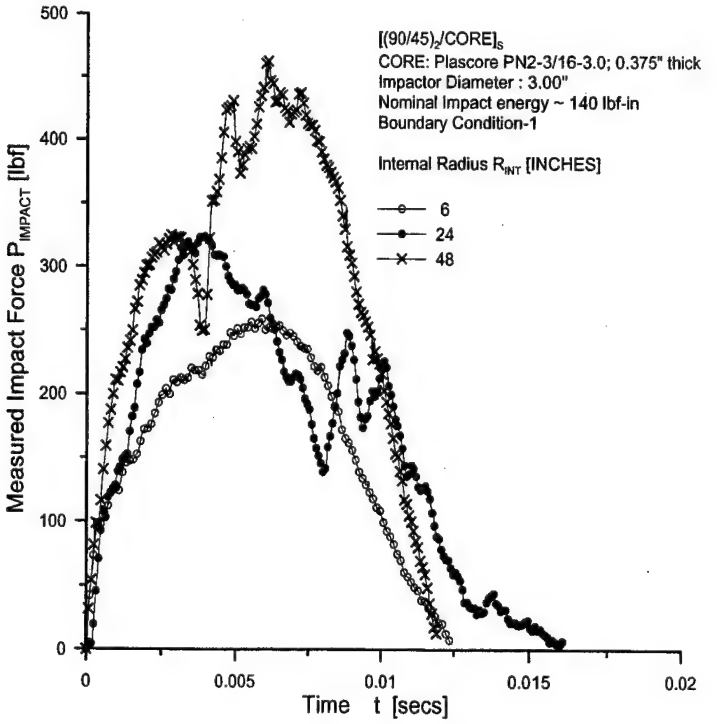

FIGURE 30. IMPACT RESPONSES OF $[(90/45)_2/CORE]_s$ SANDWICH PANELS WITH DIFFERENT INTERNAL RADIUS R_{INT} AT NOMINAL IMPACT ENERGY OF 140 lbf-in

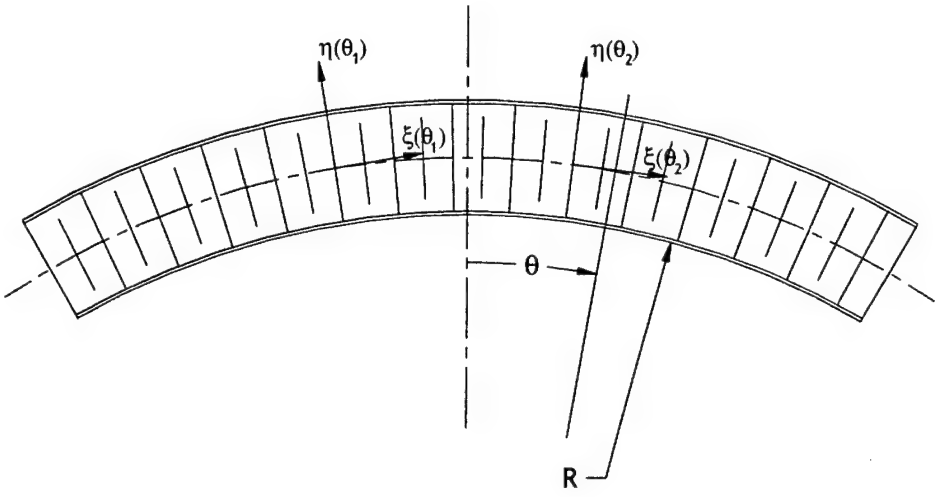

FIGURE 31. ILLUSTRATION OF ORIENTATION OF CELL WALLS ALONG THE SURFACE OF THE CURVED PANEL AND THE PRINCIPAL MATERIAL DIRECTIONS AS A FUNCTION OF THE ANGULAR COORDINATE θ

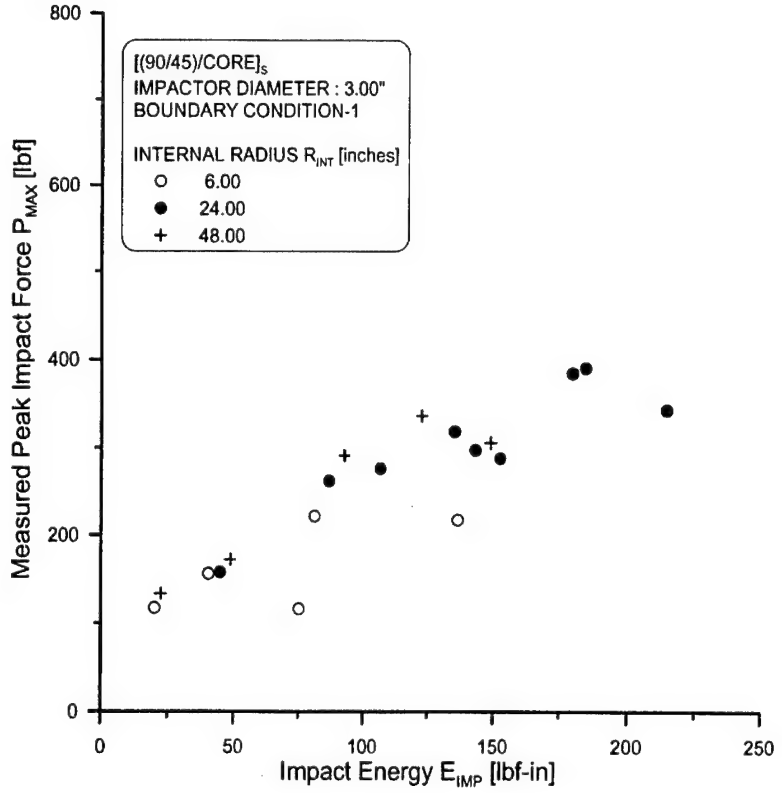

FIGURE 32. PEAK IMPACT FORCE AT VARIOUS ENERGY LEVELS FOR $[(90/45)/CORE]_s$ SPECIMENS WITH DIFFERENT R_{INT}

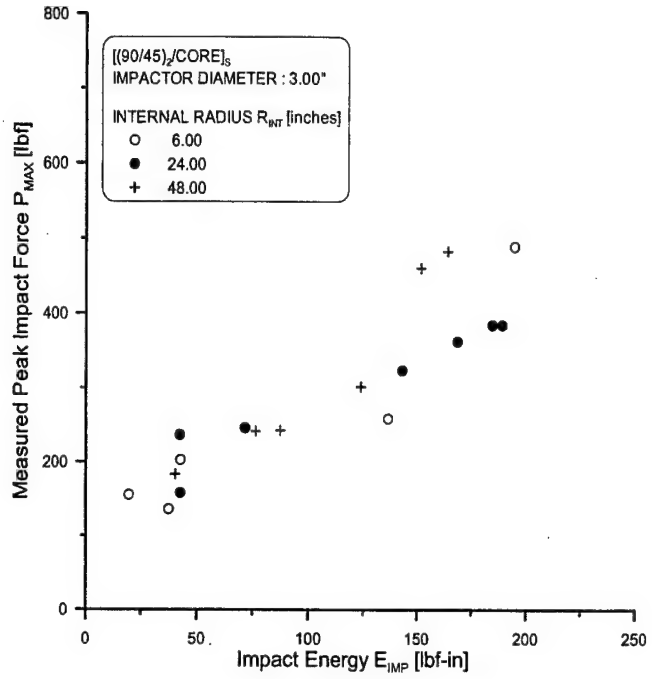

FIGURE 33. PEAK IMPACT FORCE AT VARIOUS ENERGY LEVELS FOR $[(90/45)_2/CORE]_s$ SPECIMENS WITH DIFFERENT R_{INT}

The effects of boundary conditions were investigated by impacting the $[(90/45)/CORE]_s$ and $[(90/45)_2/CORE]_s$ sandwich panels with internal radius R_{INT}=24″ with the boundary conditions described in section 5.1. The typical impact responses of $[(90/45)_2/CORE]_s$ sandwich panels impacted with a 3″ impactor with a nominal impact energy of 40 lbf-in is shown in figure 34. The impact force increases with the increasing boundary constraint. In addition, the less stiffer boundary constraints (1 and 2) tend to produce a secondary impact past the first peak.

The effects of boundary constraint on the peak impact force recorded during the impact tests for the $[(90/45)/CORE]_s$ and $[(90/45)_2/CORE]_s$ sandwich panels are summarized in figures 35 and 36, respectively. The stiffening effect of constraining the translation of the supports (boundary condition-1) is evident from both figures. However, no significant differences were observed between boundary conditions -2 and -3. This implies that constraining the rotation and the translation does not increase the bending stiffness of the curved panels significantly.

The effects of core density on the impact response of curved sandwich panels was studied by conducting a limited number of tests on $[(90/45)_2/CORE]_s$ sandwich panels with core densities of 3.0 , 4.5, and 6.0 lb/ft^3. The peak impact forces recorded during the impact tests are summarized in figure 37. A marginal increase was observed when the core density of 6.0 lbf/ft^3 was used. Perhaps the stiffening effect of core density was offset by the effects of panel curvature.

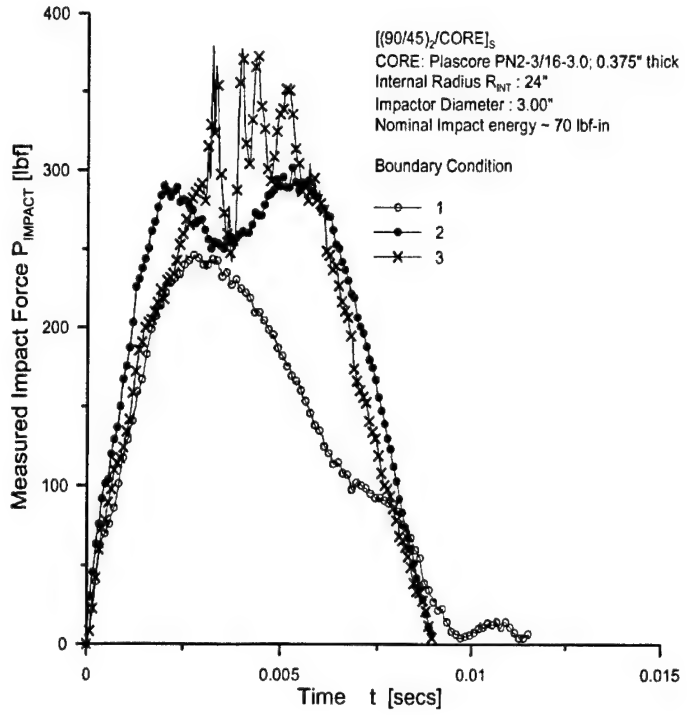

FIGURE 34. IMPACT RESPONSES OF $[(90/45)_2/CORE]_s$ WITH R_{INT}=24″ AND DIFFERENT BOUNDARY CONDITIONS IMPACTED WITH 3.00″ IMPACTOR WITH NOMINAL ENERGY OF 70 lbf-in

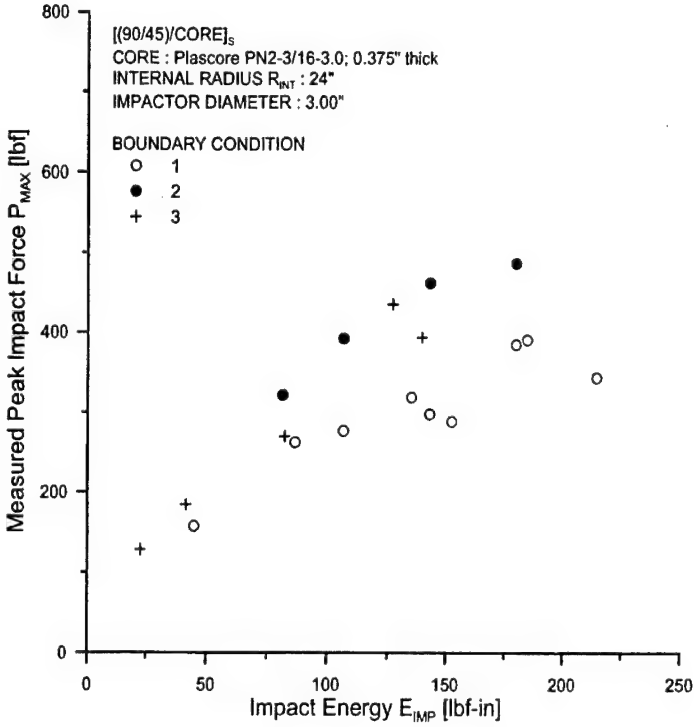

FIGURE 35. PEAK IMPACT FORCE AT VARIOUS ENERGY LEVELS FOR $[(90/45)/CORE]_s$ SPECIMENS WITH DIFFERENT BOUNDARY CONDITIONS

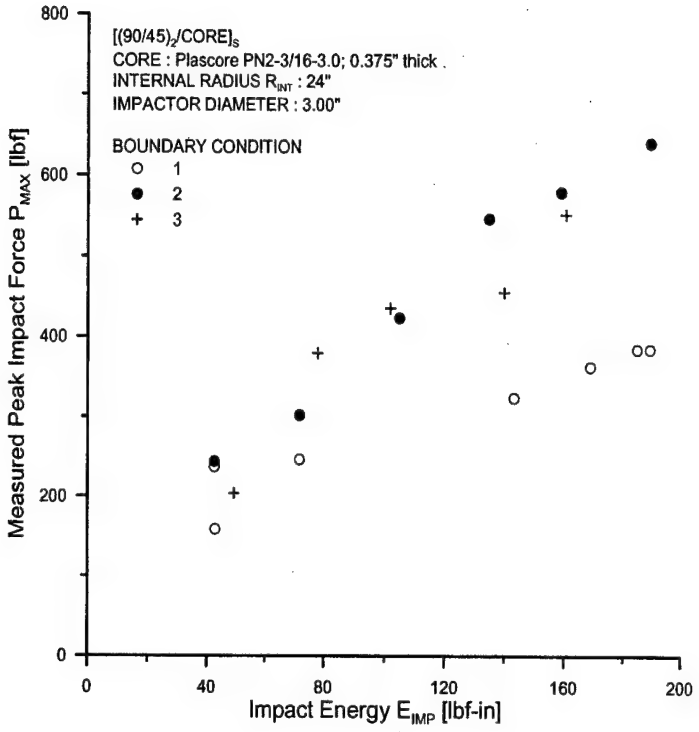

FIGURE 36. PEAK IMPACT FORCE AT VARIOUS ENERGY LEVELS FOR $[(90/45)_2/CORE]_S$ SPECIMENS WITH DIFFERENT BOUNDARY CONDITIONS

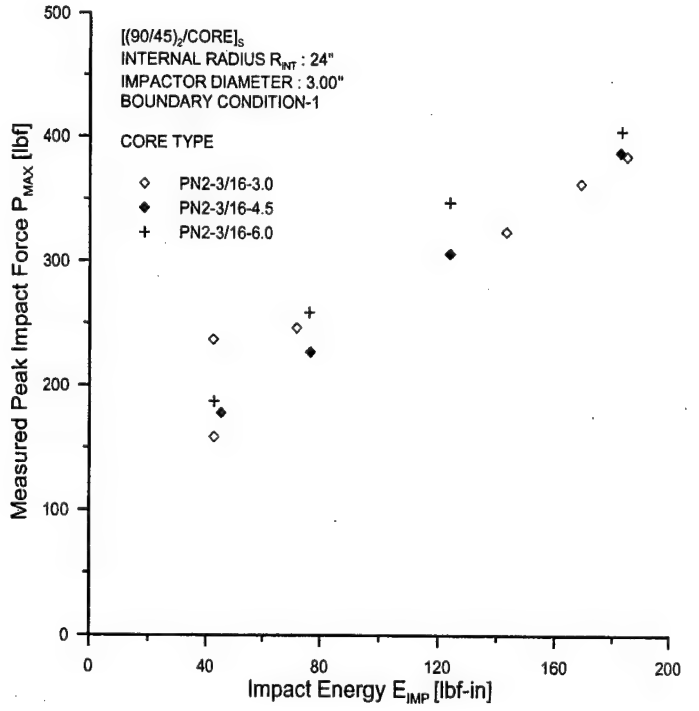

FIGURE 37. PEAK IMPACT FORCE FOR $[(90/45)_2/CORE]_S$ SANDWICH PANELS WITH DIFFERENT DENSITY CORES

The aforementioned results are for the 3″ diameter impactor only. Tests were also conducted with a 1.00″ diameter impactor. The curved sandwich panels suffered skin fractures at relatively low energy levels when impacted with the 1.00″ diameter impactor. The impactor size and the curvature of the sandwich panels limit the region over which the contact loads are distributed. The smaller contact regions lead to an early skin fracture initiation. The planar damage size was saturated with the initiation of skin fracture and no trends could be observed for the range of impact energies investigated with the 1.00″ diameter impactor.

5.5.2 Damage Characterization.

The impacted sandwich panels were inspected for any impact damage using TTU C-scan and the maximum residual indentation was measured using the setup described in reference 2. The TTU C-scan was used to quantify the planar damage area, which corresponds to the planar extent of core damage [2].

The effects of panel curvature on the planar damage area created in $[(90/45)/CORE]_s$ and $[(90/45)_2/CORE]_s$ sandwich panels are summarized in figures 38 and 39, respectively. The planar damage area was observed to increase with decreasing R_{INT}. This can again be attributed to reduced core strength because of the alignment of the cell walls along the radial direction. The ends of the cell walls at their interface with the impacted skin experience a component of shear in addition to the normal forces. The shear component is instrumental in reducing the transverse compressive strength of the core. Thus, in a specimen with smaller R_{INT}, the core adjacent to the point of impact will experience a higher shear component leading to a lower failure strength of the core.

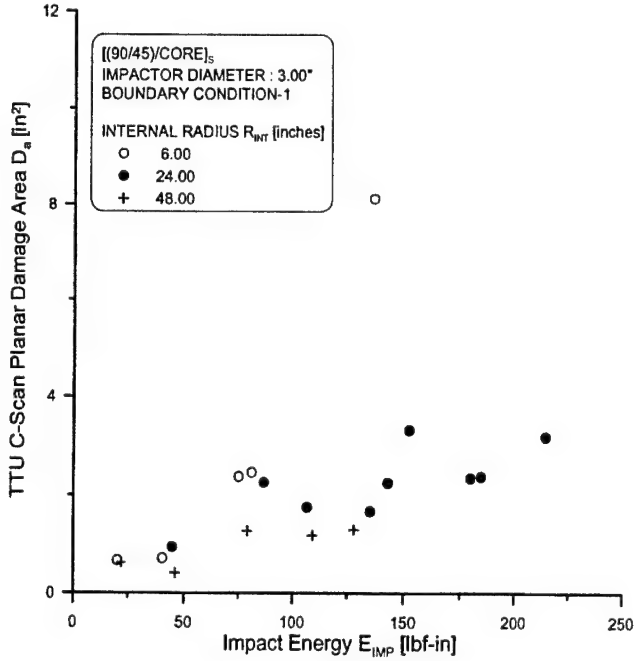

FIGURE 38. PLANAR DAMAGE AREA FOR $[(90/45)/CORE]_s$ SANDWICH PANELS WITH DIFFERENT INTERNAL RADII R_{INT}

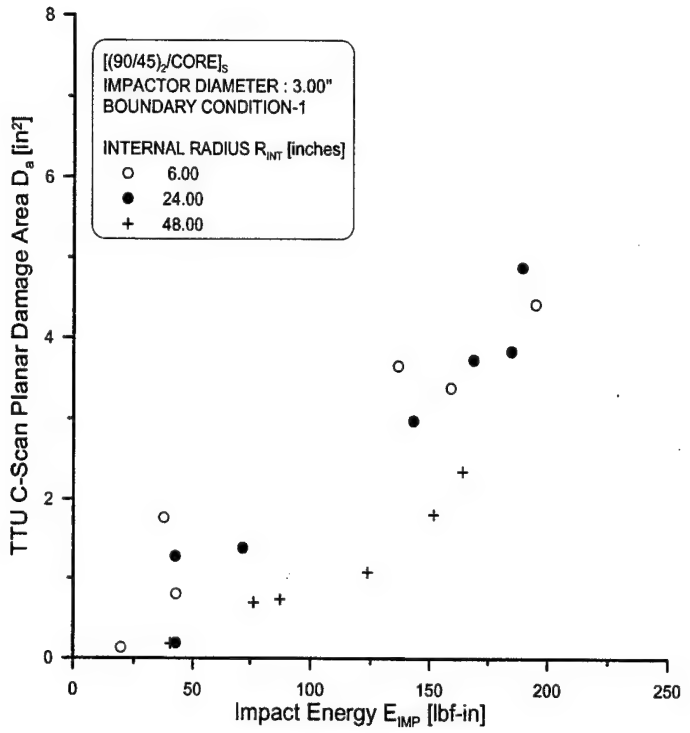

FIGURE 39. PLANAR DAMAGE AREA FOR $[(90/45)_2/CORE]_s$ SANDWICH PANELS WITH DIFFERENT INTERNAL RADII R_{INT}

In contrast to the planar damage area, the maximum residual indentation depths increased with an increase in internal radius R_{INT}. Unlike flat panels [2], the curved panels did not suffer appreciable permanent residual indentations. It can be observed from figures 40 and 41 that the maximum residual indentations rarely exceeded the nominal ply thickness (0.008″) of the facesheet material. In addition, the residual indentations for R_{INT}=48″ are consistently higher compared to R_{INT}=6″ and 24″. This is in contrast to the impact damages due to the 1.00″ impactor, which were predominantly facesheet fractures associated with large indentation depths (see section 5.5.1).

The low residual indentations in curved sandwich panels can be attributed to the high restoring force associated with the curved facesheets. The facesheets collapse on the core during the loading phase creating damage in the core. During unloading, the facesheet tends to pull itself back to its undeformed position [4], while the core tends to pull it down creating the residual indentation. In curved panels, the moments generated in the skin are higher compared to the flat panels and, thus, relatively low indentations will be observed. Therefore, visual inspections for sandwich structures impacted with larger diameter (blunt) impactors will be more difficult. For smaller impactors, the impacted damage will be more conspicuous because of the presence of skin fractures.

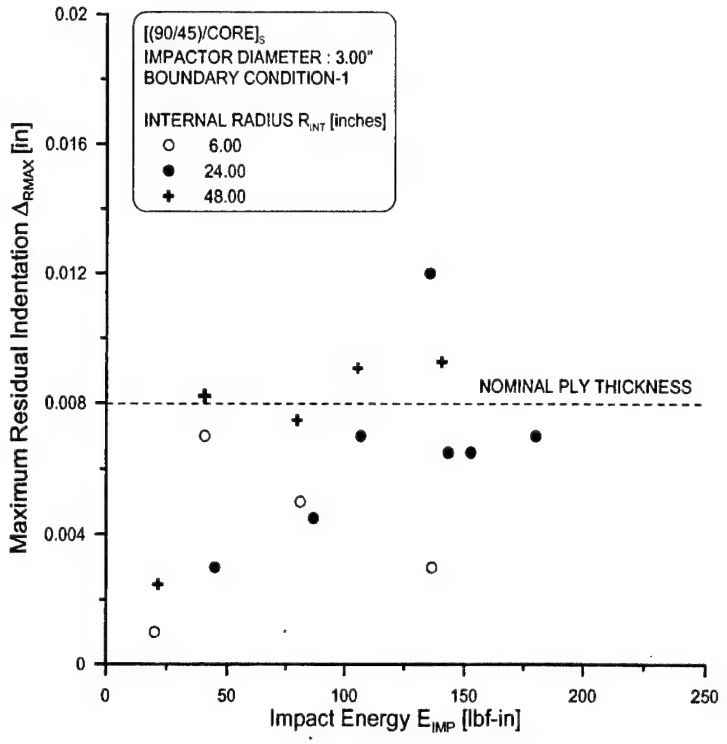

FIGURE 40. MAXIMUM RESIDUAL INDENTATION FOR $[(90/45)/CORE]_s$ SANDWICH PANELS WITH DIFFERENT INTERNAL RADII R_{INT}

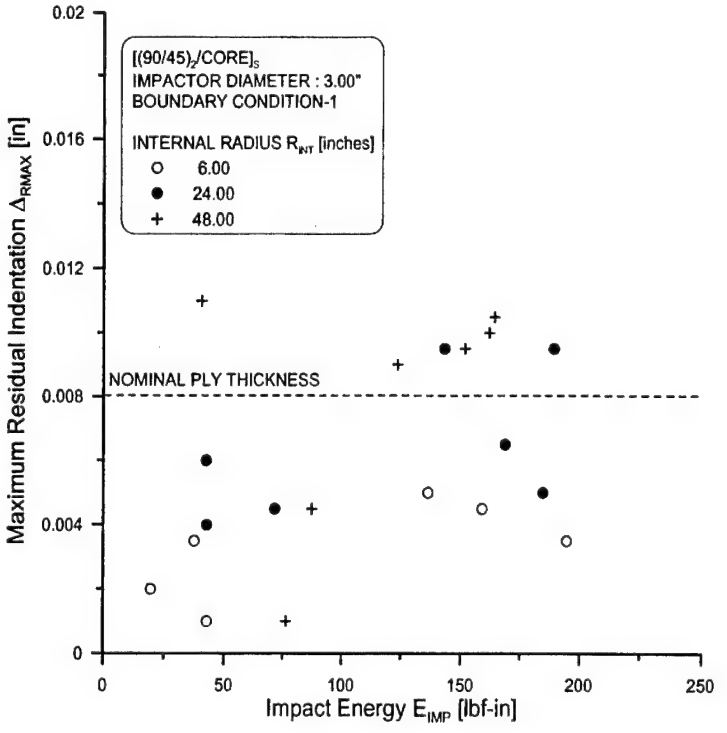

FIGURE 41. MAXIMUM RESIDUAL INDENTATION FOR $[(90/45)_2/CORE]_s$ SANDWICH PANELS WITH DIFFERENT INTERNAL RADII R_{INT}

6. FATIGUE BEHAVIOR OF IMPACT-DAMAGED SANDWICH PANELS.

The behavior of impact-damaged sandwich panels under the action of fatigue loads was investigated experimentally. The impact damage states due to the 3″ diameter impactor were of particular interest because of the high degradation of residual strengths associated with such damage states and also the difficulties in detecting them using nondestructive inspection. The fatigue lives associated with different levels of impact damage in both honeycomb core and foam core sandwich panels were studied. The details of the various aspects of the fatigue-testing program are reported in the following sections.

The impact damage states selected for fatigue study correspond to two distinct regions of the residual strength degradation curve illustrated in figure 42. The data correspond to sandwich specimens impacted with a 3″ diameter impactor at different energy levels. The lower energy level (E_1) corresponds to the knee region of the curve, where the normalized residual strength (NCAI) ranges between 0.8 to 0.6 (typical). The higher energy level (E_2) corresponds to the asymptote of the curve, where the NCAI is about 0.5 or lower (typical). The damage corresponding to these energy ranges is purely subsurface (core) damage with no visible skin damage. The typical planar damage areas corresponding to these energy levels are shown on the right in figure 42.

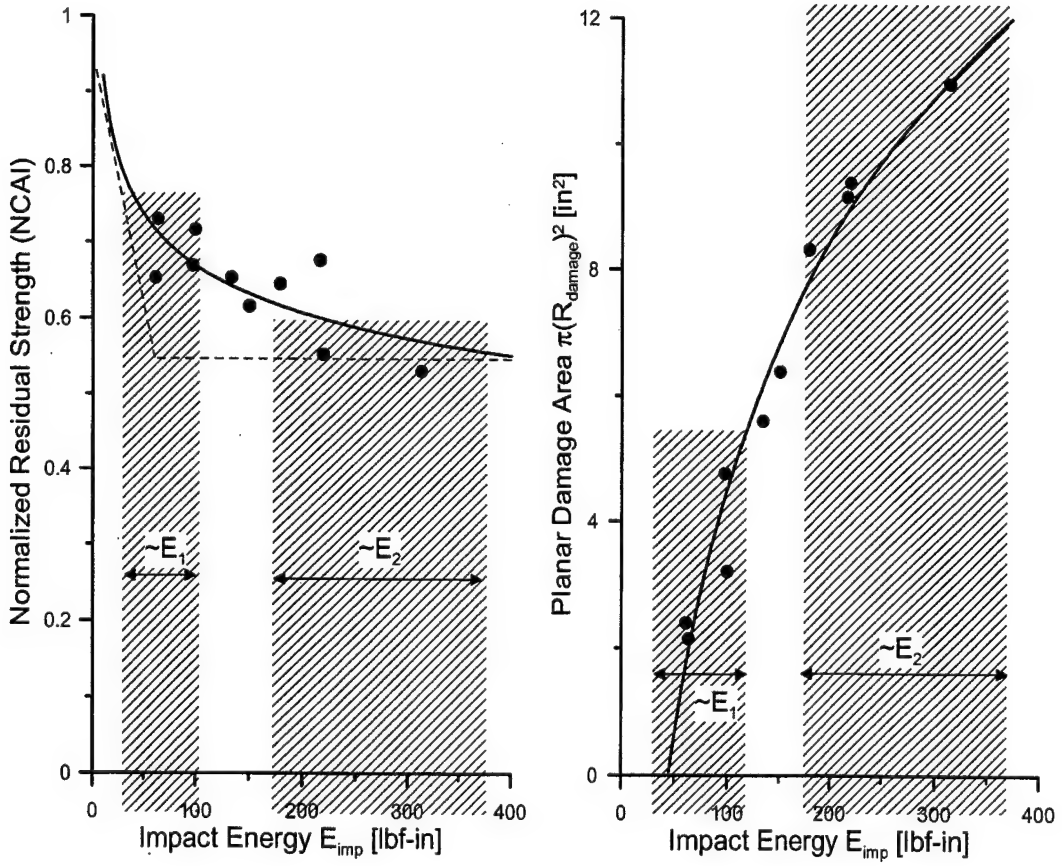

FIGURE 42. TYPICAL RANGES OF IMPACT ENERGY LEVELS FOR FATIGUE PROGRAM

The primary objectives of this exercise are:

1. To study the fatigue life of sandwich specimens with two levels of impact damage at different stress levels.

2. Observe the growth of damage if any, e.g., $2R_{damage}$.

3. Monitor further degradation of residual strength due to a prespecified infinite life N_{∞}.

6.1 MATERIAL SYSTEMS AND SANDWICH CONFIGURATIONS.

The behavior of impact damage in both honeycomb and foam core sandwich panels was investigated. The honeycomb core sandwich panels were used with NB321/3K70 plain weave carbon facesheets, while the foam core sandwich panels used NB321/7781 satin weave fiberglass facesheets. The sandwich configurations used in the current study are summarized in table 6.

TABLE 6. MATERIAL SYSTEMS AND SANDWICH CONFIGURATIONS USED IN THE FATIGUE PROGRAM

Sandwich Type	Honeycomb Core Panels	Foam Core Panels
Facesheet Material	NB321/3K70 Plain Weave Carbon prepreg.	NB321/7781 Satin Weave Fiberglass prepreg.
Layup Schedules	$[(90/45)/CORE]_s$, $[(90/45)_2/CORE]_s$	
Core Material	Plascore PN2-3/16-4.5; 0.75″ thick	Divinycell HT-70; 0.75″ thick
Adhesive	Hysol 9628.060 PSF NW film adhesive	

6.2 FATIGUE SPECIMEN FABRICATION.

The fatigue test specimen fabrication method followed the same procedure reported in reference 2. However, since the specimens were subjected to cycling loading, the wearing out of the loaded edges of the facesheet was a concern. Hence, the ends of the sandwich specimens were reinforced by potting the cores by a suitable material. In this section, the potting procedures for honeycomb and foam core sandwich panels are described.

The regions of the sandwich specimens that were reinforced with potting compound are illustrated in figure 43. The specimens were potted along the edges to a nominal depth of 0.50″. The honeycomb core panels were potted along their width without any gaps, while the foam core sandwich panels were potted across the width with suitable intervals of foam core left intact.

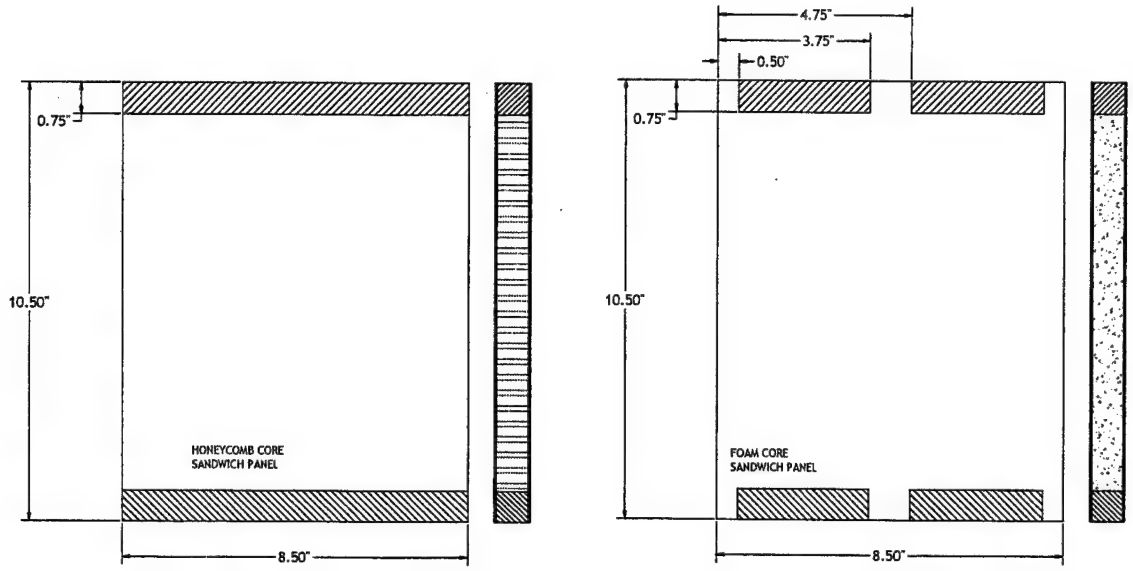

FIGURE 43. POTTING REGIONS FOR HONEYCOMB CORE AND FOAM CORE SANDWICH SPECIMENS

The honeycomb cores were potted prior to the fabrication of the sandwich panel. The preform cores were potted, as shown in the figure 44. The potting compound used was EPOCAST 1652-A/B, a two-part paste (mix ratio 100/12), which has a cured compressive strength that exceeds 7000 psi. The facesheet preforms were then assembled with the core and the sandwich assembly cured in an autoclave. The potting compound, thus, cured along with the sandwich skins. The sandwich panel was then cut to appropriate dimensions to obtain sandwich specimens with potted ends.

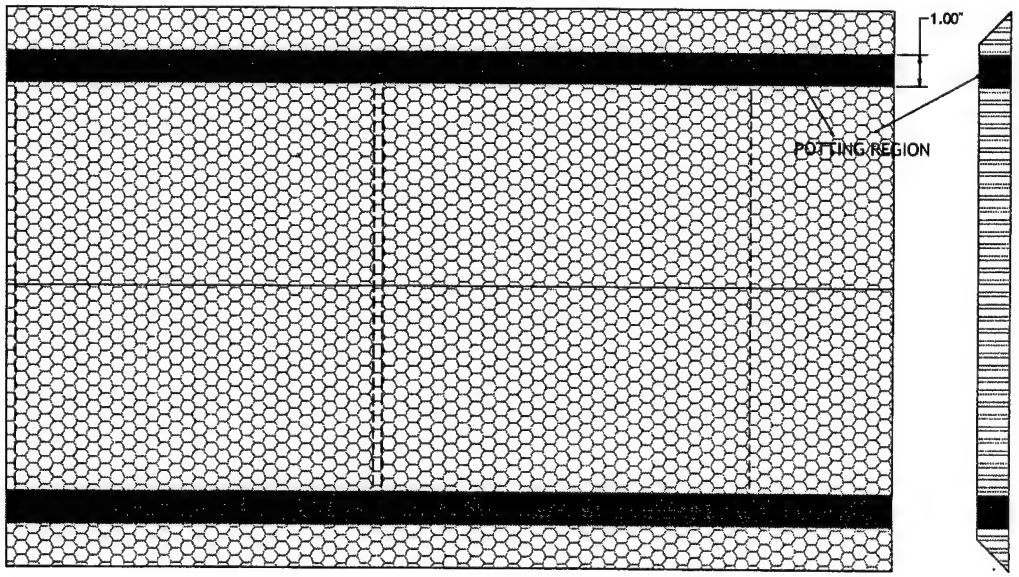

FIGURE 44. POTTING OF PREFORM HONEYCOMB CORE PRIOR TO FABRICATION OF SANDWICH PANELS

Unlike honeycomb core sandwich panels, the foam core panels could not be potted prior to the cure cycle. The specimens were first cut to size from their parent panels and the core material was removed along the edges, as illustrated in figure 45. The facesheets along the edges were then reinforced by mounting stiffeners (aluminum angles) using a double-sided adhesive tape, as shown in the figure. The stiffeners support and prevent the skins from distorting due to the shrinkage of potting resin during the curing process. The recess, which was formed by removing the core, was then filled with a room temperature cured epoxy resin system (Shell 823 resin with Shell 915 hardener, mix ratio 100-14%), and allowed to cure for 24 hours. The stiffeners were then removed and the ends of the specimen were machined (surface ground) to the required dimensions.

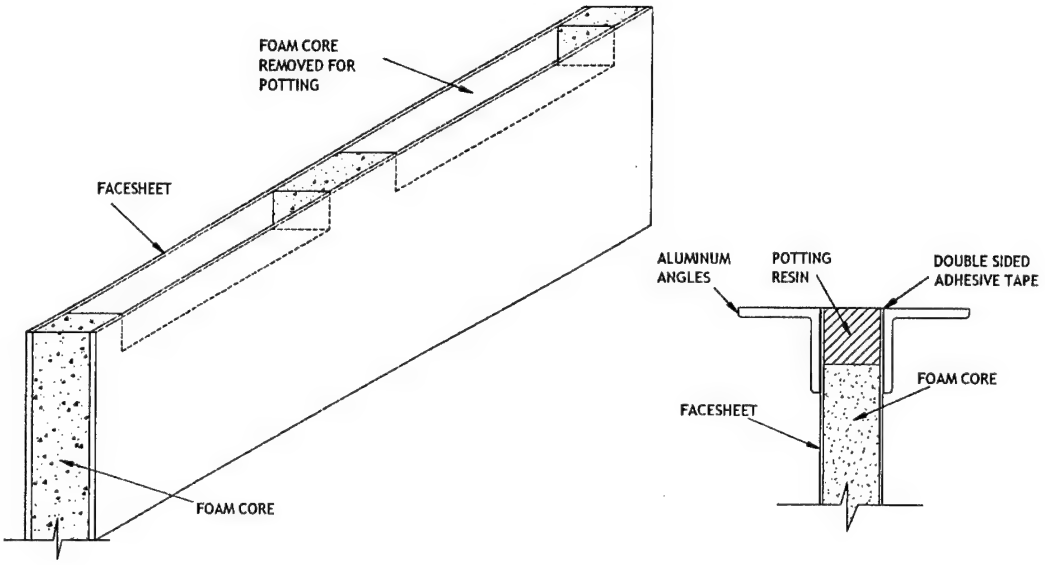

FIGURE 45. ILLUSTRATION OF PROCEDURE FOR POTTING FOAM CORE SANDWICH PANELS

6.3 FATIGUE TEST PROGRAM AND TEST MATRIX.

The fatigue testing program was divided into three phases. The first phase consisted of the generation of the static residual strength data for sandwich panels impacted with different impact energy levels. The characteristic residual strength degradation curve (curve fit) was then analyzed to select two candidate impact energy levels (E_1 and E_2) for use in the fatigue program. In the second phase, the experimental data from the residual strength test of the specimens impacted with the candidate energy levels was analyzed to select the stress/load[2] levels (N_{yy}) for fatigue loads leading to potential damage growth. The third phase consisted of the fatigue testing of the impact-damaged sandwich specimens, monitoring the damage growth, and residual strength testing of specimens that successfully completed the predefined infinite life N_∞, to assess any further degradation in residual strength. The entire fatigue program is summarized in the flowchart shown in figure 46.

[2] The residual strengths were expressed in terms of the stress resultants N_{yy} (lbf/in) rather than the stress (σ_{yy}). Thus, throughout this report, the word load rather than stress will be associated with the nomenclature for defining the fatigue tests, e.g., stress ratio will be referred to as the load ratio.

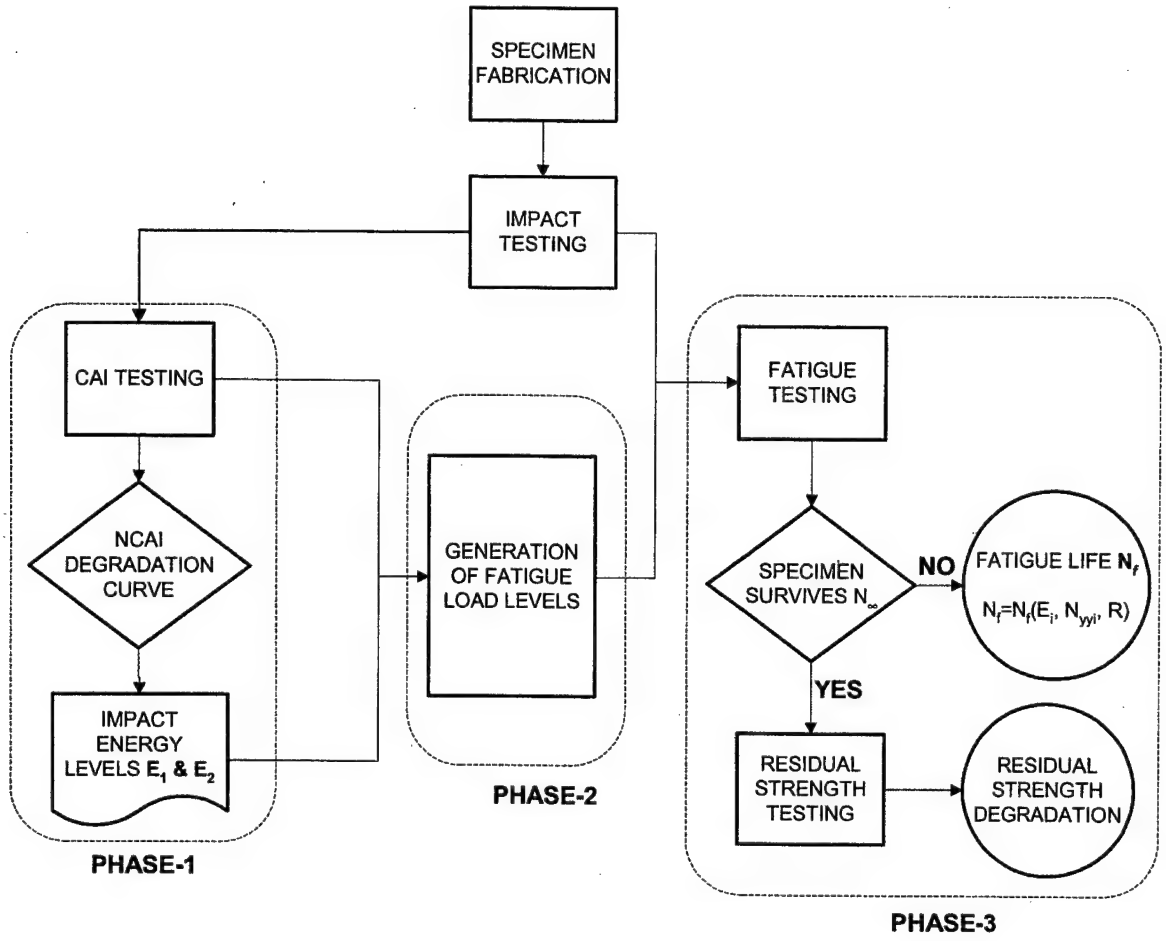

FIGURE 46. OVERVIEW OF THE FATIGUE PROGRAM

Since the fatigue life of the impact-damaged sandwich specimen is not known a priori, the load levels selected were only initial estimates. The loads were increased or decreased appropriately to introduce failures or run-outs (i.e., survive N_∞) to obtain meaningful data.

In this study, four different sandwich configurations were chosen for the fatigue program. These sandwich configurations are representative of thin-skinned sandwich structures. Each sandwich configuration was impacted with two different energy levels (E_1 and E_2) using a 3″ diameter impactor. The sandwich panel impacted with a preselected energy level was then fatigued at four different minimum load levels $N_{yy\text{-}MINIMUM}$ (refer to figure 47). The test at each load level was in turn repeated with three different load ratios R_1, R_2, and R_3 (figure 47), the load ratio R defined as the ratio of the minimum load to the maximum load. The test matrix summarizing the various combinations of impact energy levels, fatigue loads, and load ratios for a single sandwich configuration is shown in table 7. A total of 24 specimens were required for a single sandwich configuration and a combined total of 96 specimens were required to cover all sandwich configurations.

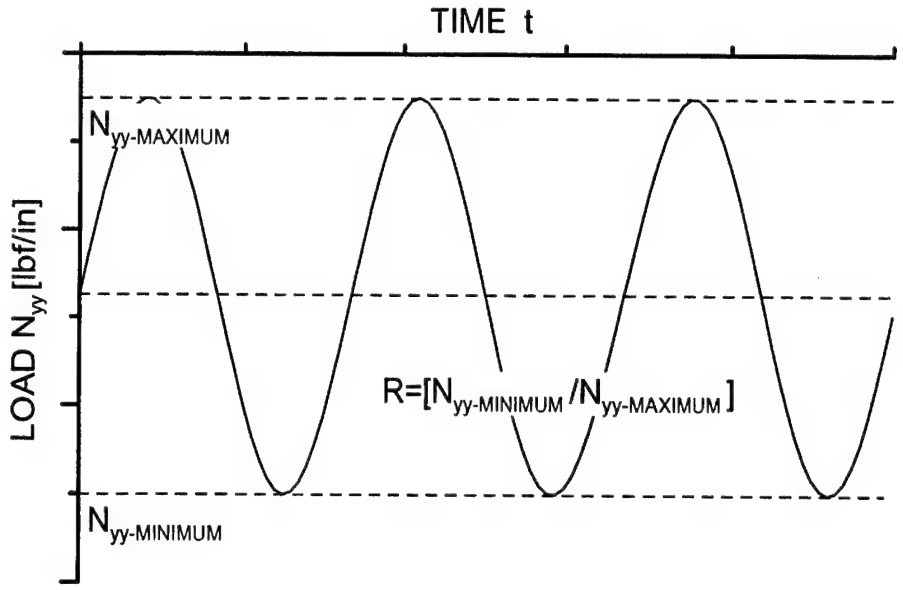

FIGURE 47. ILLUSTRATION OF FATIGUE LOADING NOMENCLATURE

TABLE 7. FATIGUE TEST MATRIX FOR A TYPICAL SANDWICH CONFIGURATION

Sandwich Configuration	Impact Energy Level	Minimum Fatigue Loads	Stress Ratios		
$[(90/45)_N/CORE]_s$	E_1	$N_{yy\text{-}MINIMUM\text{-}1}$	R_1	R_2	R_3
		$N_{yy\text{-}MINIMUM\text{-}2}$	R_1	R_2	R_3
		$N_{yy\text{-}MINIMUM\text{-}3}$	R_1	R_2	R_3
		$N_{yy\text{-}MINIMUM\text{-}4}$	R_1	R_2	R_3
	E_2	$N_{yy\text{-}MINIMUM\text{-}1}$	R_1	R_2	R_3
		$N_{yy\text{-}MINIMUM\text{-}2}$	R_1	R_2	R_3
		$N_{yy\text{-}MINIMUM\text{-}3}$	R_1	R_2	R_3
		$N_{yy\text{-}MINIMUM\text{-}4}$	R_1	R_2	R_3

The test matrix in table 7 was implemented with the following specifications for the fatigue loading.

1. The tests were conducted at a frequency $f = 2$Hz.
2. The infinite life N_∞, was assumed to be 150,000 cycles.
3. The load ratios used were, $R_1 = 10$, $R_2 = 5$, and $R_3 = 2$.
4. The specimens were inspected at intervals of 25,000 cycles for damage growth.

   a. Compliance tests: The foam core and honeycomb core sandwich panels were statically loaded to about 40% of the minimum fatigue load level, the compliance associated with end-shortening, and out-of-plane displacement at the impact location used as a measure of damage growth.

   b. TTU C-scan: The honeycomb cores were inspected for growth in planar damage size in addition to the compliance measurements.

6.4 EXPERIMENTAL PROCEDURE.

The sandwich specimen configuration, instrumentation, and test procedure followed during the residual strength tests and the fatigue tests are described in this section. The sandwich specimen geometry and strain gage locations for the static residual strength tests and the fatigue tests are illustrated in figure 48. The specimens tested statically to generate the residual strength degradation curve were instrumented with five strain gages, as shown in figure 48. The end-shortening of the specimen was measured using a deflectometer and the out-of-plane displacement at the center of damage (impact location) was measured using a LVDT, as described in section 4. The details of the boundary conditions and test fixture used can be found in reference 2.

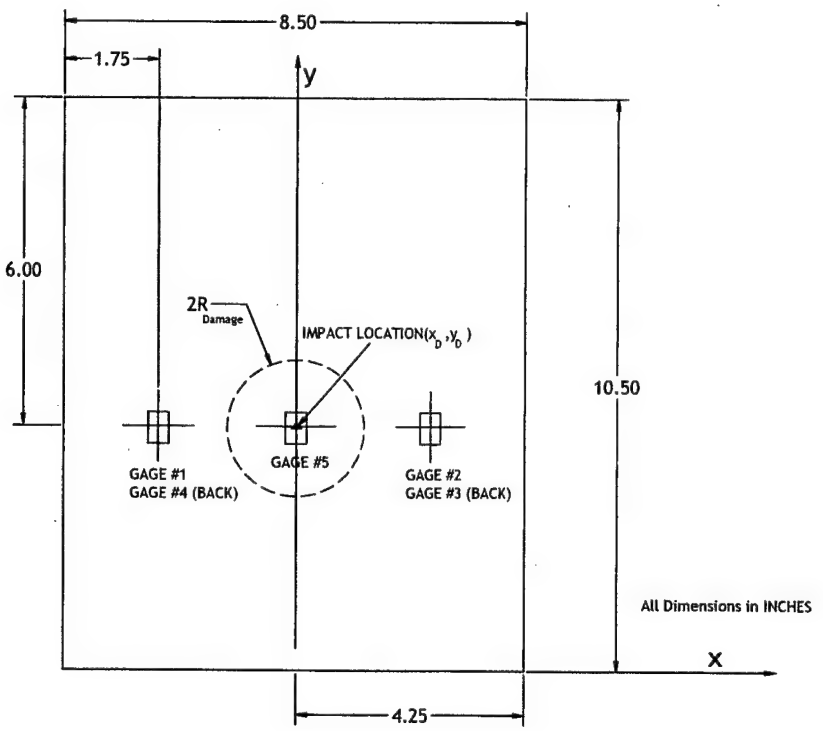

FIGURE 48. GEOMETRY OF TEST SPECIMEN AND LOCATION OF STRAIN GAGES

The sandwich specimens that were subjected to fatigue loading were instrumented with three far-field strain gages (1, 2, and 3), which were used to balance the load distribution in the sandwich skins using appropriate brass shims. The three strain gages, the deflectometer, and the LVDT were used during the compliance tests only. The deflectometer and the LVDT were disassembled from the test setup for the fatigue tests. In addition, the strain gages were disconnected from their respective excitation voltages to extend the life of the gages under fatigue loads.

The compliance and fatigue tests were controlled using the MTS Flextest IIs control system along with the Basic Testware computer program. The fatigue tests were conducted under load control mode, while the compliance tests were conducted under displacement control mode at a rate of 0.05 in/min.

6.5 RESULTS AND DISCUSSION.

The experimental results obtained during the three phases of the fatigue program are summarized in the following sections.

6.5.1 Residual Strength Degradation Curves and Energy Levels.

The CAI testing of impact-damaged sandwich panels was conducted to generate the residual strength degradation curves to be used for identifying candidate impact energy levels for the fatigue program. The CAI data for the four sandwich configurations are presented in figures 49 to 52. The candidate energy levels are also identified on the respective figures. Note that a distinct knee was not evident for some of the sandwich configurations and the selection of the lower energy level E_1 was subjective in nature. In addition, the higher energy level E_2 for honeycomb core sandwich panels was limited to 150 lbf-in, as higher energy levels tended to create visible skin damage. It was observed that the foam core sandwich panels with fiberglass facesheets were relatively more damage tolerant than the honeycomb core panels with carbon facesheets.

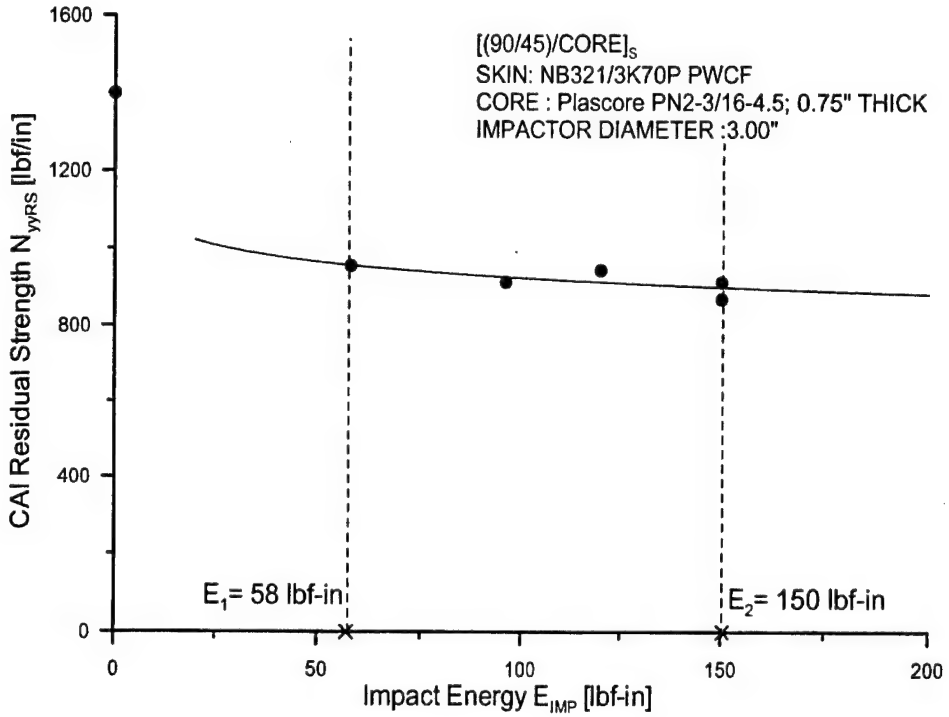

FIGURE 49. IMPACT ENERGY LEVELS FOR $[(90/45)/CORE]_s$ SANDWICH PANELS (HONEYCOMB CORE) BASED ON CAI DATA

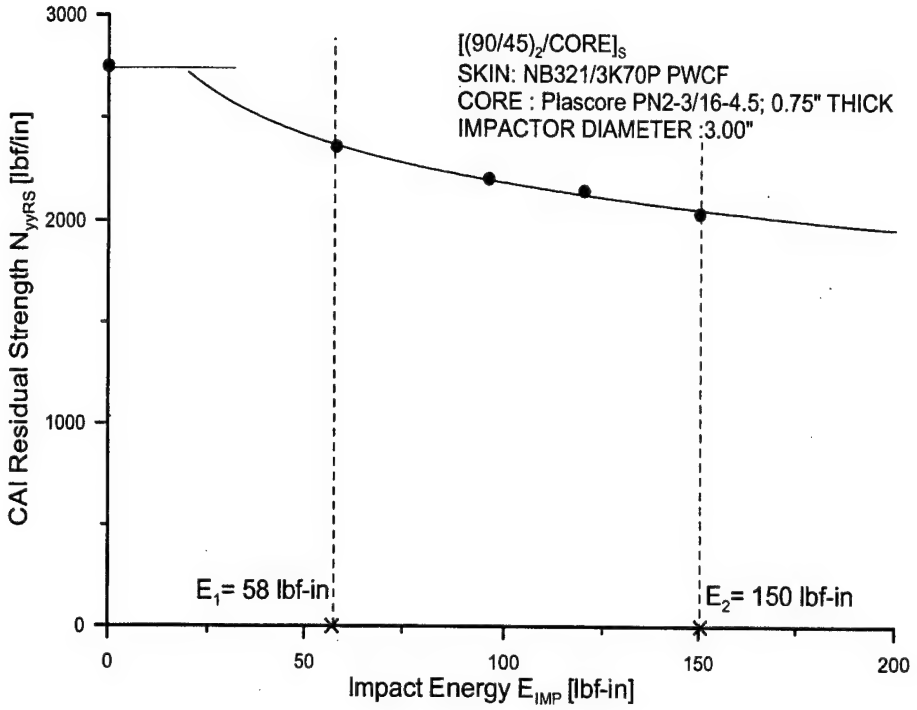

FIGURE 50. IMPACT ENERGY LEVELS FOR $[(90/45)_2/CORE]_s$ SANDWICH PANELS (HONEYCOMB CORE) BASED ON CAI DATA

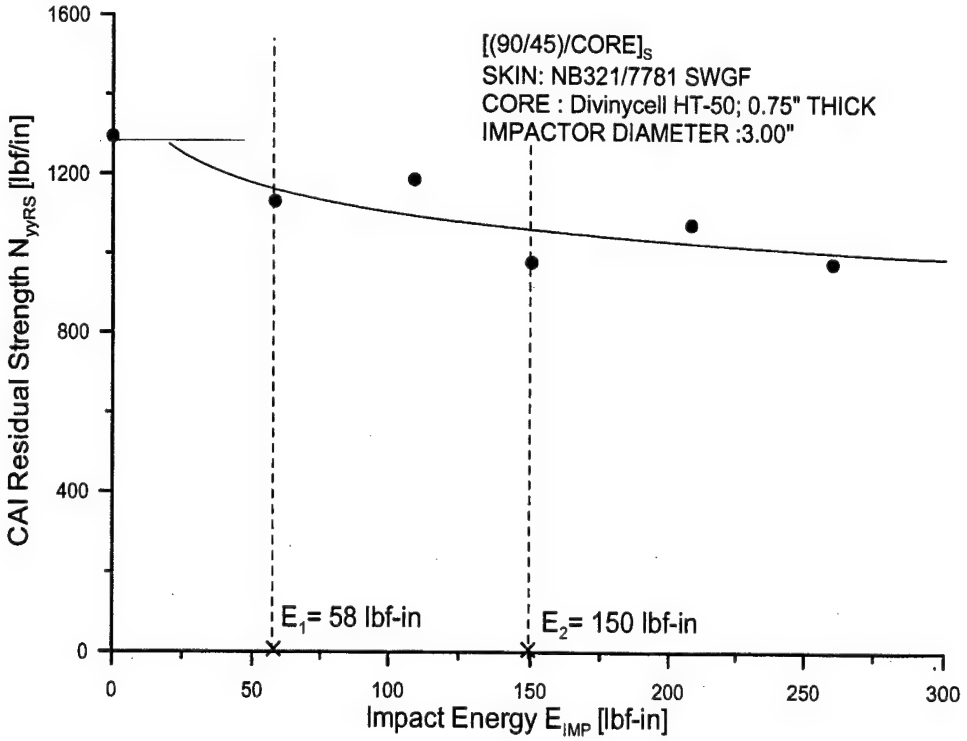

FIGURE 51. IMPACT ENERGY LEVELS FOR $[(90/45)/CORE]_s$ SANDWICH PANELS (FOAM CORE) BASED ON CAI DATA

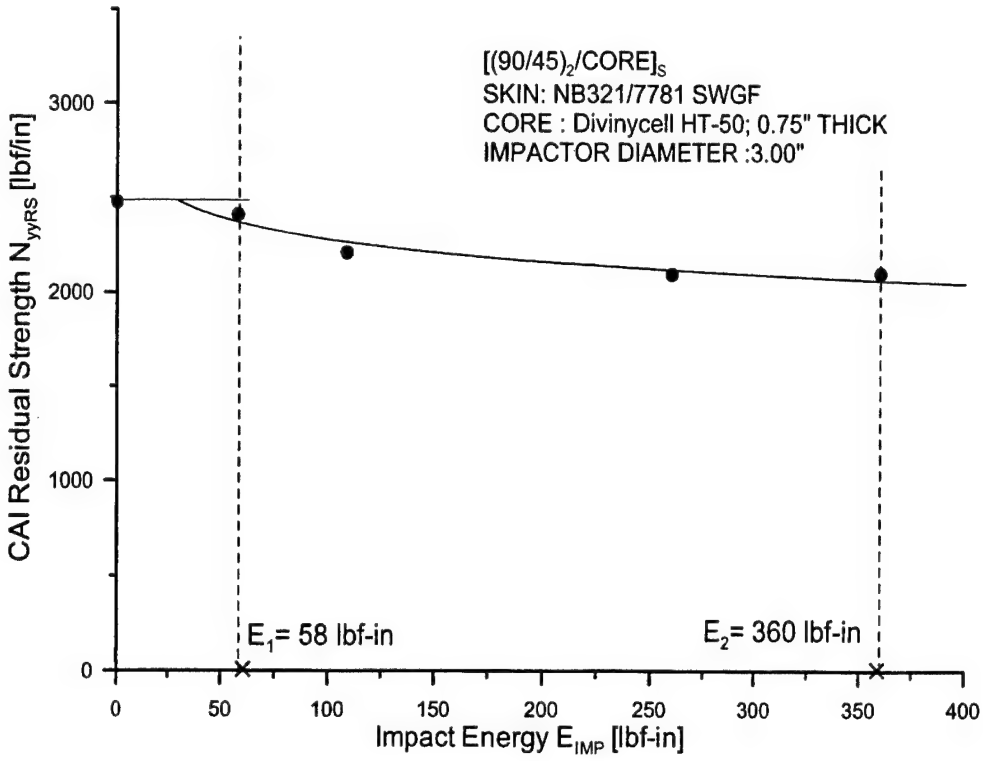

FIGURE 52. IMPACT ENERGY LEVELS FOR $[(90/45)_2/CORE]_s$ SANDWICH PANELS (FOAM CORE) BASED ON CAI DATA

The impact energy levels selected for the four different sandwich configurations are summarized in table 8.

TABLE 8. IMPACT ENERGY LEVELS FOR FATIGUE SPECIMENS

Sandwich Configuration	Facesheet Material	Core Material	Impact Energy Levels (lbf-in)	
			E_1	E_2
$[(90/45)/CORE]_s$	NB321/3K70 P PWCF	Plascore PN2-3/16-4.5 Honeycomb	58	150
$[(90/45)_2/CORE]_s$			58	150
$[(90/45)/CORE]_s$	NB321/7781 SWGF	Divinycell HT-70 Foam	58	150
$[(90/45)_2/CORE]_s$			58	360

The damage states corresponding to the above energy levels were barely visible. The planar damage diameter for the $[(90/45)/CORE]_s$ honeycomb core panels was 1.08″ (E_1) and 1.95″ (E_2), and the corresponding indentation levels were 0.011″ and 0.02″, respectively. The average planar damage diameter for the $[(90/45)_2/CORE]_s$ honeycomb core panels was 1.22″ (E_1) and 2.1″ (E_2), and the corresponding indentation levels were 0.005″ and 0.015″, respectively. The planar damage radius for the foam core panels, however, could not be determined due to the lack of appropriate NDI equipment. However, the average residual indentations for all foam core

sandwich panels were no greater than 0.01″ and 0.035″ at energy levels E_1 and E_2, respectively, with no visible skin damage.

6.5.2 Fatigue Load Levels.

The CAI test data for the sandwich specimens corresponding to the impact energy levels listed in the previous table were analyzed to generate fatigue loads. The test data of particular interest were the displacement and the strain at the impact location (gage no. 5). The presence of a characteristic knee or damage in slope, corresponding to the initiation of dimple growth and the initiation of additional core crushing within the original damage region, was used as a starting point for the selection of fatigue load levels. The remaining load levels were chosen based on the type of core used in the sandwich panel. Since the honeycomb core panels exhibit the ability to arrest the dimple past the knee, the higher load levels were selected past this point. However, because the foam core panel cannot contain the dimple, the load levels below the knee were selected as the remaining fatigue load levels. In the absence of a prominent knee in the data, the fatigue load levels were arbitrarily chosen between 50% to 80% of the failure load, as in figure 53.

The plots of the residual strength tests for the sandwich panels impacted with the energy levels listed in table 8 are shown in figures 53 to 60. The fatigue load levels are indicated on each of the plots by dashed lines to show their relation with respect to the dimple behavior during the tests.

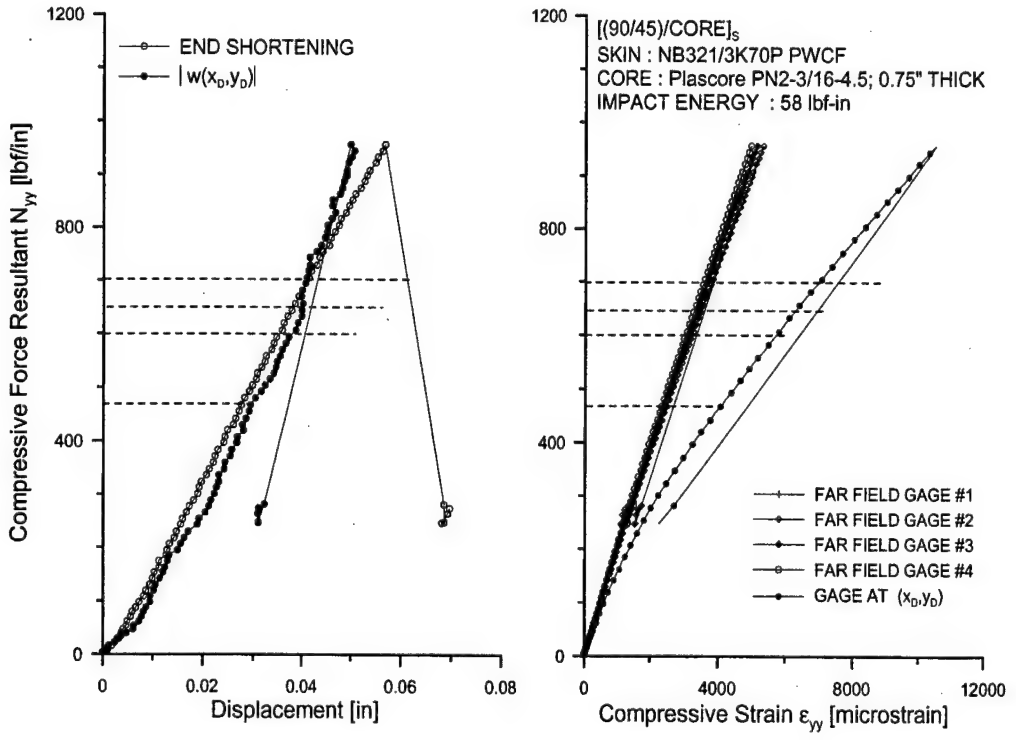

FIGURE 53. CAI TEST DATA FOR $[(90/45)/CORE]_s$ SPECIMEN HONEYCOMB CORE IMPACTED WITH ENERGY LEVEL E_1=58 lbf-in

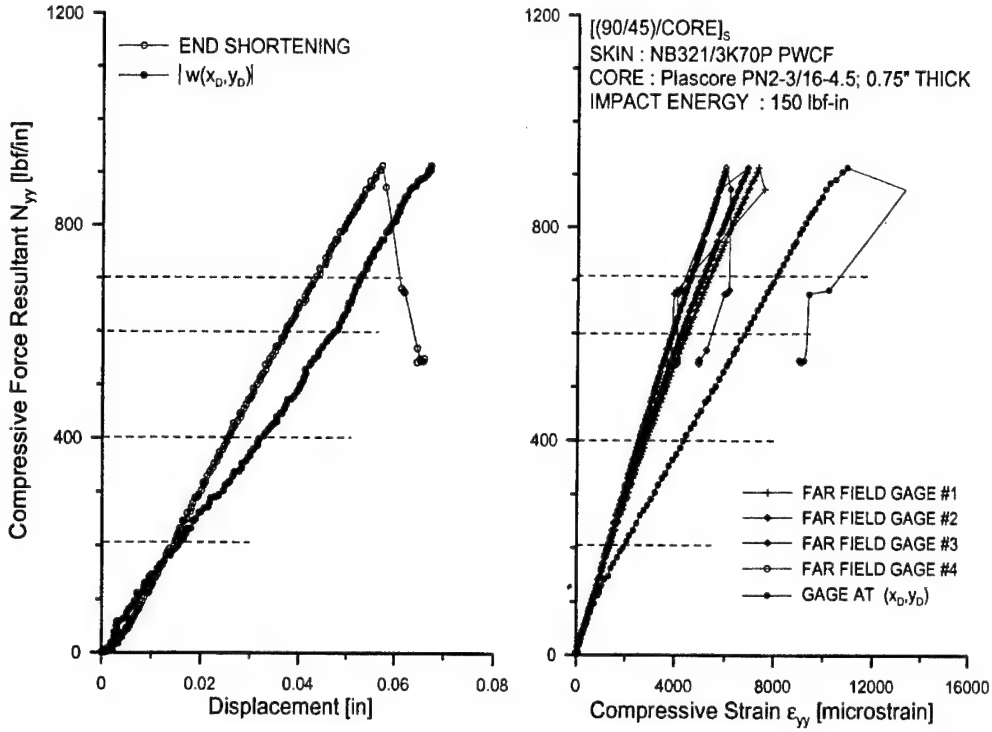

FIGURE 54. CAI TEST DATA FOR $[(90/45)/CORE]_S$ SPECIMEN HONEYCOMB CORE IMPACTED WITH ENERGY LEVEL E_2=150 lbf-in

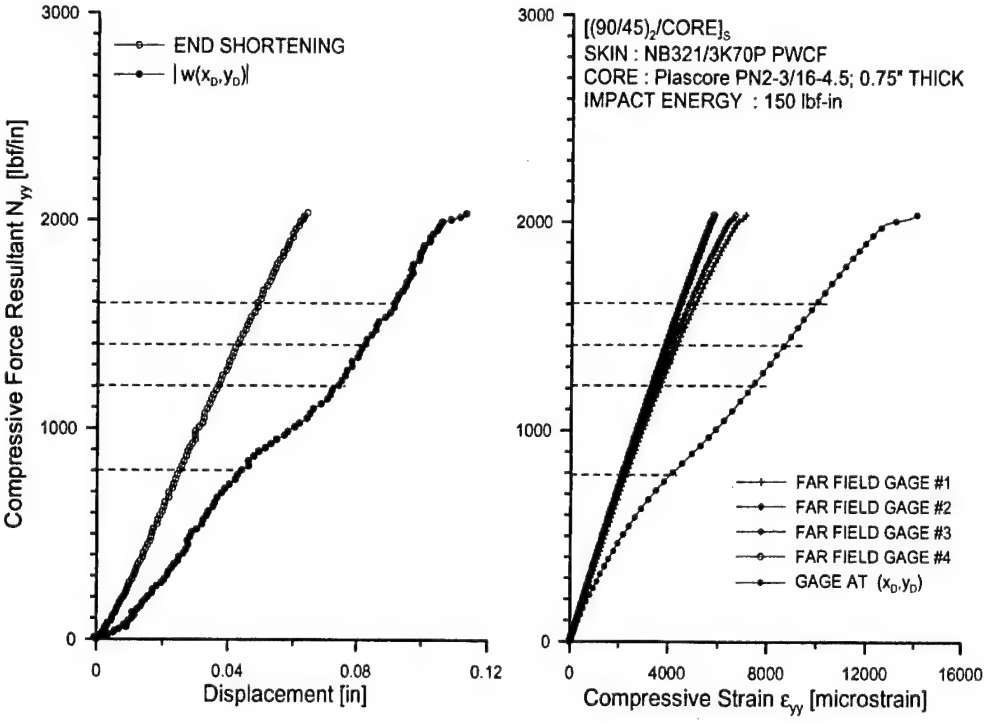

FIGURE 55. CAI TEST DATA FOR $[(90/45)_2/CORE]_S$ SPECIMEN HONEYCOMB CORE IMPACTED WITH ENERGY LEVEL E_1=58 lbf-in

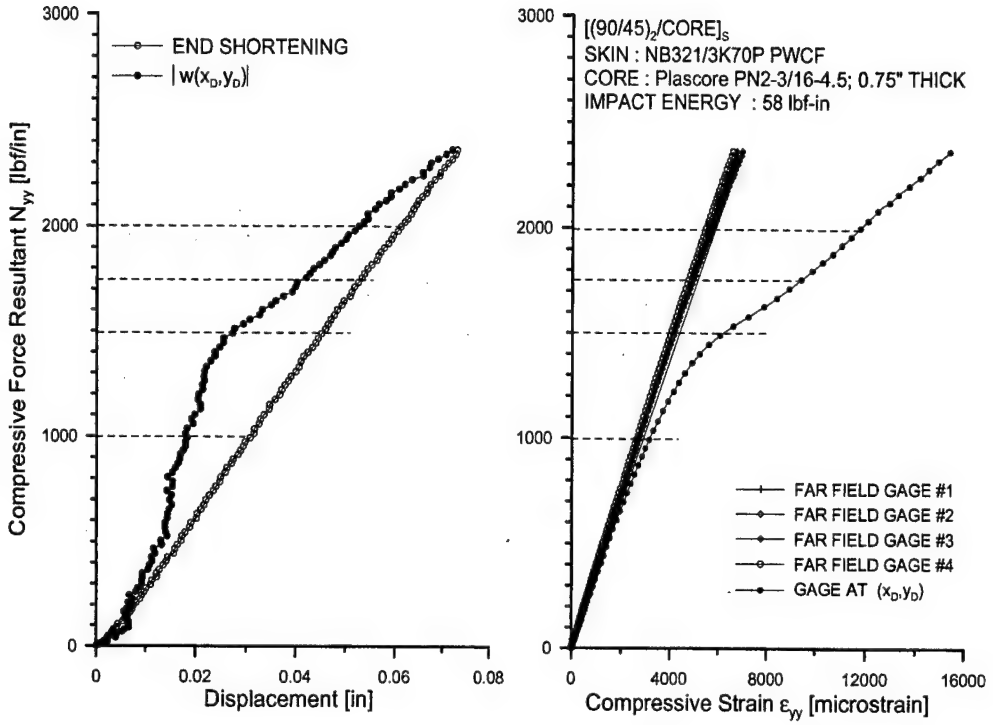

FIGURE 56. CAI TEST DATA FOR $[(90/45)_2/CORE]_s$ SPECIMEN HONEYCOMB CORE IMPACTED WITH ENERGY LEVEL E_2=150 lbf-in

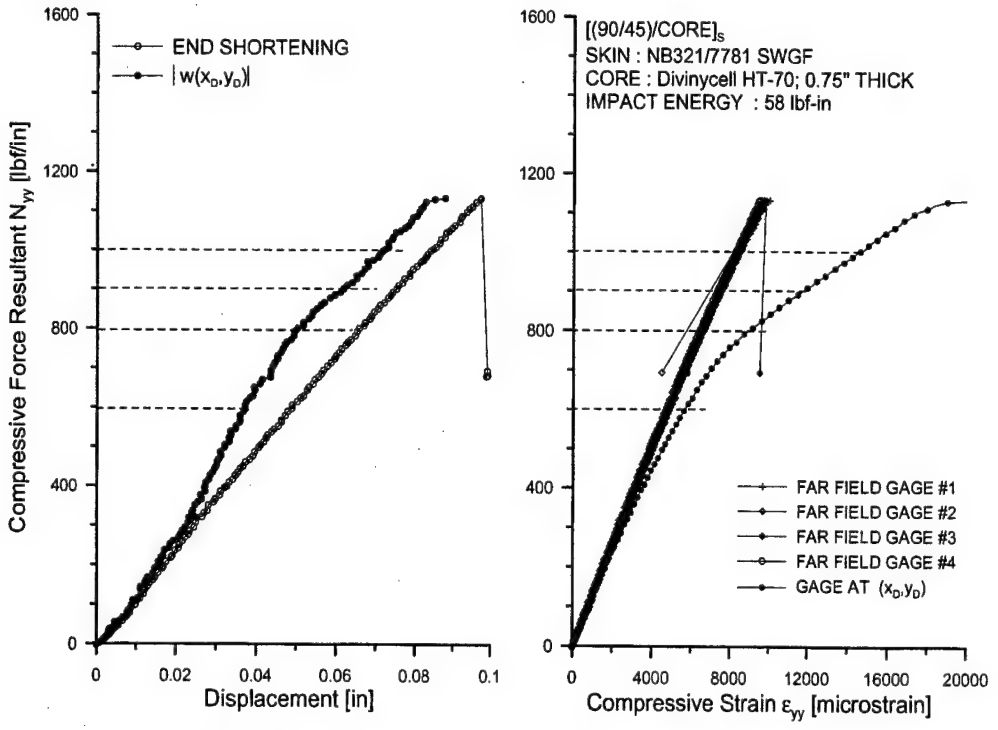

FIGURE 57. CAI TEST DATA FOR $[(90/45)/CORE]_s$ SPECIMEN FOAM CORE IMPACTED WITH ENERGY LEVEL E_1=58 lbf-in

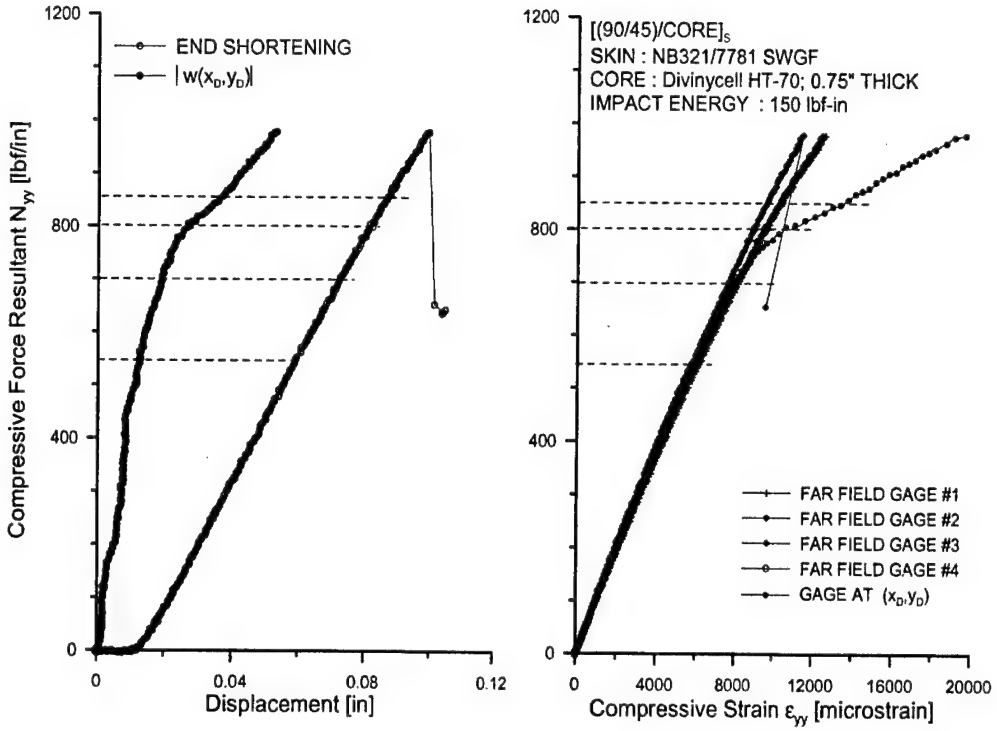

FIGURE 58. CAI TEST DATA FOR $[(90/45)/CORE]_s$ SPECIMEN FOAM CORE IMPACTED WITH ENERGY LEVEL E_2=150 lbf-in

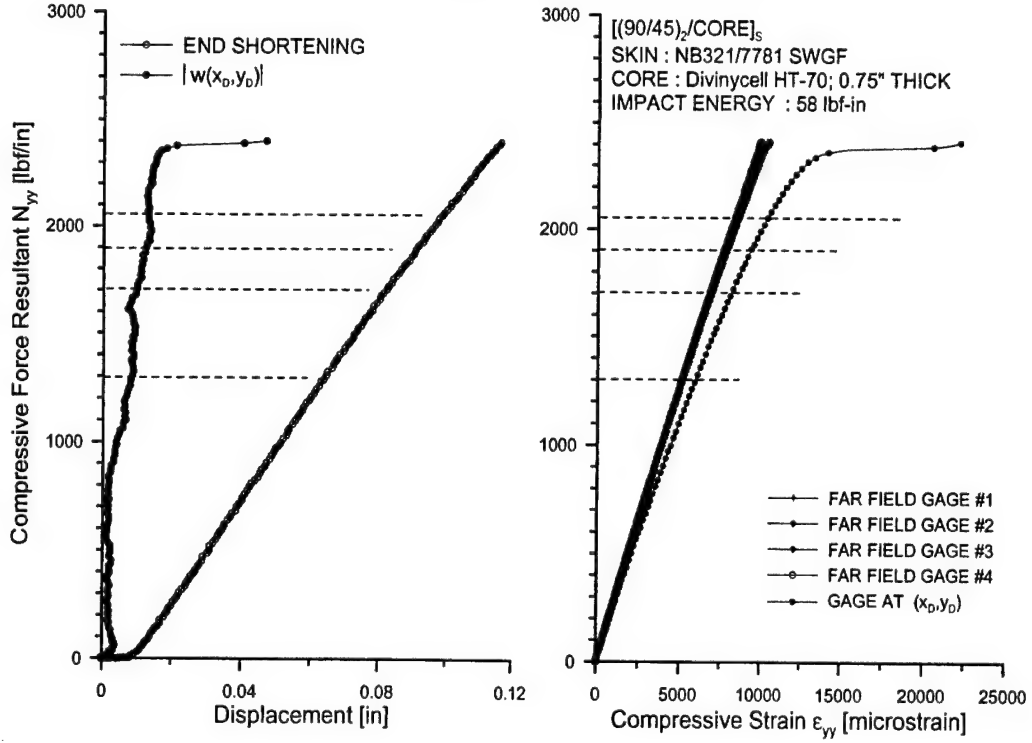

FIGURE 59. CAI TEST DATA FOR $[(90/45)_2/CORE]_s$ SPECIMEN FOAM CORE IMPACTED WITH ENERGY LEVEL E_1=58 lbf-in

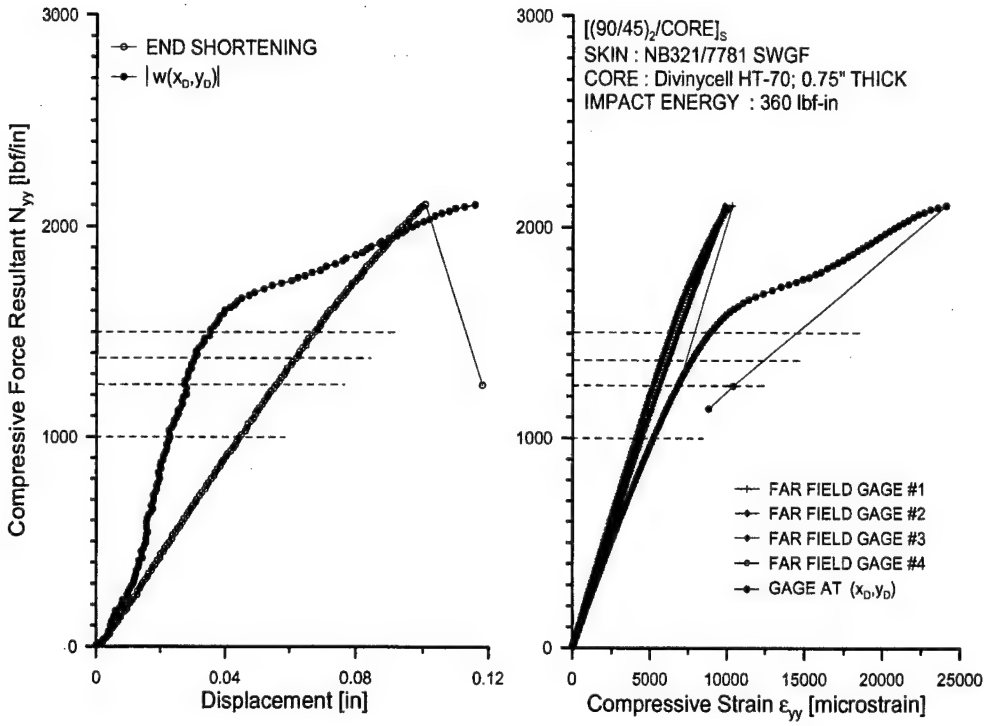

FIGURE 60. CAI TEST DATA FOR $[(90/45)_2/CORE]_s$ SPECIMEN HONEYCOMB CORE IMPACTED WITH ENERGY LEVEL E_2=360 lbf-in

The fatigue load levels indicated in the previous figures are summarized in table 9. The load levels form the minimum compressive loads ($N_{yy\text{-}MINIMUM}$) under fatigue loading. The maximum fatigue loads and the amplitude were obtained based on the load ratio R.

TABLE 9. FATIGUE LOAD LEVELS FOR SANDWICH SPECIMEN

Sandwich Configuration	Minimum Fatigue Load Levels $N_{yy\text{-}MINIMUM}$ (lbf-in)		
	Level	Impact Energy Level	
		E_1	E_2
$[(90/45)/CORE]_s$ NB321/3K70 PWCF facesheets Honeycomb core	1	475	201
	2	600	402
	3	656	600
	4	712	700
$[(90/45)_2/CORE]_s$ NB321/3K70 PWCF facesheets Honeycomb core	1	1000	800
	2	1500	1200
	3	1750	1400
	4	2000	1600
$[(90/45)/CORE]_s$ NB321/7781SWGF facesheets Foam core	1	600	550
	2	800	700
	3	900	800
	4	1000	850
$[(90/45)_2/CORE]_s$ NB321/7781 SWGF facesheets Foam core	1	1300	1000
	2	1700	1250
	3	1900	1375
	4	2050	1500

6.5.3 Fatigue Testing Results.

6.5.3.1 Fatigue Life.

The sandwich specimens were subjected to fatigue loading using the load levels and load ratios defined in the previous sections. The number of cycles to failure, N_f, at each load level and load ratio combination were recorded. The specimens surviving N_∞ (=150,000) cycles were subsequently tested to failure under static loading to assess any further degradation in residual strength. The plots of the fatigue life at different minimum load levels for the sandwich configurations are shown in figures 61 to 68. The figures also indicate the static strength of the virgin specimen and the static residual strength of a similar specimen prior to fatigue loading. The following observations were made regarding the fatigue life of sandwich specimens at different load levels.

a. The fatigue life curve (S-N curve) could not be generated due to the limited data set. The model fitting procedure presented by Sendeckyj [11] requires a minimum of m+2 uncensored (i.e., not a runout) data points at m+1 stress levels, where 'm' is the number of parameters for the fatigue model. Thus, if use a two-parameter model is used, then every stress level would need at least four uncensored data points.

b. At the higher fatigue loads, the early failures were attributed to impingement on the static strength distribution. The S/N curve was very flat and comparable to other composite structures. No significant trend could be observed with load ratio as the number of replicates were too small.

c. The threshold load, below which no degradation due to the fatigue cycling, was 65% of static CAI strength for carbon/epoxy facesheet panels for impact energies up to 150 lbf-in. For fiberglass/epoxy facesheet panels, the threshold was 75% of static CAI strength for impact energies up to 150 lbf-in and 50% of static CAI strength for the panel that sustained 360 lbf-in energy impact.

d. The strain thresholds for no fatigue damage were approximately 3500 μ of far-field strain for the carbon/epoxy facesheet panels. The strain threshold is somewhat unreliable for thin facesheet panels as the higher impact energy (150 lbf-in) caused significant stiffness loss and, hence, the panel with more damage failed at a higher strain level. Similar conclusions can be drawn for fiberglass/epoxy panels, where the lowest measured far-field threshold strain was 7000 μ.

e. The TTU C-scan inspection of honeycomb core sandwich panels did not indicate a significant increase in damage size ($2R_{damage}$). Additional destructive tests at shorter intervals may be necessary to observe the growth of core damage across the thickness of the specimen.

f. The growth of skin damage (delaminations) discussed in section 2 could not be observed for carbon facesheets (honeycomb core panels). The decrease in fatigue life may be a combination of growth in the skin and core damage states. The skin damage growth, if any, may be observed using sandwich panels with fiberglass facesheets.

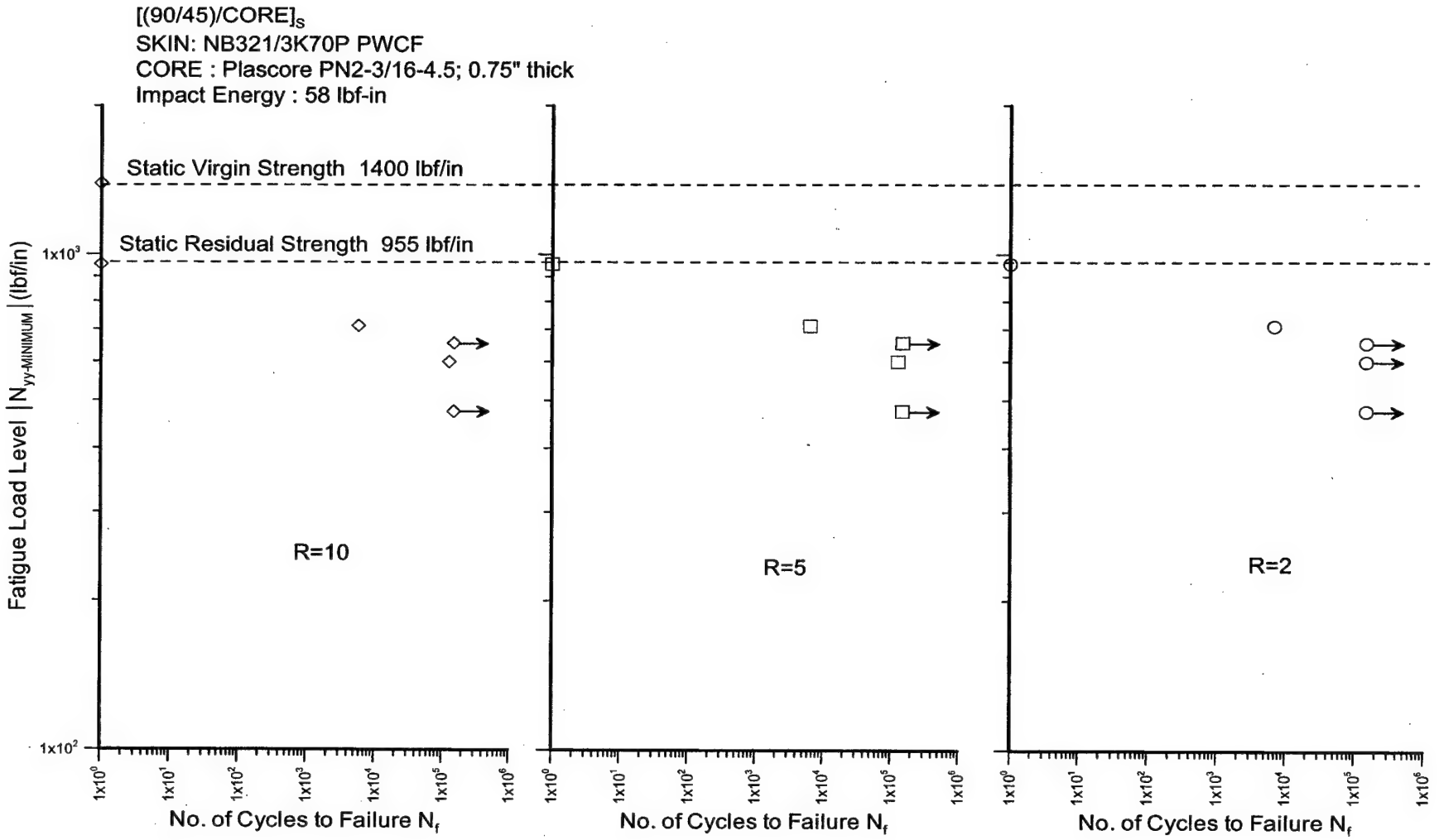

FIGURE 61. FATIGUE LIFE DATA FOR $[(90/45)/CORE]_s$ SANDWICH PANELS WITH HONEYCOMB CORE IMPACTED WITH AN IMPACT ENERGY OF 58 lbf-in

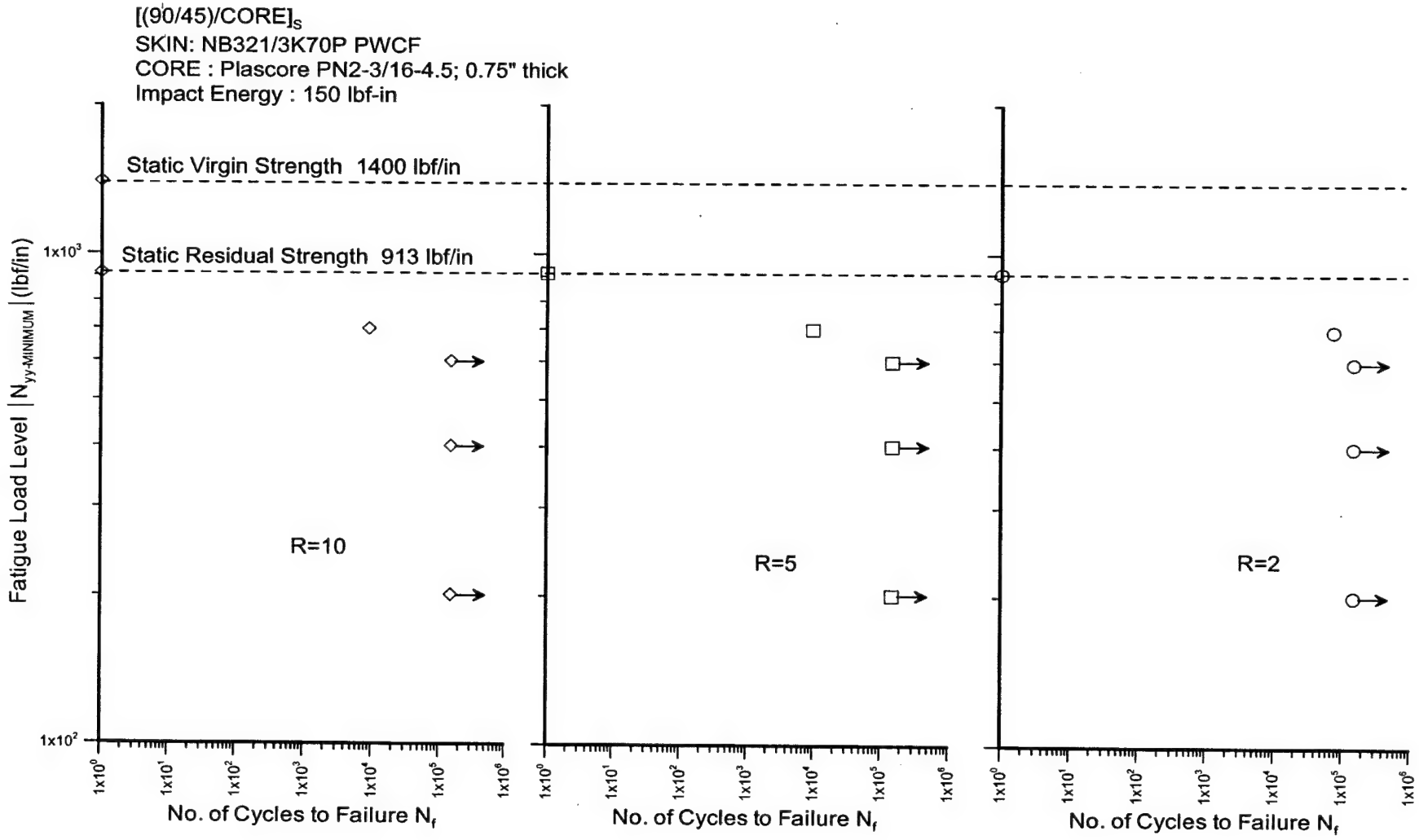

FIGURE 62. FATIGUE LIFE DATA FOR $[(90/45)/CORE]_s$ SANDWICH PANELS WITH HONEYCOMB CORE IMPACTED WITH AN IMPACT ENERGY OF 150 lbf-in

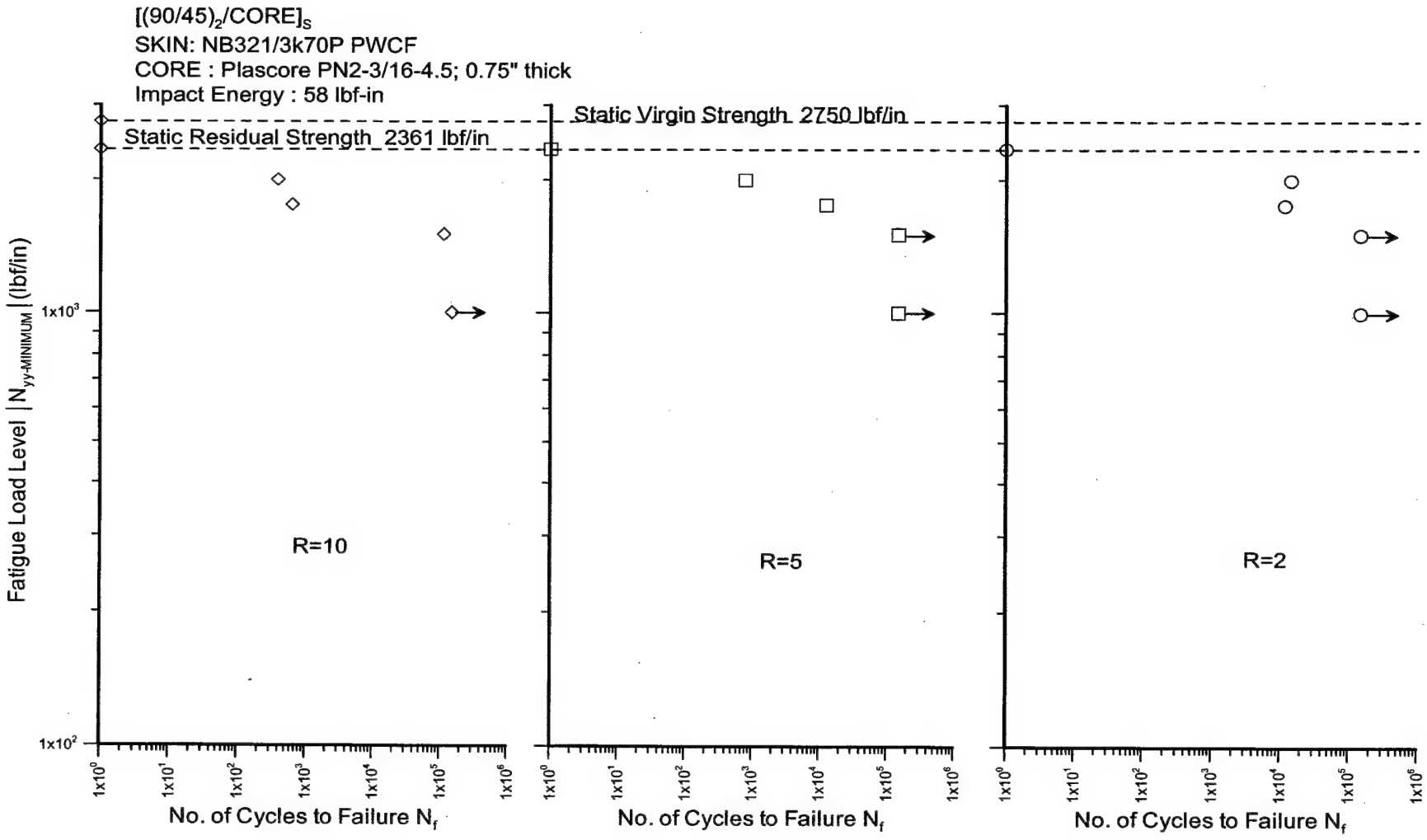

FIGURE 63. FATIGUE LIFE DATA FOR $[(90/45)_2/CORE]_s$ SANDWICH PANELS WITH HONEYCOMB CORE IMPACTED WITH AN IMPACT ENERGY OF 58 lbf-in

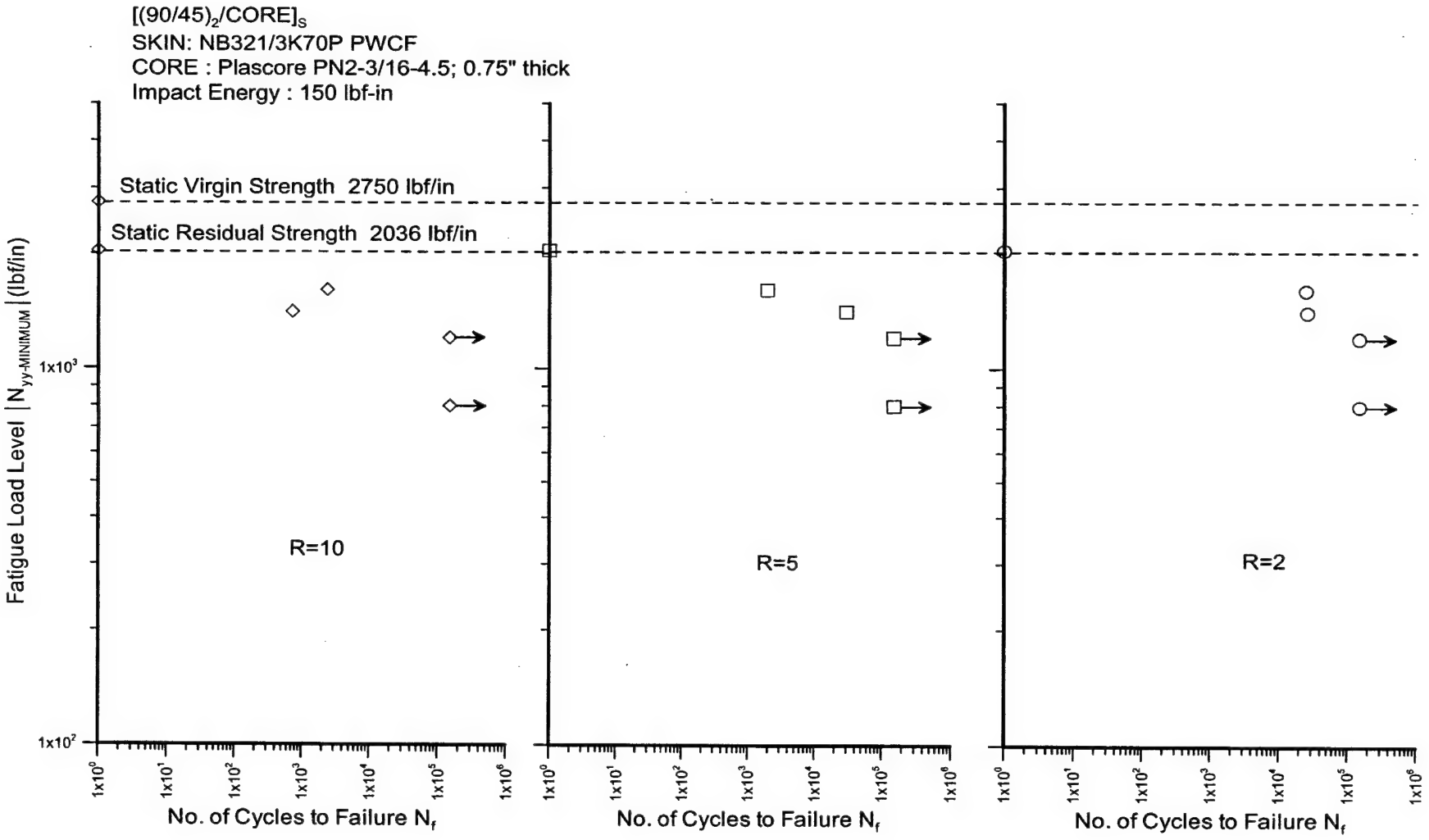

FIGURE 64. FATIGUE LIFE DATA FOR $[(90/45)_2/CORE]_s$ SANDWICH PANELS WITH HONEYCOMB CORE IMPACTED WITH AN IMPACT ENERGY OF 150 lbf-in

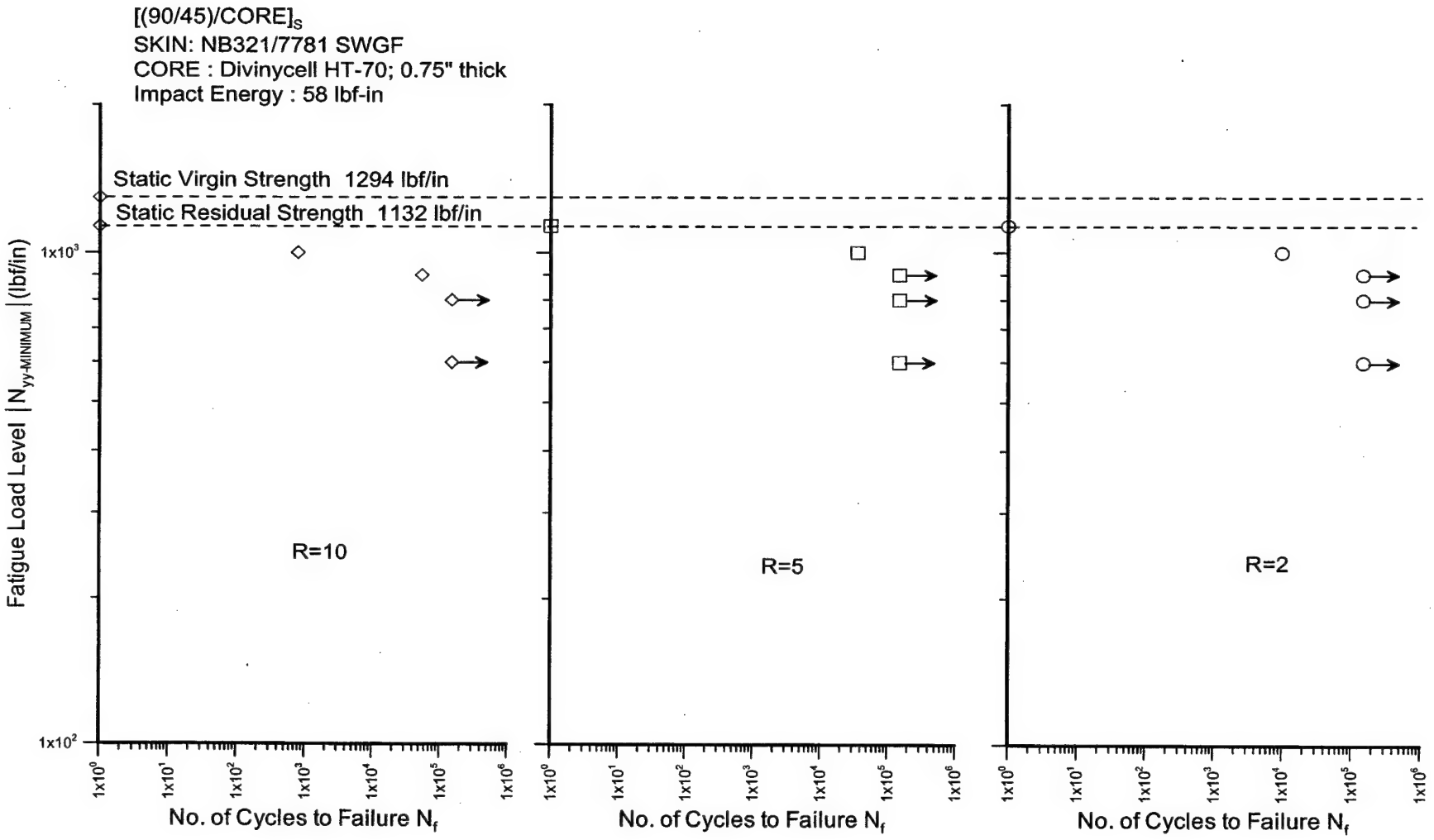

FIGURE 65. FATIGUE LIFE DATA FOR $[(90/45)/CORE]_s$ SANDWICH PANELS WITH FOAM CORE IMPACTED WITH AN IMPACT ENERGY OF 58 lbf-in

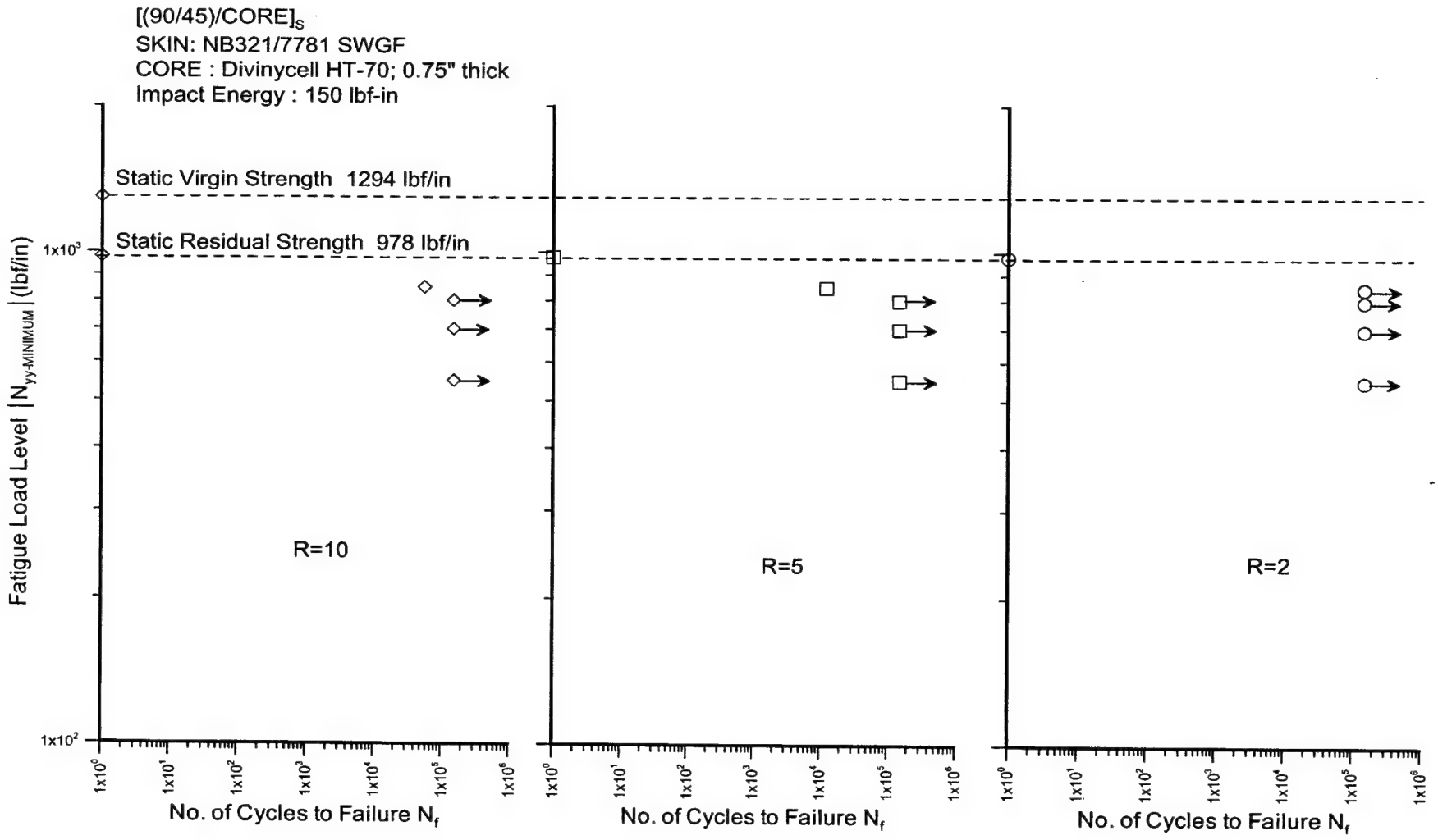

FIGURE 66. FATIGUE LIFE DATA FOR $[(90/45)/CORE]_s$ SANDWICH PANELS WITH FOAM CORE IMPACTED WITH AN IMPACT ENERGY OF 150 lbf-in

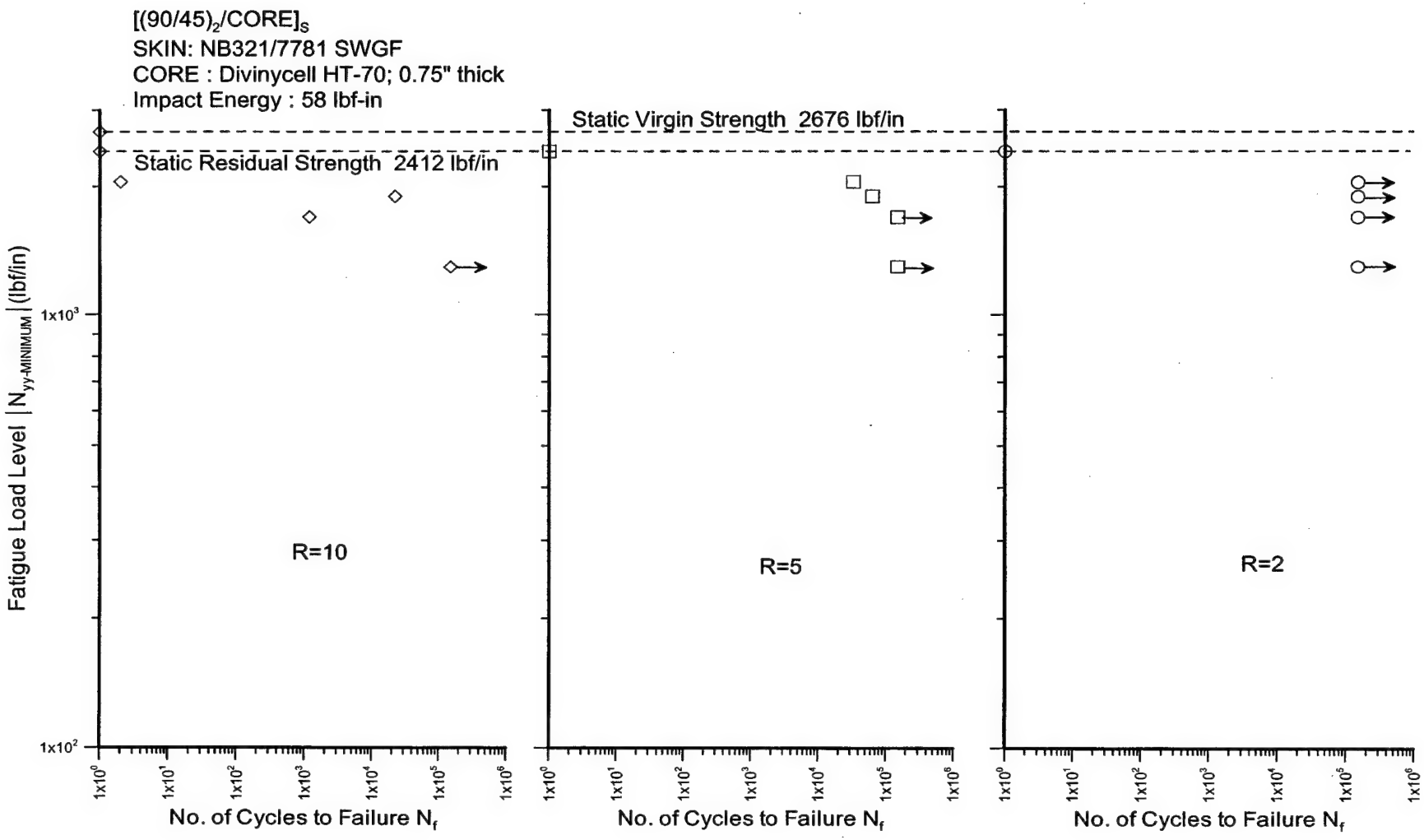

FIGURE 67. FATIGUE LIFE DATA FOR $[(90/45)_2/CORE]_s$ SANDWICH PANELS WITH FOAM CORE IMPACTED WITH AN IMPACT ENERGY OF 58 lbf-in

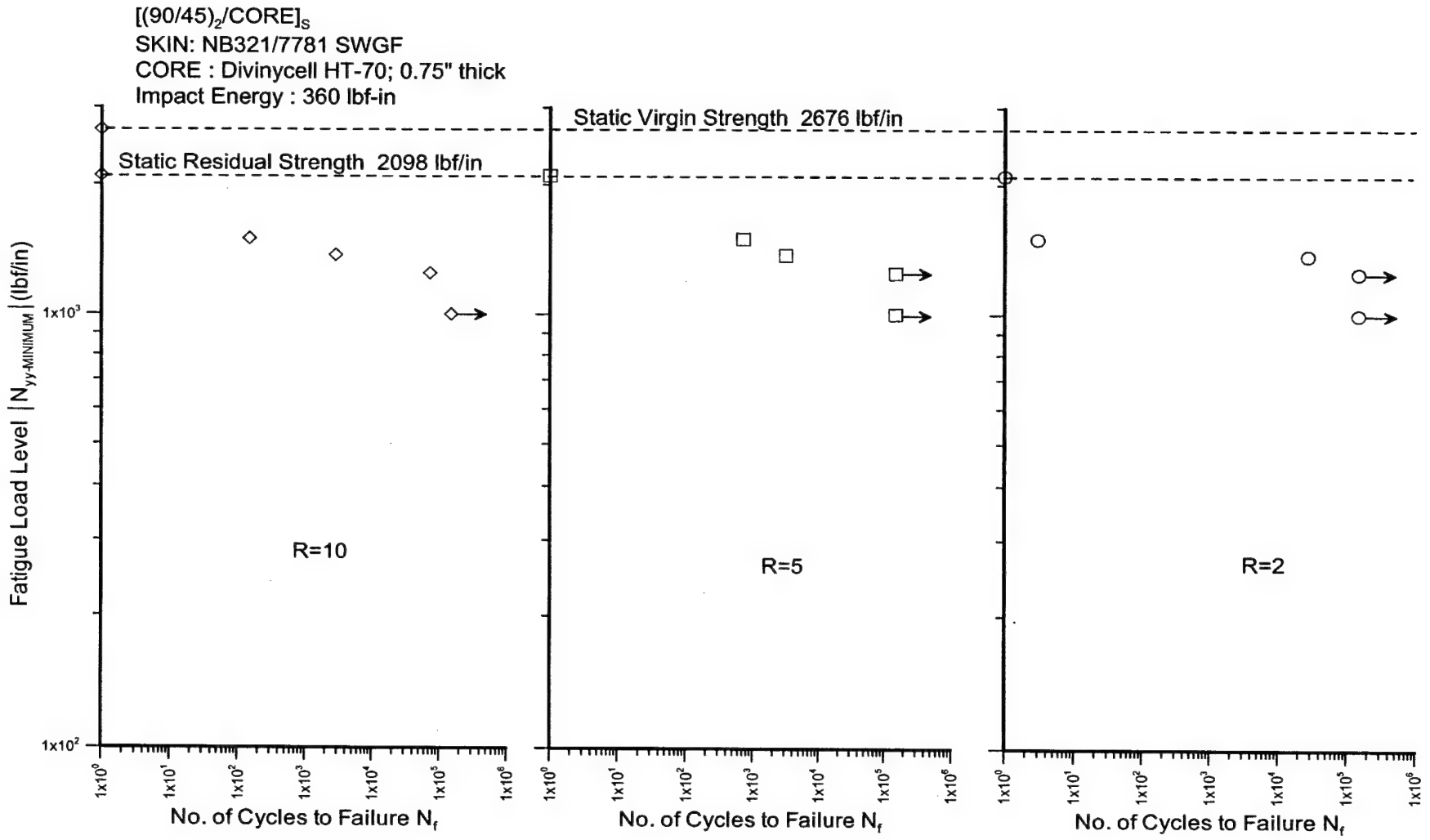

FIGURE 68. FATIGUE LIFE DATA FOR $[(90/45)_2/CORE]_s$ SANDWICH PANELS WITH FOAM CORE IMPACTED WITH AN IMPACT ENERGY OF 360 lbf-in

6.5.3.2 Residual Strength Degradation.

The degradation of residual strength of sandwich specimen due to fatigue loading was determined from static residual strength tests on the specimens surviving N_∞ cycles (run-out). The residual strength degradation was defined in terms of a normalized run-out residual strength defined below.

$$Normalized\ Run\text{-}Out\ Residual\ Strength = \frac{N_{yy-\infty}}{N_{yyRS-Ei}}$$

where $N_{yy-\infty}$ is the minimum load level at which the specimen survived N_∞ and $N_{yyRs-Ei}$ is the static residual strength of sandwich specimen impacted with impact energy level E_i (i=1,2). The normalized run-out residual strengths were plotted versus a normalized minimum load level defined as follows.

$$Normalized\ Minimum\ Load\ Level = \frac{N_{yy-MINIMUM}}{N_{yyRS-Ei}}$$

The plots of normalized run-out residual strength vs normalized minimum load levels for the sandwich configurations investigated are shown in figures 69 to 76. The data points lying on the x axis indicate specimens that did not survive N_∞ at that particular load level. Based on the experimental data, the following observations were made.

a. $[(90/45)/CORE]_s$ panels with carbon fabric facesheets and honeycomb core (see figures 69 and 70)

   1. For impact energy level E_1 (58 lbf-in), no significant degradation was observed for the minimum load levels between 50% and 70% (approx.) of the static residual strength. Some of the specimens exhibited an increase in residual strength (e.g., see figure 74), which can be attributed to small amount of testing. A scatter in data is implied based on the above observation.

   2. For impact energy level E_2 (150 lbf-in), no significant degradation was observed for minimum load levels between 20% to 70% (approx.) of the static residual strength, for load ratios of 5 and 2. However, for the load ratio of 10, the degradation in residual strength increased from 0% to 20% when the minimum load in fatigue was increased from 20% to 70% of the static residual strength.

b. $[(90/45)_2/CORE]_s$ panels with carbon fabric facesheets and honeycomb core (see figures 71 and 72)

   1. For impact energy level E_1, an average degradation in residual strength of 10% was observed for load levels less than 50% (R=10), 65% (R=5), and 70% (R=2) of the static residual strength.

2. For impact energy level E_2, an average degradation in residual strength of up to 15% was observed for load levels less than 60% (all load ratios) of the static residual strength.

c. $[(90/45)/CORE]_s$ panels with fiberglass fabric facesheets and foam core (see figures 73 and 74)

1. For impact energy level E_1, there was no significant degradation in residual strength for minimum load levels lower than 80% (approx.) of the static residual strength.

2. For impact energy level E_2, the residual strength degradation was negligible at all stress levels less then 80% (approx.) of the static residual strength, for load ratios of 10 and 2. A degradation of about 18% was observed for a minimum fatigue load level corresponding to 70% of the static residual strength when the load ratio was 5.

d. $[(90/45)_2/CORE]_s$ panels with fiberglass fabric facesheets and foam core (see figures 75 and 76)

1. For impact energy level E_1, the average degradation was 5% for minimum load levels lower than 90% (approx.) of the static residual strength and a load ratio of 2. When the load level was about 55% of the static residual strength, an average degradation of 10% was observed at all three load ratios.

2. For impact energy level E_2, (360 lbf-in) the average degradation was 30% for minimum load levels lower than 60% (approx.) of the static residual strength at all load ratios.

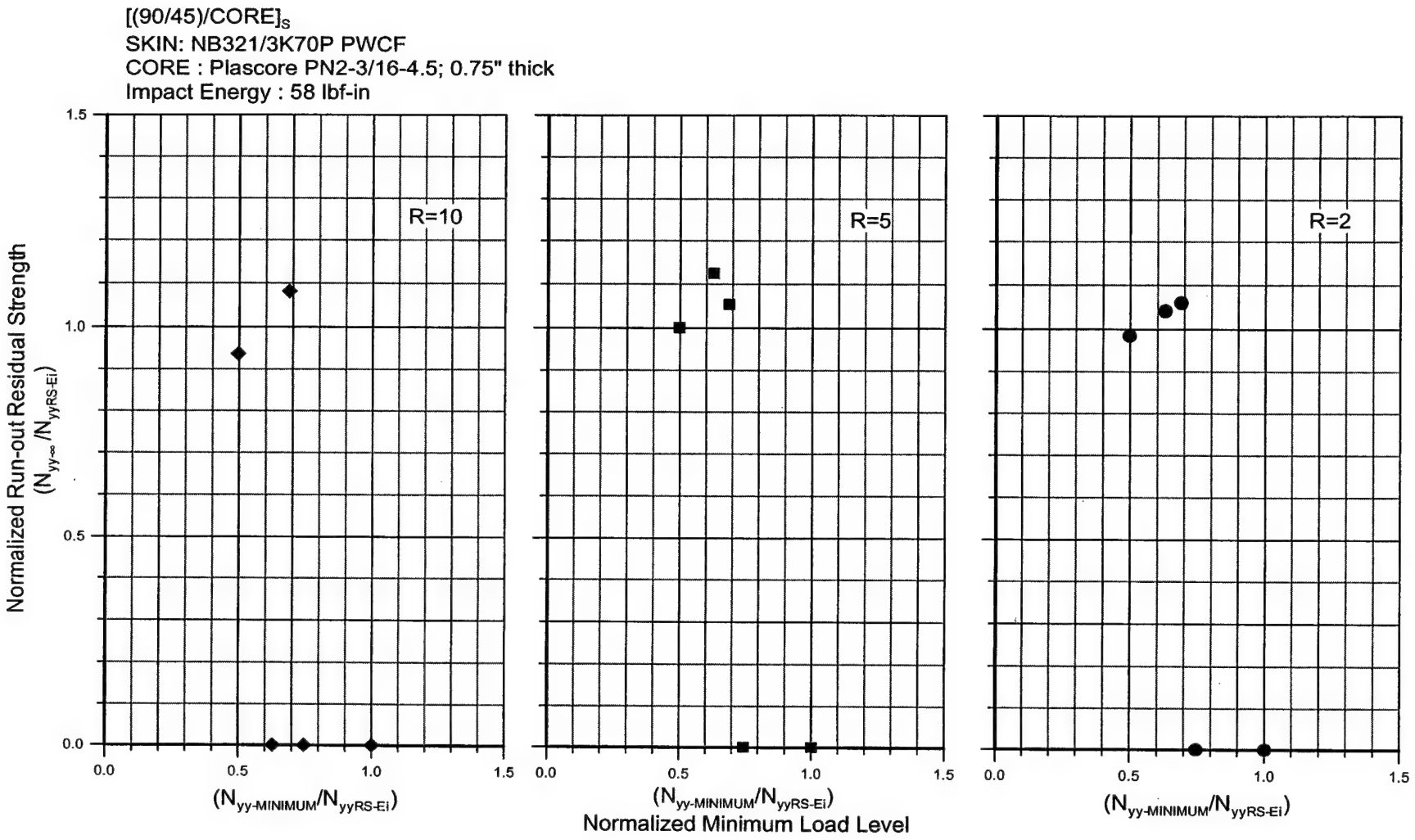

FIGURE 69. RESIDUAL STRENGTH DEGRADATION FOR $[(90/45)/CORE]_s$ SANDWICH PANELS WITH HONEYCOMB CORE IMPACTED WITH AN IMPACT ENERGY OF 58 lbf-in

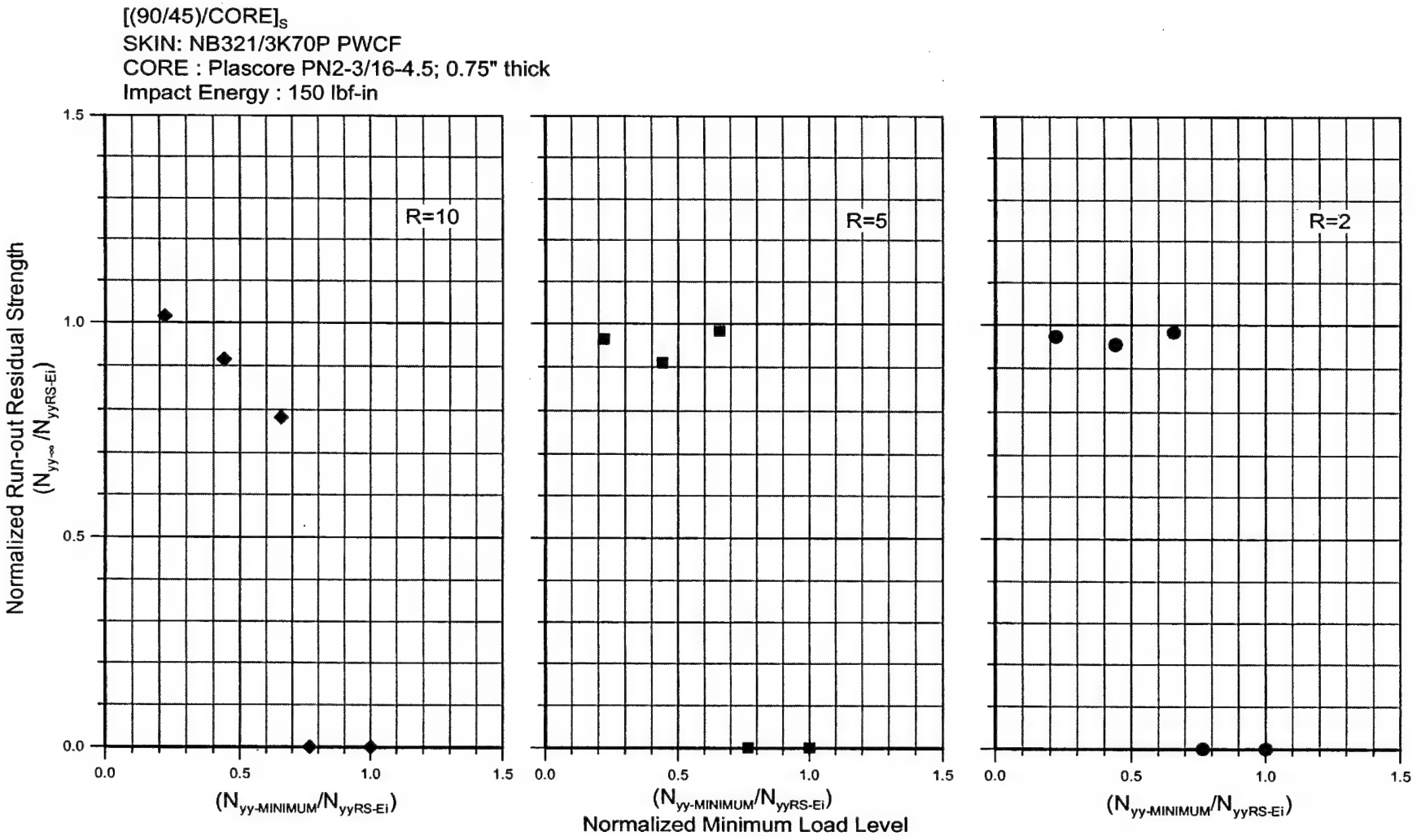

FIGURE 70. RESIDUAL STRENGTH DEGRADATION FOR $[(90/45)/CORE]_s$ SANDWICH PANELS WITH HONEYCOMB CORE IMPACTED WITH AN IMPACT ENERGY OF 150 lbf-in

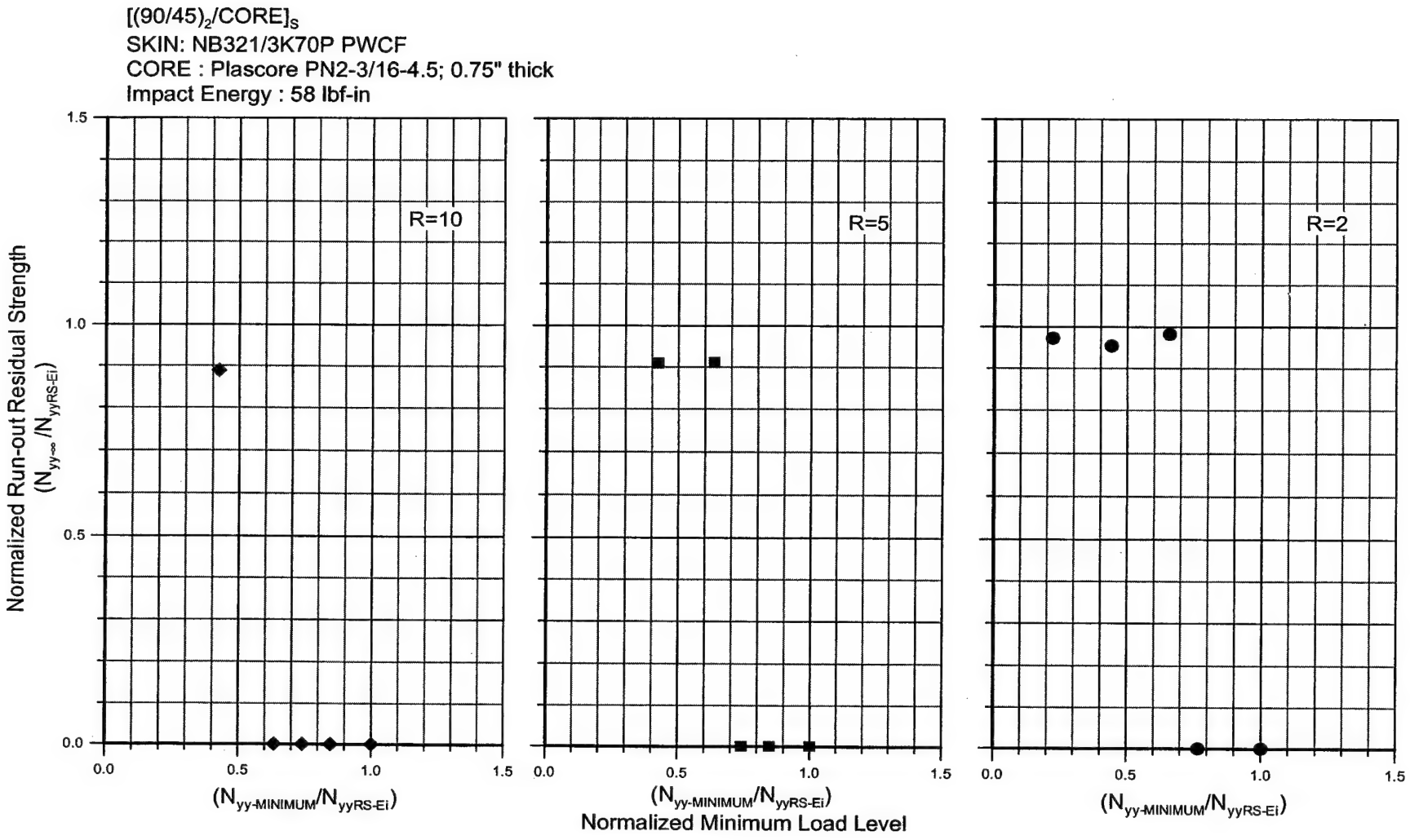

FIGURE 71. RESIDUAL STRENGTH DEGRADATION FOR $[(90/45)_2/CORE]_s$ SANDWICH PANELS WITH HONEYCOMB CORE IMPACTED WITH AN IMPACT ENERGY OF 58 lbf-in

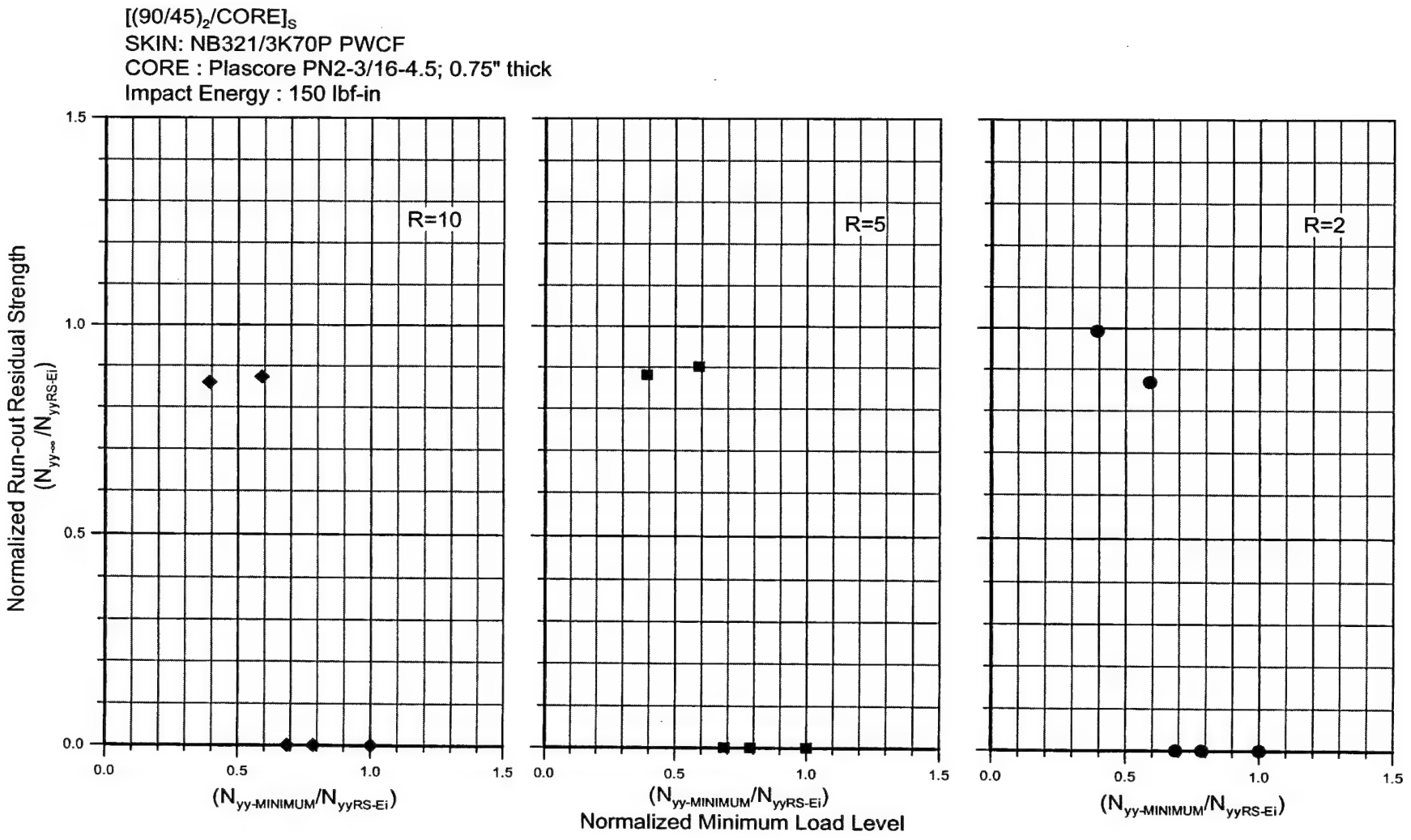

FIGURE 72. RESIDUAL STRENGTH DEGRADATION FOR $[(90/45)_2/CORE]_s$ SANDWICH PANELS WITH HONEYCOMB CORE IMPACTED WITH AN IMPACT ENERGY OF 150 lbf-in

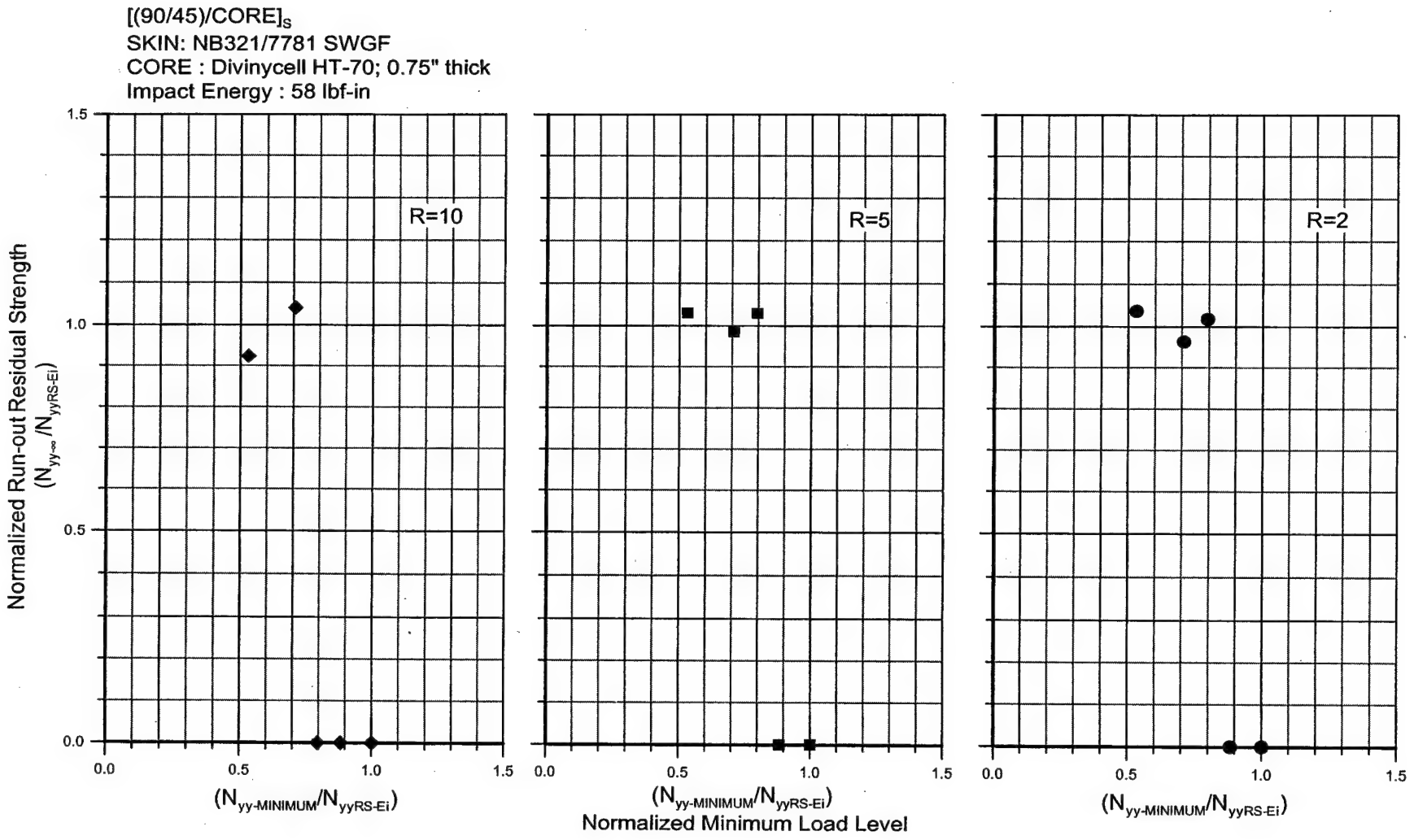

FIGURE73. RESIDUAL STRENGTH DEGRADATION FOR $[(90/45)/CORE]_s$ SANDWICH PANELS WITH FOAM CORE IMPACTED WITH AN IMPACT ENERGY OF 58 lbf-in

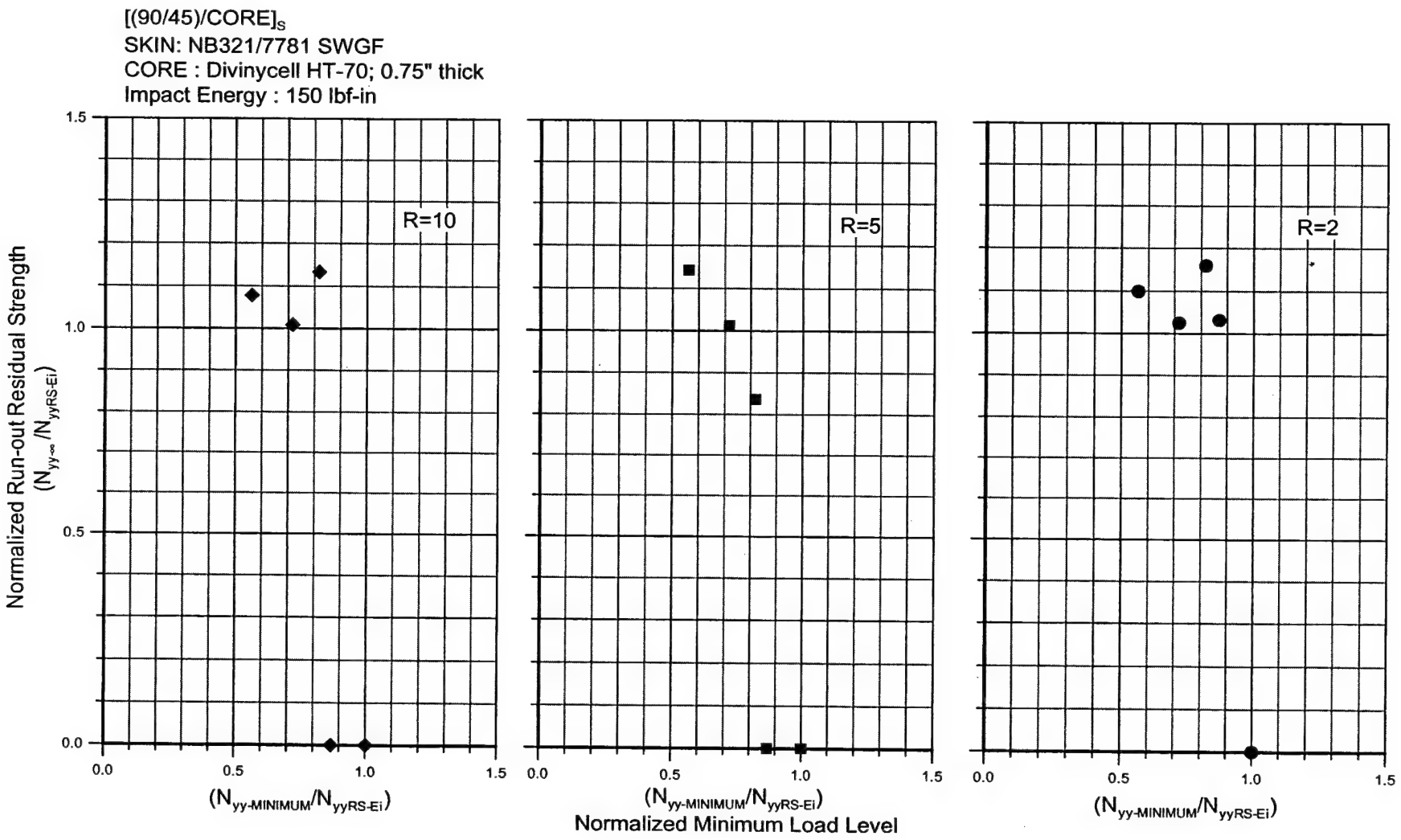

FIGURE 74. RESIDUAL STRENGTH DEGRADATION FOR $[(90/45)/CORE]_s$ SANDWICH PANELS WITH FOAM CORE IMPACTED WITH AN IMPACT ENERGY OF 150 lbf-in

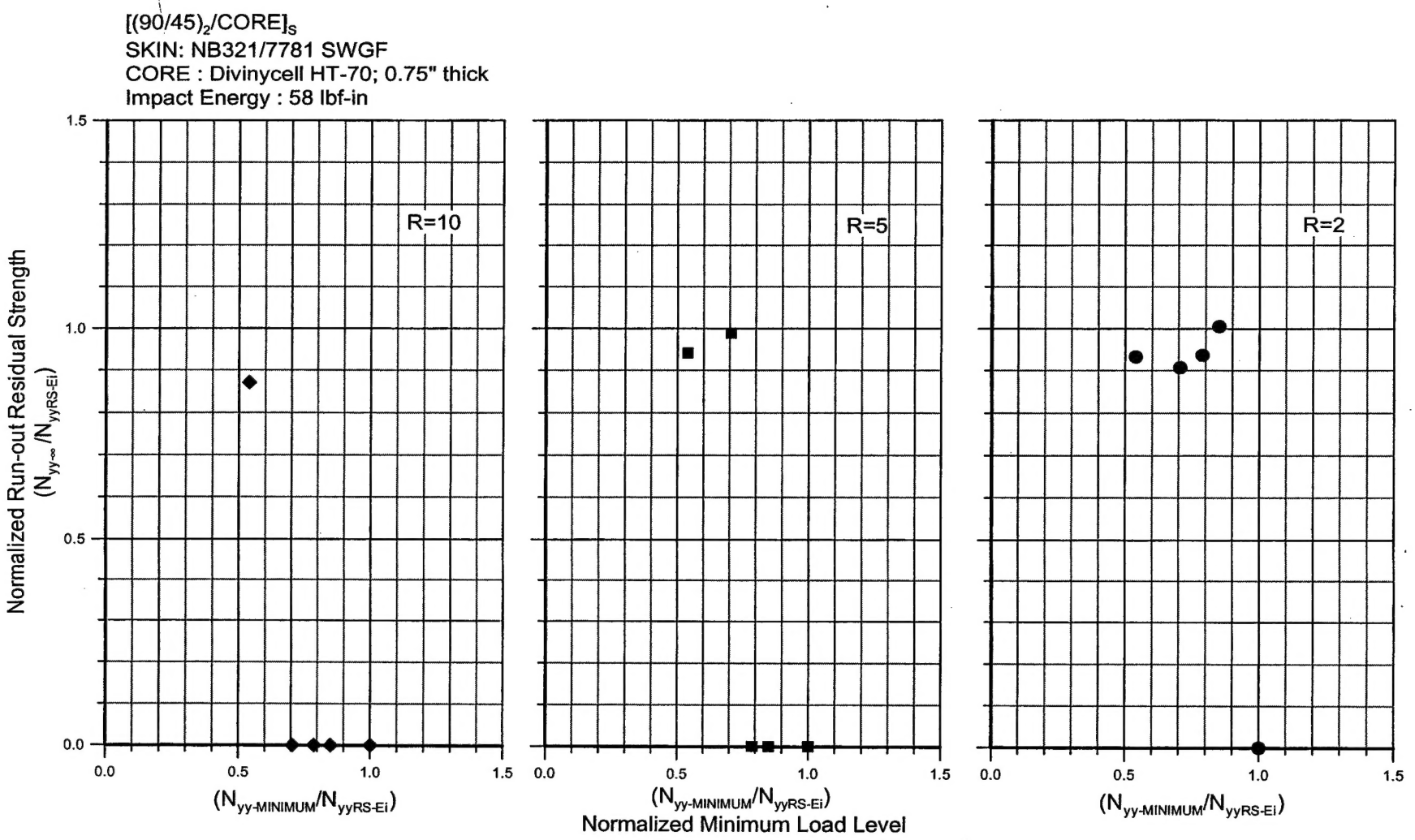

FIGURE 75. RESIDUAL STRENGTH DEGRADATION FOR $[(90/45)_2/CORE]_s$ SANDWICH PANELS WITH FOAM CORE IMPACTED WITH AN IMPACT ENERGY OF 58 lbf-in

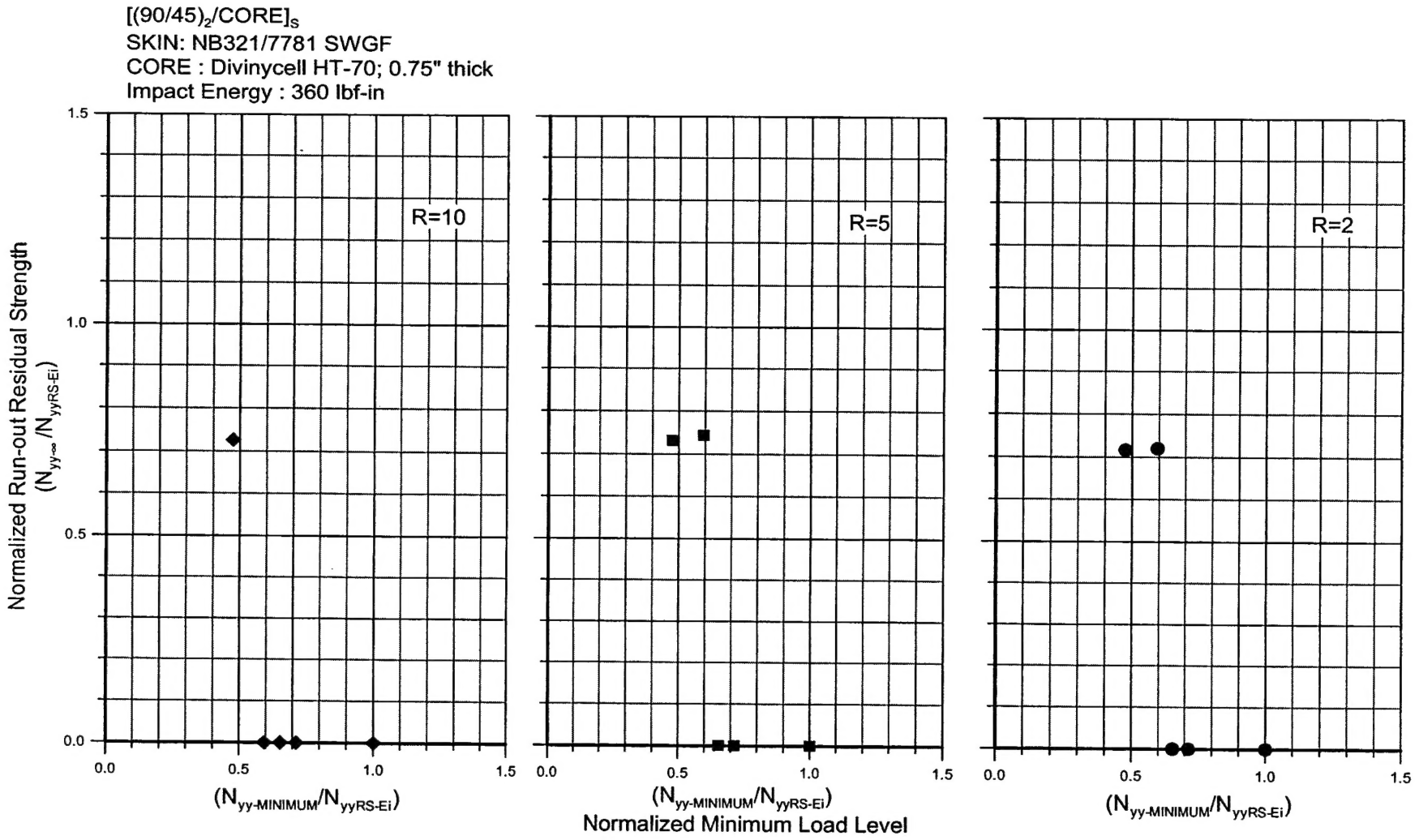

FIGURE 76. RESIDUAL STRENGTH DEGRADATION FOR $[(90/45)_2/CORE]_s$ SANDWICH PANELS WITH FOAM CORE IMPACTED WITH AN IMPACT ENERGY OF 360 lbf-in

7. CONCLUSIONS.

The work presented describes the nature of damage states based on destructive sectioning and nondestructive inspection techniques in thin-gage composite sandwich panels. The effects of panel curvature were also characterized with respect to these damage states. In addition, a limited fatigue investigation was conducted to characterize any damage growth that occurred and might influence possible inspection intervals throughout the service life of the structure.

The detectability of impact damage states in sandwich panels due to blunt impactors using different field inspection techniques was experimentally investigated for different facesheet and core combinations. The impact damage in honeycomb core sandwich panels was better detected using instruments that exploit the local vibrational characteristics of the sandwich structure, while the damage in foam core panels was more amenable to acoustic-based techniques. The effect of facesheet stiffness on the sensitivity of the field inspection techniques was investigated and the results are reported.

The behavior of the impact damage states due to blunt impactors under in-plane compressive loads was investigated in detail. The impact damage behaved in a characteristic sequence of events leading to contrasting final failure modes. The sequence of events was dependent on the facesheet stiffness and the transverse compressive properties of the core material. The facesheet thickness (flexural stiffness) was observed to govern the propagation of dimple, leading to either a skin fracture failure mode (thin facesheets) or a buckling failure mode (thick facesheets).

The effects of panel curvature on the impact damage resistance of sandwich panels were experimentally investigated for limited sandwich configurations. The effects of the radius of cylindrical panels, boundary conditions, facesheet type, and core type are summarized. The decrease in the radius of curvature, which increased the global bending stiffness but decreased the local contact stiffness increased the susceptibility to damage for sharp impacts and decreased the susceptibility for blunt impacts. The curved panel behavior was characterized in terms of the impact responses and the damage metrics.

The fatigue behavior of honeycomb core and foam core sandwich panels with impact damage due to 3″ diameter impactor was investigated. The effect of load ratio and load level on the fatigue life was observed. However, no significant trend could be observed with load ratio as the number of replicates were too small. The load/life was very flat and exhibited a well-known composites sudden death behavior. At higher fatigue loads, the early failures were attributed to impingement on the static strength distribution.

The threshold load, below which no degradation due to the fatigue cycling, was 65% of static CAI strength for carbon/epoxy facesheet panels for impact energies up to 150 lbf-in. For fiberglass/epoxy facesheets, the threshold is 75% of static CAI strength for impact energies up to 150 lbf-in and 50% of static CAI strength for the panel that sustained 360 lbf-in energy impact.

The specimens surviving the predefined infinite life of 150,000 cycles were further tested for degradation in residual strength. Except for foam core sandwich panels with fiberglass/epoxy facesheets impacted at a 30 lbf-ft energy level, where the residual strength degradation was 30%,

the fatigue cycling did not degrade the static strength. It should be noted that the fatigue cycling was at strain levels much higher than would be expected in service.

8. REFERENCES.

1. J. Tomblin, T. Lacy, B. Smith, S. Hooper, A. Vizzini, and S. Lee, "Review of Damage Tolerance for Composite Sandwich Airframe Structures," FAA William J. Hughes Technical Center, Atlantic City International Airport, New Jersey, DOT/FAA/AR-99/49, August 1999.

2. John S. Tomblin, Raju, K.S., Liew, J., and Smith, B.L., "Impact Damage Characterization and Damage Tolerance of Composite Sandwich Airframe Structures," FAA William J. Hughes Technical Center, Atlantic City International Airport, New Jersey, DOT/FAA/AR-00/44, January 2001.

3. K.S. Raju and J.S. Tomblin, "Damage Characteristics in Sandwich Panels Subjected to Static Indentation Using Spherical Indentors," 42nd AIAA/ASME/ASCE/AHS/ASC Structures, Structural Dynamics, and Materials Conference, 16-19 April 2001, Seattle, WA.

4. K.S. Raju, "The Static Indentation Behavior of Composite Sandwich Panels With Thin Quasi-Isotropic Skins," Ph.D. Dissertation, Department of Aerospace Engineering, Wichita State University, December 2001.

5. David K. Hsu, John J. Peters, Dong Fei, Daniel J. Barnard, and Vinay Dayal, "Imaging of Flaws in Composite Honeycomb Aircraft Structures Using Instrumented Tap Test," *SPIE Proceedings on Nondestructive Evaluation of Aging Materials and Composites*, Vol. 3585, G.Y. Baaklini, C.A. Libowitz, and E.S. Boltz, eds., 1999, pp. 236-245.

6. Mitsui Woodpecker, Mitsui & Co. (U.S.A), Inc., 1001 Fourth Avenue, Suite 4000, Seattle, WA 98154-1196.

7. SAE ARP5089, Aerospace Recommended Practice.

8. Lacy et al., "Damage Resistance Characterization of Sandwich Composites Using Response Surfaces," FAA William J. Hughes Technical Center, Atlantic City International Airport, New Jersey, DOT/FAA/AR-01/71, March 2002.

9. Gary Georgeson, Scott Lea, and Jeff Hansen, "Electronic Tap Hammer for Composite Damage Assessment," SPIE Proceedings, Vol. 2945, *Nondestructive Evaluation of Aging Aircraft, Airports and Aerospace Hardware*, R.D. Rempt and A.L. Broz, eds., 1996.

10. K.S. Raju and J.S. Tomblin, "Compressive Behavior of Impact-Damaged Thin Skinned Honeycomb Core Sandwich Panels," to be published.

11. Sendeckyj, G.P., "Fitting Models to Composite Materials Fatigue Data," *Test Methods and Design Allowables for Fibrous Composites, ASTM STP 734,* C.C. Chamis, ed., American Society for Testing and Materials, 1981, pp. 245-260.

*U.S. GOVERNMENT PRINTING OFFICE: 2002/504-042/60026